

Design and Implementation of Control Concepts for Image-Guided
Object Movement

Von der Fakultät für Maschinenbau
der Gottfried Wilhelm Leibniz Universität Hannover
zur Erlangung des akademischen Grades
Doktor-Ingenieur
genehmigte Dissertation
von

M.Eng Manusak Janthong
geboren am 02.03.1973 in Kanchanaburi, Thailand

2006

1. Referent: Prof. Dr.-Ing. E. Reithmeier
2. Referent: Prof. Dr.-Ing. L. Overmeyer
Vorsitz: Prof. Dr.-Ing. G. Poll

Tag der Promotion: 17.07.2006

Abstract

3D inverted pendulum at IMR was constructed by [Bro06] in order to study the stabilization with visual feedback for the patient table of the radiotherapy. This research is a further work from [Bro06] so as to implement the various control schemes for controlling 3D inverted pendulum with helping a CMOS camera.

In this research the camera calibration, which differs with [Bro06], is used to establish a relationship between 2D image- and 3D world coordinates of the pendulum. The pin-hole model is used to be the camera model. To determinate the unknown parameters of the camera model, the non-linear least squares are used to estimate these parameters.

Lagrange's theory is utilized to derive the dynamics of 3D inverted pendulum, including some parameters such as the inclination angle of the camera and xy -table.

In the control of 3D inverted pendulum two problems is defined such as (1) regulation problem (2) tracking problem. The aim of the regulation problem is to stabilize the pendulum and maintain the cart at the middle of the xy -table and the other is to stabilize the pendulum while the cart is tracking a circle path. The control techniques for the regulation problem are PID, state feedback, model reference adaptive control (MRAC) using full state feedback and non-linear control. In case of the tracking problem the control techniques are state feedback, robust tracking control, MRAC using full state feedback and non-linear control plus MRAC for output tracking.

The experimental results of both two problems are compared to the corresponding numerical simulation results and the performance of each controller is illustrated.

Keywords: control engineering, 3D inverted pendulum, visual feedback

Kurzfassung

Das inverse 3D-Pendel wurde am IMR [Bro06] konstruiert, um die Positionierung eines Patienten während der Strahlentherapie mit Bildrückführung zu untersuchen. Die Arbeit dient weiter dazu verschiedene Regelkonzepten zur Regelung eines inversen 3D-Pendels mit einer CMOS Kamera zu erforschen.

Die Kamerakalibrierung dieser Arbeit, die sich von [Bro06] unterscheidet, wird verwendet, um ein Beziehung zwischen 2D Bild- und 3D Welt-Koordinaten des Pendels zu erhalten. Für die Kalibrierung wird das Pin-Hole Modell benutzt und mit Hilfe der Methode der kleinsten Fehlerquadrate die unbekannt Parameter geschätzt.

Zur Bestimmung der Dynamik des Pendels, auch unter Berücksichtigung von Kippwinkeln der Kamera und des Tisches, wird das Lagrangesche Theorem verwendet.

Im ersten Schritt ist das Ziel der Regelung des inversen 3D-Pendels, das Pendel in der stabilen aufrechten Lage an einer Position zu halten. Im zweiten Schritt soll sich das Pendel stabil auf einer Bahn (z. B. auf einem Kreis) bewegen. Für die Stabilisierung in der aufrechten Lage werden PID-Regler, Zustandsregler, MRAC-Regler mit Vollzustandsrückführung und nicht-linearer Regler verwendet. Für die Bahnregelung auf dem Kreis werden Zustandsregler, MRAC-Regler mit Vollzustandsrückführung und nichtlineare Regler einschließlich MRAC-Regler für Output Tracking benutzt.

Für beide Aufgabenstellungen werden die Simulationsergebnisse mit den experimentellen Resultaten verglichen und diskutiert.

Schlagwörter: Regelungstechnik, inverses 3D-Pendel, Bildrückführung

Acknowledgments

I would first like to thank my advisor Prof. Dr.-Ing. E. Reithmeier for giving me the opportunity to contribute to my project, advice, insight, and guidance along the way. I am grateful for the opportunity of working with him, for the possibilities of visiting several colleagues, and for making me put things in the right perspective. I'd like to thank all people in Institut für Mess- und Regelungstechnik (IMR), Leibniz Universität Hannover who have provided me with their advice. I'd also like to thank Rajamangala University of Technology Thunyaburi, Thailand for financial support throughout my study.

I am grateful to the members of my promotion committee for thorough reading my manuscript: Prof. Dr.-Ing. L. Overmeyer, Institut für Transport- und Automatisierungstechnik (ITA) and Prof. Dr.-Ing. G. Poll, Institut für Maschinenelemente, Konstruktionstechnik und Tribologie (IMKT).

Finally, I greatly thank my beloved family in Thailand, all my friends for always being there when I needed them and all Thai people in Hannover whose name I did not mention explicitly. A special word of thanks goes to my wife, Patcharin Janthong, for all her love, moral support and help.

Hannover, in July 2006

Manusak Janthong

Table of Contents

Abstract	I
Kurzfassung	II
Acknowledgments	III
Table of Contents	IV
List of Figures	VI
List of Tables	IX
1 Introduction	1
1.1 State of the Art.....	1
1.2 Research Objective and Outline of the Thesis.....	8
2 Preliminary Works at IMR	10
3 System Modeling	12
3.1 Lagrange's Equations.....	12
3.2 Modeling of Inverted Pendulum.....	13
3.2.1 Dynamics of 2D Inverted Pendulum.....	13
3.2.2 Dynamics of 3D Inverted Pendulum.....	15
3.3 Modeling of Motor and Cart.....	22
4 Control Design and Simulation	23
4.1 Background Control Theory.....	23
4.1.1 Non-linear Control.....	23

4.1.2	Model Reference Adaptive Control (MRAC).....	26
4.1.2.1	MRAC using Full State Feedback.....	27
4.1.2.2	MRAC for Output Tracking.....	29
4.1.3	Robust Tracking Control.....	30
4.2	Control Design.....	32
4.2.1	Regulation Problem.....	32
4.2.1.1	PID Controller.....	34
4.2.1.2	State Feedback.....	34
4.2.1.3	Non-linear Controller.....	36
4.2.1.4	MRAC using Full State Feedback.....	40
4.2.1.5	Simulation Results.....	44
4.2.2	Tracking Problem.....	48
4.2.2.1	State Feedback.....	48
4.2.2.2	MRAC using Full State Feedback.....	49
4.2.2.3	Robust Tracking Controller.....	52
4.2.2.4	Non-linear Controller & MRAC for Output Tracking.....	54
4.2.2.5	Simulation Results.....	57
5	Experiments and Results	70
5.1	Camera Calibration.....	70
5.2	Control Experiments and Results.....	75
5.2.1	Regulation Problem.....	75
5.2.2	Tracking Problem.....	79
6	Conclusion and Further Development	91
6.1	Conclusion.....	91
6.2	Further Development.....	92
	Bibliography	94
	Lebenslauf	100

List of Figures

1.1	Single link inverted pendulum-cart system.....	2
1.2	Vision feedback diagram to stabilize a pendulum.....	3
1.3	Double inverted pendulum-cart system	4
1.4	Tribble inverted pendulum-cart system	5
1.5	Rotary inverted pendulum or Furuta pendulum.....	5
1.6	Laboratory setup for Furuta pendulum.....	6
1.7	2DOF inverted pendulum.....	7
1.8	Balancing a pendulum with planar robot.....	8
2.1	Radiotherapy at Alfried Krupp hospital.....	10
2.2	Actual experiment system of 3D inverted pendulum at IMR.....	11
3.1	Coordinate description of 2D inverted pendulum.....	13
3.2	Coordinate description of 3D inverted pendulum.....	15
4.1	Structure of approximate feedback linearization control.....	24
4.2	Structure of MRAC using full state feedback.....	27
4.3	Structure of MRAC for output tracking	29
4.4	Structure of robust tracking control.....	30
4.5	Block diagram of pendulum, motor and cart.....	32
4.6	PID controller and compensator for regulation problem.....	34
4.7	State feedback and estimator for regulation problem.....	35
4.8	Projection of the pendulum onto xz - and yz -planes.....	36
4.9	Approximate feedback linearization for regulation problem.....	37
4.10	MRAC using full state feedback for regulation problem.....	40
4.11	Comparison of the simulation responses of the inclination angle ψ for regulation problem.....	45
4.12	Comparison of the simulation responses of the inclination angle ϑ for regulation problem.....	45
4.13	Comparison of the simulation responses of the cart position x for regulation problem.....	46

4.14 Comparison of the simulation responses of the cart position y for regulation problem.....	46
4.15 Comparison of the simulation responses of the control signal along x -axis for regulation problem.....	47
4.16 Comparison of the simulation responses of the control signal along y -axis for regulation problem.....	47
4.17 State feedback for tracking problem.....	48
4.18 MRAC using full state feedback for tracking problem.....	51
4.19 Robust tracking control for tracking problem.....	53
4.20 Nonlinear control plus MRAC for output tracking for tracking problem.....	56
4.21 Comparison of the simulation responses of the inclination angle ψ for constant angular velocity case of tracking problem.....	59
4.22 Comparison of the simulation responses of the inclination angle ϑ for constant angular velocity case of tracking problem.....	59
4.23 Comparison of the simulation responses of the cart position x for constant angular velocity case of tracking problem.....	60
4.24 Comparison of the simulation responses of the cart position y for constant angular velocity case of tracking problem.....	61
4.25 Comparison of the simulation responses of the cart position on xy -plane for constant angular velocity case of tracking problem.....	62
4.26 Comparison of the simulation responses of the control signal along x -axis for constant angular velocity case of tracking problem.....	63
4.27 Comparison of the simulation responses of the control signal along y -axis for constant angular velocity case of tracking problem.....	63
4.28 Comparison of the simulation responses of the inclination angle ψ for inconstant angular velocity case of tracking problem.....	65
4.29 Comparison of the simulation responses of the inclination angle ϑ for inconstant angular velocity case of tracking problem.....	65
4.30 Comparison of the simulation responses of the cart position x for inconstant angular velocity case of tracking problem.....	66
4.31 Comparison of the simulation responses of the cart position y for inconstant angular velocity case of tracking problem.....	67
4.32 Comparison of the simulation responses of the cart position on xy -plane for inconstant angular velocity case of tracking problem.....	68
4.33 Comparison of the simulation responses of the control signal along x -axis for inconstant angular velocity case of tracking problem.....	69
4.34 Comparison of the simulation responses of the control signal along y -axis for inconstant angular velocity case of tracking problem.....	69
5.1 Camera calibration.....	71
5.2 A planar model object or pattern.....	72
5.3 Description of the coordinates U and V in camera calibration process.....	73
5.4 Comparison of the experimental responses of the inclination angle ψ for regulation problem.....	76
5.5 Comparison of the experimental responses of the inclination angle ϑ for regulation problem.....	76

5.6 Comparison of the experimental responses of the cart position x for regulation problem.....	77
5.7 Comparison of the experimental responses of the cart position y for regulation problem.....	77
5.8 Comparison of the experimental responses of the control signal along x -axis for regulation problem.....	78
5.9 Comparison of the experimental responses of the control signal along y -axis for regulation problem.....	78
5.10 Comparison of the experimental responses of the inclination angle ψ for constant angular velocity case of tracking problem.....	80
5.11 Comparison of the experimental responses of the inclination angle ϑ for constant angular velocity case of tracking problem.....	80
5.12 Comparison of the experimental responses of the cart position x for constant angular velocity case of tracking problem.....	81
5.13 Comparison of the experimental responses of the cart position y for constant angular velocity case of tracking problem.....	82
5.14 Comparison of the experimental responses of the cart position on xy -plane for constant angular velocity case of tracking problem.....	83
5.15 Comparison of the experimental response of the control signal along x -axis for constant angular velocity case of tracking problem.....	84
5.16 Comparison of the experimental responses of the control signal along y -axis for constant angular velocity case of tracking problem.....	84
5.17 Comparison of the experimental responses of the inclination angle ψ for inconstant angular velocity case of tracking problem.....	86
5.18 Comparison of the experimental responses of the inclination angle ϑ for inconstant angular velocity case of tracking problem.....	86
5.19 Comparison of the experimental responses of the cart position x for inconstant angular velocity case of tracking problem.....	87
5.20 Comparison of the experimental responses of the cart position y for inconstant angular velocity case of tracking problem.....	88
5.21 Comparison of the experimental responses of the cart position on xy -plane for inconstant angular velocity case of tracking problem.....	89
5.22 Comparison of the experimental responses of the control signal along x -axis for inconstant angular velocity case of tracking problem.....	90
5.23 Comparison of the experimental responses of the control signal along y -axis for inconstant angular velocity case of tracking problem.....	90

List of Tables

4.1	Reference inputs along x - and y -axes.....	57
5.1	Comparison of the measured and estimated results of the pattern.....	74

To my Parents, Jaroon and Somjit Janthong

To my brother, Purilap Janthong

To my sister, Nuntawan Janthong

To my loving wife, Patcharin Janthong

Chapter 1

Introduction

This chapter describes the physical behaviours of the inverted pendulum including the literature survey of the inverted pendulum about the controllers used to stabilize and swing-up in Chapter 1.1. The objective and outline of this research are detailed in Chapter 1.2.

1.1 State of the Art

Balancing of an inverted pendulum is a classic problem in the field of control which considerably interests in many fields such as mechanics, physics, applied mathematics and etc., because the inverted pendulum system exhibits non-linear, unstable and non-minimum phase dynamics. This system inherently has two equilibriums, one of which is stable while the other is unstable. The stable equilibrium corresponds to a state in which the pendulum is pointing downwards. If the pendulum is released from any position other than precisely straight up, then it falls and oscillates about the stable equilibrium with decreasing amplitude until it comes to rest. Therefore, the stable equilibrium requires no control input to be achieved this position and is uninteresting from a control perspective. The unstable equilibrium corresponds to a state in which the pendulum points strictly upwards and requires a control input to maintain this position. The basic control objective of the inverted pendulum problem is to maintain the unstable equilibrium position when the pendulum initially starts in an upright position.

For this section the main aim is a brief review of the literature on control schemes for the various kinds of the inverted pendulum as following.

Planar inverted pendulum

The planar inverted pendulum mounted on the cart is a basic control problem of the inverted pendulum and has several types such as single pendulum, double pendulum and triple pendulum. The control problem of the pendulum can be divided into two problems such as stabilizing and swing-up. Both were studied with various control theory as following

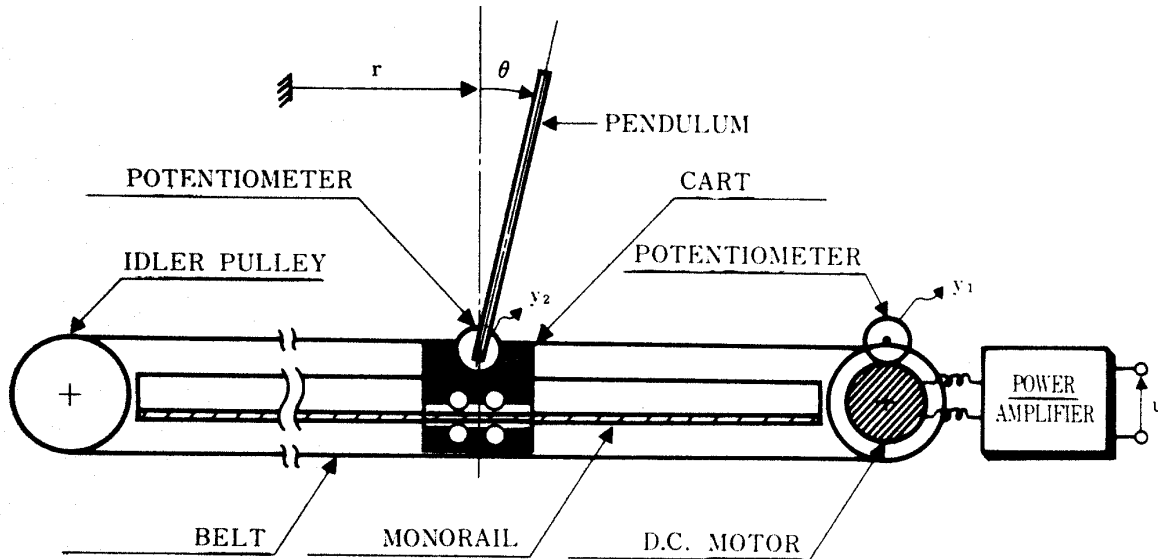


Figure 1.1 Single link inverted pendulum-cart system [Mor76]

For single inverted pendulum, a single link pendulum mounted on the cart and the control system [Mor76] was designed for stabilizing and swing-up problems of the pendulum. There were two types of controllers: (1) a feedforward controller that is to swing-up the pendulum from its pending position to upright position; (2) a linear feedback controller with a full state observer base on LQR in order to keep the pendulum on the cart in the upright position.

Neural network control is presented in [Ish91] [Wil91]. A neural network controller with the back propagation algorithm is designed by [Ish91] for the inverted pendulum. [Ish91] had applied their controller to stabilize the actual inverted pendulum and succeeded to stabilize it after 164 trials for learning. [Wil91] proposed a learning architecture for training a neural network controller to provide the appropriate force to balance the inverted pendulum. The training process is performed using the back propagation algorithm. Their system uses two neural networks, one for the identification and the other for the controlling. The identification network learns to identify the system dynamics while the controlling network simultaneously changes its characteristics using the result of the identification network to control the inverted pendulum.

The grey prediction of the first-order model combined with a PD controller is proposed by [Hua00] to control the inverted pendulum and the parameters of the grey model are estimated by using a least-squares scheme. Their control object is to swing up the pendulum from a stable position to an unstable position and control the position of the cart to the origin of the track.

[Ren96] used the approximate linearization controller to design according to the Guzella and Isidori algorithm [Guz93]. This algorithm is tried to solve the quadratic linearization problem to find a non-linear transformation and a state feedback control law. This control law is applied to the inverted pendulum for test bench with real time software.

Actually the inclination angle of the pendulum is measured by an encoder. But there were a number of researchers, who used the vision feedback from the camera to compute the inclination angle of the inverted pendulum [Mag98] [Wen00]. To determine of the inclination angle of the pendulum [Mag98], the colour of the pendulum is specified to be black and the background is white and two horizontal lines are drawn in the image information from the camera and then the position of the greatest dark/bright transition is found. This position is represented as the column number. As the distance between two horizontal line is known. Therefore, the inclination angle can be determined by using a simple trigonometric function. [Mag98] developed the fuzzy-logic controller to control the experimental inverted pendulum with conventional triangular membership functions to fuzzify the data measured by the vision system. [Wen00] used the camera for determining the cart position and inclination angle of the pendulum using pattern matching algorithm and developed LQR controller with full state observer to stabilize the pendulum. Their experiment is based on the graphical language LabVIEW.

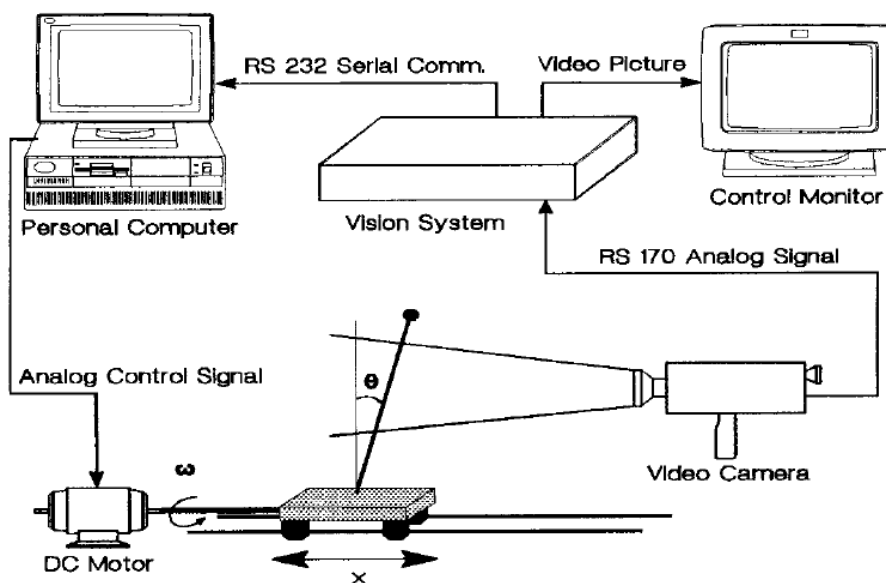


Figure 1.2 Vision feedback diagram to stabilize a pendulum [Mag98]

For double inverted pendulum, [Hen04] studied the swing-up control of the pendulum. They developed the controllers for swing-up and stabilizing in three steps: (1) to swing-up the first pendulum using energy control method (2) to swing-up the second pendulum using energy control method while stabilizing the first pendulum using sliding mode control method (3) stabilizing both of the pendulums in upright position using sliding mode control method.

[Fuj00] proposed a self-tuning controller for stabilizing the double inverted pendulum by combining two controllers together such as PID and Neural networks controller. They used neural networks to adjust the gain parameters of PID controller, in which the minimum cost function for tuning is the squared error between the actual output and the desired values. And they called this controller as the self-tuning neuro-PID.

Generally the control of the inverted pendulum, the friction forces between the cart and rail are neglected. However there was a researcher group [Fan01] who investigates the double inverted pendulum system which the friction forces cannot be cancelled and cause large limit cycles. The friction compensator term based on the modified first-order Dahl model is added into the feedback gain that is designed using linear-quadratic regulator from the linearized system for stabilizing the pendulum.

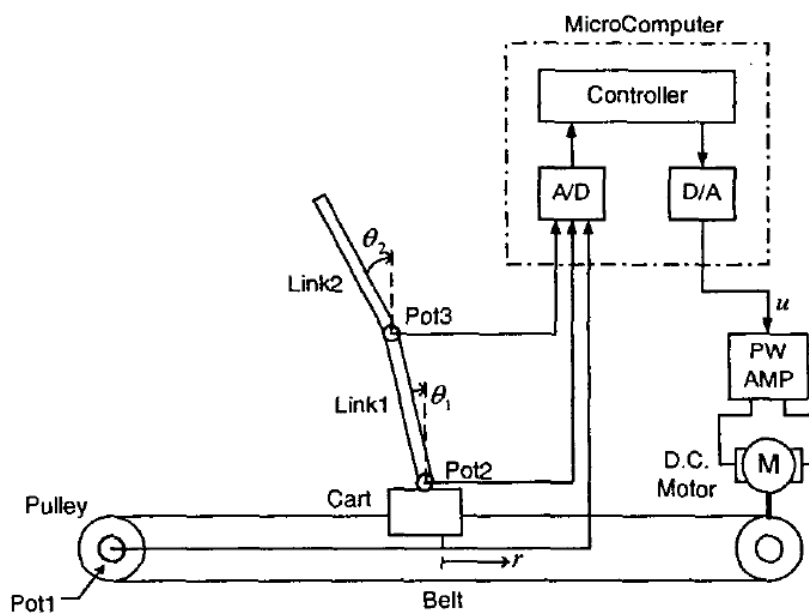


Figure 1.3 Double inverted pendulum-cart system [Fan01]

For triple inverted pendulum, [Elt98] constructed the dynamic model of a triple link inverted pendulum including non-linear friction terms and proposed a simple linear transformation to obtain the set of non-linear equations in the Denavit-Hartenberg coordinate system. They designed a non-linear numerical optimization technique. First they found the feedback gain matrix by minimizing the time-multiplied quadratic performance index. The feedback gain matrix is used as the starting value for the non-linear numerical optimization technique to solve a optimize set of the feedback gain matrix.

[Med97] designed a robust controller for a triple inverted pendulum based on a discrete-time linear quadratic regulator theory via a robust reduce order estimator to stabilize the pendulum.

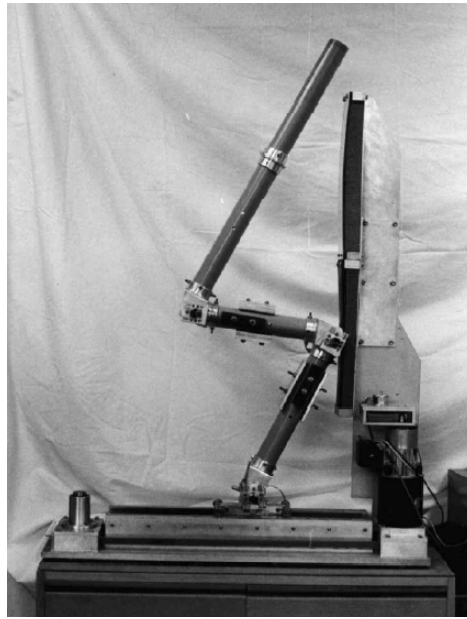


Figure 1.4 Triple inverted pendulum-cart system [Med97]

Rotary Inverted Pendulum

The Rotary inverted pendulum, also known as the Furuta pendulum, is one of the challenging type of the pendulum. K. Furuta from the Tokyo Institute of Technology first developed this inverted pendulum. The experiment is called the TITech pendulum. This type has the pendulum attached to a rotating arm instead of a cart moving on a straight line as shown in Figure 1.5. The objective is to swing up the pendulum and make it stable at the upright position with two different but appealing control problems such as swing up and stabilizing. The various control algorithms have been proposed for swing up and stabilize control problems as following.

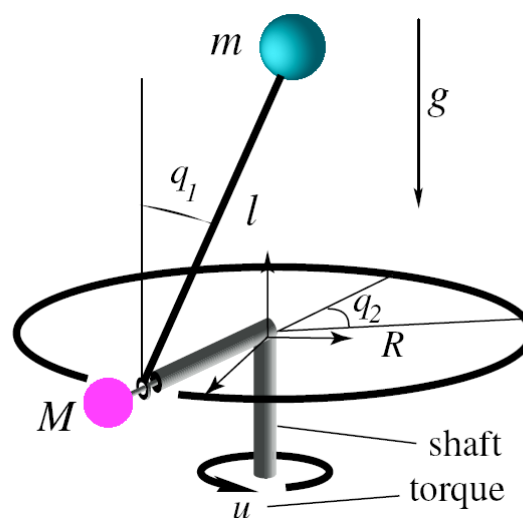


Figure 1.5 Rotary inverted pendulum or Furuta pendulum [Nai02]

The sliding mode control was considered in [Gro96]. For sliding surface design, the position of the tip of the rotating arm and the inclination angle of the pendulum are defined to be a function of the angle of the rotating arm. The simulations are tested for two cases of stabilizing at the inclination angle of the pendulum: (1) 45 degrees, (2) 0 degrees. The former case, it is not stable but the latter one, it converges to its desired value after the rotating arm turns over three revolutions.

The non-linear controller was developed in [Sug98] [Nai02] for stabilizing the Furuta pendulum. [Sug98] used the approximate linearization technique [Kre84] by transforming the non-linear system of the Furuta pendulum into the Brunowsky canonical form, the feedback gain matrix of the linearized system is then solved by LQR. The proposed controller can stabilize the system when the inclination angle of the pendulum is less than 45 degrees (No load) and 41 degrees (load 0.038 kg on the top of the pendulum), while the linear controller without non-linear compensation works only when the inclination angle of the pendulum is less than 35 degrees (No load) and 15 degrees (load 0.038 [kg] on the top of the pendulum). [Nai02] assumed the Furuta pendulum system looks like the inverted pendulum on the cart that is constrained to move in a circle rather than along a line. Therefore, they derived a non-linear control law for stabilizing the Furuta pendulum and transforming the Furuta pendulum into the planar pendulum on the cart plus a gyroscopic force (normal form) that satisfies the simplified matching conditions.



Figure 1.6 Laboratory setup for Furuta pendulum [Wan04]

Minimum time swing up problem was solved in [Xu01] and [Wan04]. The time optimal control of a non-linear system for the Furuta pendulum with Pontryagin's Maximum principle is proposed by [Xu01]. Their control is divided into three steps. Firstly, feedforward time optimal control is used to swing up to the neighbourhood of the upright position from the pending position and then, LQR is used to stabilize the pendulum at the upright position using the linearized model of the pendulum to find the feedback gain matrix. Finally, the switching

algorithm is specified as: if the absolute of the inclination angle of the pendulum is less than 0.5 radius, the control stage is changed from the swing-up control to the stabilizing control. [Wan04] designed PID controller for swing-up control plus an impulsive or pulse-step feedforward that is to be tuned through several iterative tuning experiments to achieve minimum time swing up. The energy of the system is used to be the switching algorithm.

2DOF Inverted Pendulum

In the recent years a new problem of the inverted pendulum occurs, that is 2DOF inverted pendulum (some paper call spatial inverted pendulum [Chi90]) shown in Figure 1.7. It has few researchers who propose its stabilizing and swing-up controllers as following:

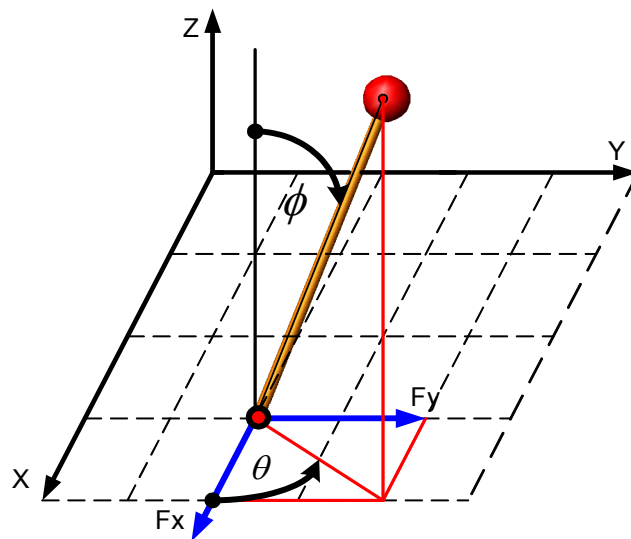


Figure 1.7 2DOF inverted pendulum

Pole placement technique is designed in [Chi90]. [Chi90] simulated 2DOF inverted pendulum mounted on the top of the cart by using universal joint, and the cart can translate in x - and y -directions. This inverted pendulum is called spatial inverted cart/pendulum. [Chi90] presented a full state feedback controller design for a state-space linear model. Taylor series and dropping second and higher order term are used to linearize the non-linear dynamic equations of motion of system about upright position. The state feedback controller based on pole placement technique is used to achieve the desired eigenvalues for the closed loop system.

The balancing act of 2DOF inverted pendulum with a robot is presented in [Spr98], [Chu99] and [Yam99]. [Spr98] used a 2DOF SCARA robot to stabilize 2DOF inverted pendulum. The pendulum is projected onto xz - and yz -planes of the inertial coordinate system. These projections are treated independently from each other and controlled individually by a state-space controller with the feedback gain matrix that is calculated according to the linear-quadratic regulator (LQR) design method along x - and y -axes, respectively. The contactless sensor system is implemented to measure the inclination angle of the pendulum. This measurement system consists of a small magnet, placed at the bottom of the pendulum to generate a static magnetic field, and two Hall-effect sensors, placed inside the end effector of the robot to give a signal proportional to the inclination angle. [Chu99] addressed the problem

of stabilities a 2DOF inverted pendulum as [Spr98] but they used a 3DOF planar direct-drive robot instead of a 2DOF SCARA robot to balance the pendulum. [Yam99] used 2 PUMA 560-like robots to hand over the stabilized inverted pendulum placed on a plate using a CCD camera for measuring the position of the pendulum. The force/position controllers are implemented to achieve strict force control. In handing over the pendulum the vertical height and the posture of the plate must be kept constant.

[Bro06] constructed 3D inverted pendulum on the cart at IMR and implemented a CMOS camera for calculating the position of the ball. To calculate the position of the ball, [Bro06] used the scanline for circular object algorithm. The angles of the pendulum are obtained by using the position of the cart and ball. [Bro06] proposed a PID controller for stabilizing 3D inverted pendulum.

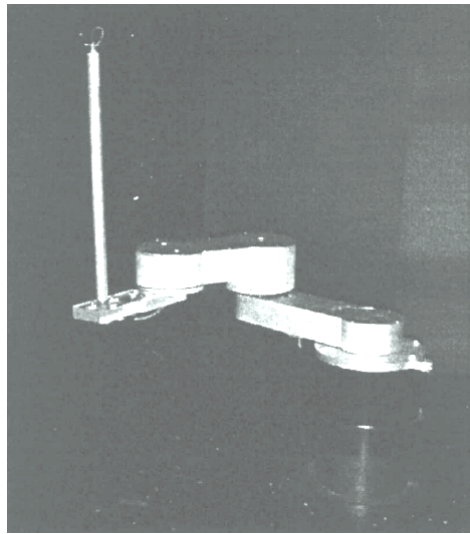


Figure 1.8 Balancing a pendulum with planar robot [Chu99]

1.2 Research Objective and Outline of the Thesis

This research is a further work from [Bro06]. The objective of this research is to design the various control algorithms to control 3D inverted pendulum with 2 control problems such as regulation and tracking. In the regulation problem the control system will be designed in order to maintain the position of the cart at the middle of the table while the pendulum is being balanced in upright position. For the tracking problem the position of the cart tracks a path while the pendulum is being stabilized. The path used in this research is specified as a circle.

This thesis is organized as follows:

Chapter 1 describes a brief state of the art, the previous works of the inverted pendulum, the objective and outline of the research.

Chapter 2 reviews the preliminary works at Institut für Mess- u. Regelungstechnik (IMR)

Chapter 3 explains the mathematical model of 2D & 3D inverted pendulum with the inclination angle of the table and camera using the Lagrange's equations.

Chapter 4 reviews the control algorithms used in this research. Various regulator and tracker controllers are designed in order to control 3D inverted pendulum, including their simulations.

Chapter 5 describes the calibration of the camera and the experimental results of the control algorithms designed in Chapter 4 are illustrated.

In Chapter 6, the conclusion and further developments are given.

Chapter 2

Preliminary Works at IMR

At Institut für Mess- u. Regelungstechnik (IMR), Leibniz Universität Hannover a pendulum structure called “3D Inverted Pendulum” has been designed. 3D inverted pendulum was constructed so as to simulate a new idea for an application of the stabilization with visual feedback. It is the stabilization of an image-guided automatic adjustable patient table of the radiotherapy. The regulation applies to the exact positioning of the center of the tumour e.g. in the head area of the patient in the reference path of rays. The image processing is used to compute the position of the tumour through the face area of the patient calculated and displayed geometrically.



Figure 2.1 Radiotherapy at Alfried Krupp hospital

In the previous work at IMR [Bro06] had designed and constructed 3D inverted pendulum system in Figure 2.2 for the simulation of the patient table in the radiotherapy. The main structure of 3D inverted pendulum consists of a xy -table and pendulum with a ball. The xy -table and the ball are referred as the table and head of the patient respectively. And a CMOS camera is used for measuring the position of the ball at the end of the pendulum. [Bro06] had implemented the tools for controlling the pendulum on xPC-Target system of MATLAB. In that research, the dynamic equations of 3D inverted pendulum is derived from Newton-Euler theory with the spin torque of the pendulum. And the dynamics of the motor and cart are identified with CMOS camera as a sensor. A first-order system is defined as a model of the motor and cart. A step response experiment is done with a bias of 1 Voltage for the identification of the unknown parameter of the model. Thus the step input is 1-10 Voltage. [Bro06] designed PID controller for the stabilization of 3D inverted pendulum.

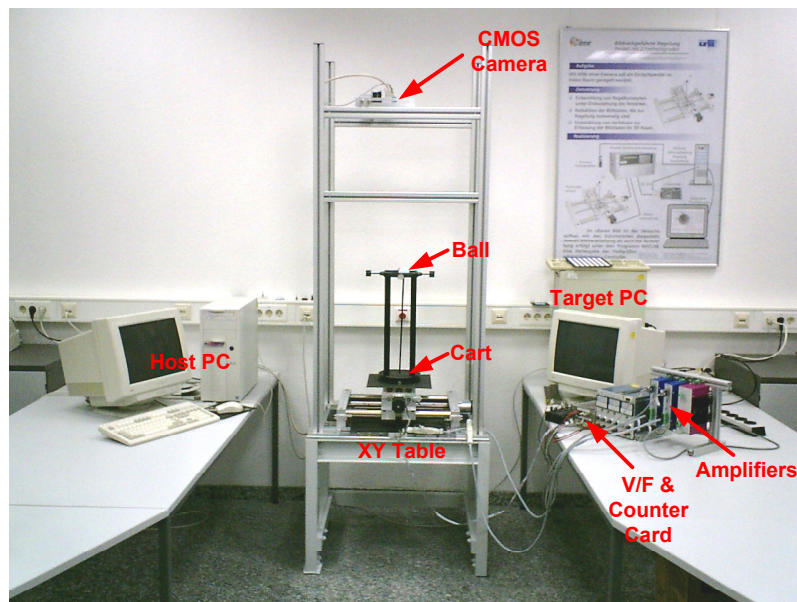


Figure 2.2 Actual experiment system of 3D inverted pendulum at IMR

Chapter 3

System Modeling

3D inverted pendulum is a special structure since it has two degrees of freedom of rotary motion of the inverted pendulum and two degrees of freedom of the translate motion of the cart. The dynamic equations of 3D inverted pendulum and cart system had been derived in the previous work [Bro06] which considered also the spin torque of the pendulum in the system. But in this research the spin torque of the pendulum will be eliminated but the inclination angles of the camera and xy -table will be considered in the system and Lagrange's equation, which is reviewed in Chapter 3.1, is used to derive the dynamic equations of 3D inverted pendulum in Chapter 3.2 and the system of the cart and motor is explained in Chapter 3.3.

3.1 Lagrange's Equations

The Lagrange's equations of motion are the method used to formulate the dynamic model of a mechanical system in term of 2 forms of energies contained in the mechanical system as: the kinetic energy and the potential energy. The Lagrange's equations in the Lagrangian function form are then given by

$$\frac{d}{dt} \left(\frac{\partial L}{\partial \dot{q}_i} \right) - \frac{\partial L}{\partial q_i} = Q_i \quad (3.1)$$

where L , q_i and Q_i are Lagrangian function, the generalized coordinates or the state variables and the generalized forces respectively. And Lagrangian function L is the difference between the kinetic and potential energy of the system as given by

$$L(q, \dot{q}) = T(q, \dot{q}) - V(q) \quad (3.2)$$

where T and V are the system's kinetic energy and the system's potential energy respectively. In addition, the generalized force Q_i contains all the given forces in the system acting along the i -th generalized coordinate. The given forces may be of two categories:

1. External forces, including the force due to gravity.
2. Forces due to friction.

The generalized force Q_i is

$$Q_i = \sum_{j=1}^N \bar{F}_j \frac{\partial \bar{r}_j}{\partial q_i} \quad (3.3)$$

where N , \bar{F} and \bar{r} are the number of the particle or rigid body in the system, the given force vector on the particle or rigid body and the position vector of the particle or rigid body respectively.

3.2 Modeling of Inverted Pendulum

3.2.1 Dynamics of 2D Inverted Pendulum

The dynamic equation of 2D inverted pendulum can be formulated from Figure 3.1. This figure also shows the parameters, which influence to the system such as the angles α and θ as the inclination angle of the table and camera respectively and they are constant but unknown. The generalized coordinates of 2D inverted pendulum are the inclination angle ψ of the inverted pendulum and the distance x of the cart along X' -axis, respectively.

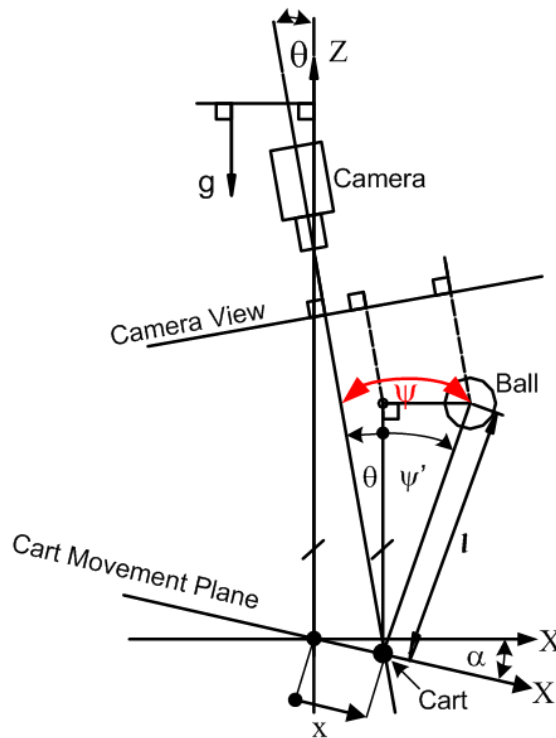


Figure 3.1 Coordinate description of 2D inverted pendulum

Consider the ball, the position vector of the ball \vec{r}_{M_B} can be given by

$$\vec{r}_{M_B} = (x \cos(\alpha) + l \sin(\psi - \theta))\vec{i} + (-x \sin(\alpha) + l \cos(\psi - \theta))\vec{k}. \quad (3.4)$$

where \vec{i} and \vec{k} are the unit vectors parallel to the X - and Z -axes and l is the length of the pendulum [m].

Differentiation of the position vector of the ball with respect to time for determining the velocity vector of the ball.

$$\dot{\vec{r}}_{M_B} = \left(\dot{x} \cos(\alpha) + l \cos(\psi - \theta) \dot{\psi} \right) \vec{i} + \left(-\dot{x} \sin(\alpha) + l \sin(\psi - \theta) \dot{\psi} \right) \vec{k} \quad (3.5)$$

In this case, the moment of inertia of the ball and rod about their center of gravity and the mass of the rod are small. Therefore, the rod mass and moment of inertia of the ball and rod can be neglected. The kinetic energy of 2D inverted pendulum can be obtained as follows

$$\begin{aligned} T &= \frac{1}{2} M_B \left(\dot{r}_{M_B} \right)^2 \\ T &= \frac{1}{2} M_B \left(\dot{x}^2 + l^2 \dot{\psi}^2 + 2l \cos(\alpha) \cos(\psi - \theta) \dot{x} \dot{\psi} - 2l \sin(\alpha) \sin(\psi - \theta) \dot{x} \dot{\psi} \right) \end{aligned} \quad (3.6)$$

where M_B is the mass of the ball [kg].

The potential energy of the inverted pendulum is

$$V = M_B g (l \cos(\psi - \theta) - x \sin(\alpha)). \quad (3.7)$$

Referring to Equation (3.2), the Lagrangian function L is written as follows

$$\begin{aligned} L &= \frac{1}{2} M_B \dot{x}^2 + \frac{1}{2} M_B l^2 \dot{\psi}^2 + M_B l \cos(\alpha) \cos(\psi - \theta) \dot{x} \dot{\psi} - M_B l \sin(\alpha) \sin(\psi - \theta) \dot{x} \dot{\psi} \\ &\quad - M_B g l \cos(\psi - \theta) + M_B g \sin(\alpha) x. \end{aligned} \quad (3.8)$$

$\frac{\partial L}{\partial q_i}$ and $\frac{d}{dt} \left(\frac{\partial L}{\partial \dot{q}_i} \right)$ terms in Equation (3.1) can be determined as follows:

$$\frac{\partial L}{\partial \psi} = -M_B l \cos(\alpha) \sin(\psi - \theta) \dot{x} \dot{\psi} - M_B l \sin(\alpha) \cos(\psi - \theta) \dot{x} \dot{\psi} + M_B g l \sin(\psi - \theta), \quad (3.9)$$

$$\frac{\partial L}{\partial \dot{\psi}} = M_B l^2 \dot{\psi} + M_B l \cos(\alpha) \cos(\psi - \theta) \dot{x} - M_B l \sin(\alpha) \sin(\psi - \theta) \dot{x}, \quad (3.10)$$

For the dynamic equation of motion of 3D inverted pendulum will be formulated from Figure 3.2. The parameters, which influence to the system such as the angle α and β as the inclination angle of the table and the angle θ and γ as the inclination angle of the camera respectively, are shown in this figure. The generalized coordinates of 3D inverted pendulum are the inclination angles ψ and ϑ of the inverted pendulum and the distances x and y of the cart along X_1 - and Y_1 -axes, respectively.

Figure 3.2 shows two frames. One is a fixed reference frame, Frame 0, or gravity frame with its origin O_0 and other is a frame of the cart movement, Frame 1, with its origin O_1 . Thus, their origins of both frames coincide but their orientations are different. Let \vec{P}_C be a position vector of the cart and \vec{P}_B be a position vector of the ball. To formulate the dynamics of 3D inverted pendulum, it's necessary to find the position vector of the ball \vec{P}_B with respect to Frame 0. It can be obtained as follows

$${}_{(0)}\vec{P}_B = {}_{(0)}\vec{P}_C + {}_{(0)}\vec{P}_{CB} \quad (3.15)$$

where ${}_{(0)}\vec{P}_C$ is the position vector of the cart with respect to Frame 0 and ${}_{(0)}\vec{P}_{CB}$ is the position vector between the cart and ball with respect to Frame 0.

The position vector of the cart \vec{P}_C with respect to Frame 0 can be determined as follows

$${}_{(0)}\vec{P}_C = {}^{01}R {}_{(1)}\vec{P}_C \quad (3.16)$$

where ${}_{(1)}\vec{P}_C$ is a position vector of the cart with respect to Frame 1 and ${}^{01}R$ is a rotation matrix of the position vector in Frame 1 into the position vector in Frame 0 and it is given by

$$\begin{aligned} {}^{01}R &= \text{Rotate}(Y_0, \alpha) \text{Rotate}(X_1, \beta) \\ {}^{01}R &= \begin{bmatrix} \cos(\alpha) & 0 & \sin(\alpha) \\ 0 & 1 & 0 \\ -\sin(\alpha) & 0 & \cos(\alpha) \end{bmatrix} \begin{bmatrix} 1 & 0 & 0 \\ 0 & \cos(\beta) & -\sin(\beta) \\ 0 & \sin(\beta) & \cos(\beta) \end{bmatrix} \\ {}^{01}R &= \begin{bmatrix} \cos(\alpha) & \sin(\alpha)\sin(\beta) & \sin(\alpha)\cos(\beta) \\ 0 & \cos(\beta) & -\sin(\beta) \\ -\sin(\alpha) & \cos(\alpha)\sin(\beta) & \cos(\alpha) \end{bmatrix}. \end{aligned} \quad (3.17)$$

Since the cart move only on x_1y_1 -plane of Frame 1. Therefore, the position vector of the cart with respect to Frame 1 can be defined as ${}_{(1)}\vec{P}_C = [x, y, 0]^T$. Then ${}_{(0)}\vec{P}_C$ can be obtained as follows

$${}_{(0)}\bar{P}_C = \begin{bmatrix} x \cos(\alpha) + y \sin(\alpha) \sin(\beta) \\ y \cos(\beta) \\ -x \sin(\alpha) + y \cos(\alpha) \sin(\beta) \end{bmatrix}. \quad (3.18)$$

Consider ${}_{(0)}\bar{P}_{CB}$, it can be determined from 2 angles ψ and \mathcal{G} . With ψ is the sum of the inclination angle ψ' about y_1 -axis measured from z_0 -axis to the projection line of the inverted pendulum on x_0z_0 -plane and the inclination angle θ of the camera. And \mathcal{G} is the sum of the inclination angle \mathcal{G}' measured from the projection line of the pendulum on x_0z_0 -plane to the pendulum rod and the inclination angle γ of the camera. ${}_{(0)}\bar{P}_{CB}$ is obtained as follows

$${}_{(0)}\bar{P}_{CB} = \begin{bmatrix} l \cos(\mathcal{G} - \gamma) \sin(\psi - \theta) \\ l \sin(\mathcal{G} - \gamma) \\ l \cos(\mathcal{G} - \gamma) \cos(\psi - \theta) \end{bmatrix}. \quad (3.19)$$

Substitute Equations (3.18) and (3.19) into Equation (3.15). Then the position vector ${}_{(0)}\bar{P}_B$ of the ball with respect to Frame 0 can be obtained as follows:

$$\begin{aligned} {}_{(0)}\bar{P}_B &= \begin{bmatrix} x \cos(\alpha) + y \sin(\alpha) \sin(\beta) \\ y \cos(\beta) \\ -x \sin(\alpha) + y \cos(\alpha) \sin(\beta) \end{bmatrix} + \begin{bmatrix} l \cos(\mathcal{G} - \gamma) \sin(\psi - \theta) \\ l \sin(\mathcal{G} - \gamma) \\ l \cos(\mathcal{G} - \gamma) \cos(\psi - \theta) \end{bmatrix} \\ {}_{(0)}\bar{P}_B &= \begin{bmatrix} x \cos(\alpha) + y \sin(\alpha) \sin(\beta) + l \cos(\mathcal{G} - \gamma) \sin(\psi - \theta) \\ y \cos(\beta) + l \sin(\mathcal{G} - \gamma) \\ -x \sin(\alpha) + y \cos(\alpha) \sin(\beta) + l \cos(\mathcal{G} - \gamma) \cos(\psi - \theta) \end{bmatrix}. \end{aligned} \quad (3.20)$$

The mathematical model for the 3D inverted pendulum is derived from the Lagrange's equations of motion (3.1) with the generalized coordinates ψ , \mathcal{G} , x and y . And the mass of the rod and moment of inertia of the ball and rod can be eliminated as well as the 2D inverted pendulum. The system's kinetic energy can be obtained as follows:

$$T = \frac{1}{2} M_B \left({}_{(0)}\dot{\bar{P}}_B \right)^2 \quad (3.21)$$

$$T = \frac{1}{2} M_B \begin{pmatrix} \dot{x}^2 + \dot{y}^2 + l^2 \cos^2(\vartheta - \gamma) \dot{\psi}^2 + l^2 \dot{\vartheta}^2 - 2l \cos(\alpha) \sin(\psi - \theta) \dot{x} \dot{\vartheta} \\ + 2l \cos(\alpha) \cos(\psi - \theta) \cos(\vartheta - \gamma) \dot{x} \dot{\psi} + 2l \cos(\beta) \cos(\vartheta - \gamma) \dot{y} \dot{\vartheta} \\ - 2l \sin(\alpha) \sin(\beta) \sin(\psi - \theta) \sin(\vartheta - \gamma) \dot{y} \dot{\vartheta} \\ + 2l \cos(\psi - \theta) \cos(\vartheta - \gamma) \sin(\alpha) \sin(\beta) \dot{y} \dot{\psi} \\ + 2l \cos(\psi - \theta) \sin(\alpha) \sin(\vartheta - \gamma) \dot{x} \dot{\vartheta} \\ + 2l \cos(\vartheta - \gamma) \sin(\alpha) \sin(\psi - \theta) \dot{x} \dot{\psi} \\ - 2l \cos(\alpha) \cos(\psi - \theta) \sin(\beta) \sin(\vartheta - \gamma) \dot{y} \dot{\vartheta} \\ - 2l \cos(\alpha) \cos(\vartheta - \gamma) \sin(\beta) \sin(\psi - \theta) \dot{y} \dot{\psi} \end{pmatrix}. \quad (3.22)$$

The system's potential energy of 3D inverted pendulum is

$$V = M_B g (-x \sin(\alpha) + y \cos(\alpha) \sin(\beta) + l \cos(\psi - \theta) \cos(\vartheta - \gamma)). \quad (3.23)$$

Substitute Equations (3.22) and (3.23) into Equation (3.2). So the Lagrangian function is

$$L = \frac{1}{2} M_B \begin{pmatrix} \dot{x}^2 + \dot{y}^2 + l^2 \cos^2(\vartheta - \gamma) \dot{\psi}^2 + l^2 \dot{\vartheta}^2 - 2l \cos(\alpha) \sin(\psi - \theta) \dot{x} \dot{\vartheta} \\ + 2l \cos(\alpha) \cos(\psi - \theta) \cos(\vartheta - \gamma) \dot{x} \dot{\psi} + 2l \cos(\beta) \cos(\vartheta - \gamma) \dot{y} \dot{\vartheta} \\ + 2l \cos(\psi - \theta) \sin(\alpha) \sin(\vartheta - \gamma) \dot{x} \dot{\vartheta} \\ + 2l \cos(\vartheta - \gamma) \sin(\alpha) \sin(\psi - \theta) \dot{x} \dot{\psi} \\ - 2l \sin(\alpha) \sin(\beta) \sin(\psi - \theta) \sin(\vartheta - \gamma) \dot{y} \dot{\vartheta} \\ + 2l \cos(\psi - \theta) \cos(\vartheta - \gamma) \sin(\alpha) \sin(\beta) \dot{y} \dot{\psi} \\ - 2l \cos(\alpha) \cos(\psi - \theta) \sin(\beta) \sin(\vartheta - \gamma) \dot{y} \dot{\vartheta} \\ - 2l \cos(\alpha) \cos(\vartheta - \gamma) \sin(\beta) \sin(\psi - \theta) \dot{y} \dot{\psi} \end{pmatrix} - M_B g (-x \sin(\alpha) + y \cos(\alpha) \sin(\beta) + l \cos(\psi - \theta) \cos(\vartheta - \gamma)). \quad (3.24)$$

$\frac{\partial L}{\partial q_i}$ and $\frac{d}{dt} \left(\frac{\partial L}{\partial \dot{q}_i} \right)$ terms in Equation (3.1) can be determined as follows:

$$\begin{aligned}
\frac{\partial L}{\partial \psi} = & -ml \cos(\alpha) \cos(\psi - \theta) \sin(\vartheta - \gamma) \dot{x} \dot{\vartheta} - ml \cos(\alpha) \cos(\vartheta - \gamma) \sin(\psi - \theta) \dot{x} \dot{\psi} \\
& - ml \cos(\psi - \theta) \sin(\alpha) \sin(\beta) \sin(\vartheta - \gamma) \dot{y} \dot{\vartheta} + mgl \cos(\vartheta - \gamma) \sin(\psi - \theta) \\
& - ml \sin(\alpha) \sin(\psi - \theta) \sin(\vartheta - \gamma) \dot{x} \dot{\vartheta} + ml \cos(\psi - \theta) \cos(\vartheta - \gamma) \sin(\alpha) \dot{x} \dot{\psi} \quad (3.25) \\
& + ml \cos(\alpha) \sin(\beta) \sin(\psi - \theta) \sin(\vartheta - \gamma) \dot{y} \dot{\vartheta} \\
& - ml \cos(\alpha) \cos(\psi - \theta) \cos(\vartheta - \gamma) \sin(\beta) \dot{y} \dot{\psi} \\
& - ml \cos(\vartheta - \gamma) \sin(\alpha) \sin(\beta) \sin(\psi - \theta) \dot{y} \dot{\vartheta},
\end{aligned}$$

$$\begin{aligned}
\frac{\partial L}{\partial \vartheta} = & -M_B l^2 \cos(\vartheta - \gamma) \sin(\vartheta - \gamma) \dot{\psi}^2 - M_B l \cos(\alpha) \cos(\vartheta - \gamma) \sin(\psi - \theta) \dot{x} \dot{\vartheta} \\
& - M_B l \cos(\psi - \theta) \sin(\alpha) \sin(\beta) \sin(\vartheta - \gamma) \dot{y} \dot{\psi} - M_B l \cos(\beta) \sin(\vartheta - \gamma) \dot{y} \dot{\vartheta} \\
& + M_B l \cos(\psi - \theta) \cos(\vartheta - \gamma) \sin(\alpha) \dot{x} \dot{\vartheta} + M_B gl \cos(\psi - \theta) \sin(\vartheta - \gamma) \\
& - M_B l \sin(\alpha) \sin(\psi - \theta) \sin(\vartheta - \gamma) \dot{x} \dot{\psi} \quad (3.26) \\
& - M_B l \cos(\alpha) \cos(\psi - \theta) \cos(\vartheta - \gamma) \sin(\beta) \dot{y} \dot{\vartheta} \\
& + M_B l \cos(\alpha) \sin(\beta) \sin(\psi - \theta) \sin(\vartheta - \gamma) \dot{y} \dot{\psi} \\
& - M_B l \cos(\alpha) \cos(\psi - \theta) \sin(\vartheta - \gamma) \dot{x} \dot{\vartheta} \\
& - M_B l \cos(\vartheta - \gamma) \sin(\alpha) \sin(\beta) \sin(\psi - \theta) \dot{y} \dot{\vartheta},
\end{aligned}$$

$$\begin{aligned}
\frac{\partial L}{\partial \dot{\psi}} = & M_B l^2 \cos^2(\vartheta - \gamma) \dot{\psi} + M_B l \cos(\alpha) \cos(\psi - \theta) \cos(\vartheta - \gamma) \dot{x} \\
& + M_B l \cos(\psi - \theta) \cos(\vartheta - \gamma) \sin(\alpha) \sin(\beta) \dot{y} \quad (3.27) \\
& + M_B l \cos(\vartheta - \gamma) \sin(\alpha) \sin(\psi - \theta) \dot{x} \\
& - M_B l \cos(\alpha) \cos(\vartheta - \gamma) \sin(\beta) \sin(\psi - \theta) \dot{y},
\end{aligned}$$

$$\begin{aligned}
\frac{\partial L}{\partial \dot{\vartheta}} = & M_B l^2 \dot{\vartheta} - M_B l \cos(\alpha) \sin(\psi - \theta) \sin(\vartheta - \gamma) \dot{x} \\
& - M_B l \sin(\alpha) \sin(\beta) \sin(\psi - \theta) \sin(\vartheta - \gamma) \dot{y} + M_B l \cos(\beta) \cos(\vartheta - \gamma) \dot{y} \\
& + M_B l \cos(\psi - \theta) \sin(\alpha) \sin(\vartheta - \gamma) \dot{x} \\
& - M_B l \cos(\alpha) \cos(\psi - \theta) \sin(\beta) \sin(\vartheta - \gamma) \dot{y},
\end{aligned} \tag{3.28}$$

$$\begin{aligned}
\frac{d}{dt} \left(\frac{\partial L}{\partial \dot{\psi}} \right) = & M_B l^2 \cos^2(\vartheta - \gamma) \ddot{\varphi} - 2M_B l^2 \cos(\vartheta - \gamma) \sin(\vartheta - \gamma) \dot{\psi} \dot{\vartheta} \\
& + M_B l \cos(\alpha) \cos(\psi - \theta) \cos(\vartheta - \gamma) \ddot{x} \\
& - M_B l \cos(\alpha) \cos(\vartheta - \gamma) \sin(\psi) \dot{x} \dot{\psi} \\
& - M_B l \cos(\alpha) \cos(\psi - \theta) \sin(\vartheta - \gamma) \dot{x} \dot{\vartheta} \\
& + M_B l \cos(\psi - \theta) \cos(\vartheta - \gamma) \sin(\alpha) \sin(\beta) \ddot{y} \\
& - M_B l \cos(\vartheta - \gamma) \sin(\alpha) \sin(\beta) \sin(\psi - \theta) \dot{y} \dot{\psi} \\
& - M_B l \cos(\psi - \theta) \sin(\alpha) \sin(\beta) \sin(\vartheta - \gamma) \dot{y} \dot{\vartheta} \\
& + M_B l \cos(\vartheta - \gamma) \sin(\alpha) \sin(\psi - \theta) \ddot{x} \\
& - M_B l \sin(\alpha) \sin(\psi - \theta) \sin(\vartheta - \gamma) \dot{x} \dot{\vartheta} \\
& + M_B l \cos(\psi - \theta) \cos(\vartheta - \gamma) \sin(\alpha) \dot{x} \dot{\psi} \\
& - M_B l \cos(\alpha) \cos(\vartheta - \gamma) \sin(\beta) \sin(\psi - \theta) \ddot{y} \\
& + M_B l \cos(\alpha) \sin(\beta) \sin(\psi - \theta) \sin(\vartheta - \gamma) \dot{y} \dot{\vartheta} \\
& - M_B l \cos(\alpha) \cos(\psi - \theta) \cos(\vartheta - \gamma) \sin(\beta) \dot{y} \dot{\psi},
\end{aligned} \tag{3.29}$$

$$\begin{aligned}
\frac{d}{dt} \left(\frac{\partial L}{\partial \dot{\mathcal{G}}} \right) &= M_B l^2 \ddot{\mathcal{G}} - M_B l \cos(\alpha) \cos(\psi - \theta) \sin(\mathcal{G} - \gamma) \dot{x} \dot{\psi} \\
&\quad - M_B l \cos(\beta) \sin(\mathcal{G} - \gamma) \dot{y} \dot{\mathcal{G}} + M_B l \cos(\psi - \theta) \sin(\alpha) \sin(\mathcal{G} - \gamma) \ddot{x} \\
&\quad - M_B l \cos(\alpha) \cos(\mathcal{G} - \gamma) \sin(\psi - \theta) \dot{x} \dot{\mathcal{G}} + M_B l \cos(\beta) \cos(\mathcal{G} - \gamma) \ddot{y} \\
&\quad - M_B l \cos(\alpha) \sin(\psi - \theta) \sin(\mathcal{G} - \gamma) \ddot{x} \\
&\quad - M_B l \sin(\alpha) \sin(\beta) \sin(\psi - \theta) \sin(\mathcal{G} - \gamma) \ddot{y} \\
&\quad - M_B l \cos(\psi - \theta) \sin(\alpha) \sin(\beta) \sin(\mathcal{G} - \gamma) \dot{y} \dot{\psi} \\
&\quad - M_B l \cos(\mathcal{G} - \gamma) \sin(\alpha) \sin(\beta) \sin(\psi - \theta) \dot{y} \dot{\mathcal{G}} \\
&\quad - M_B l \sin(\alpha) \sin(\psi - \theta) \sin(\mathcal{G} - \gamma) \dot{x} \dot{\psi} \\
&\quad + M_B l \cos(\psi - \theta) \cos(\mathcal{G} - \gamma) \sin(\alpha) \dot{x} \dot{\mathcal{G}} \\
&\quad - M_B l \cos(\alpha) \cos(\psi - \theta) \sin(\beta) \sin(\mathcal{G} - \gamma) \ddot{y} \\
&\quad + M_B l \cos(\alpha) \sin(\beta) \sin(\psi - \theta) \sin(\mathcal{G} - \gamma) \dot{y} \dot{\psi} \\
&\quad - M_B l \cos(\alpha) \cos(\psi - \theta) \cos(\mathcal{G} - \gamma) \sin(\beta) \dot{y} \dot{\mathcal{G}}
\end{aligned} \tag{3.30}$$

$$\text{and } Q_i = 0. \tag{3.31}$$

The Lagrange's equations of motion of the 3D inverted pendulum can be derived as follows:

$$\frac{d}{dt} \left(\frac{\partial L}{\partial \dot{\psi}} \right) - \frac{\partial L}{\partial \psi} = 0 \tag{3.32}$$

$$\text{and } \frac{d}{dt} \left(\frac{\partial L}{\partial \dot{\mathcal{G}}} \right) - \frac{\partial L}{\partial \mathcal{G}} = 0. \tag{3.33}$$

Substitute Equations (3.25) to (3.31) into Equations (3.32) and (3.33). The dynamic equations of 3D inverted pendulum are then following:

$$\begin{aligned}
& M_B l^2 \cos^2(\vartheta - \gamma) \ddot{\psi} - 2M_B l^2 \cos(\vartheta - \gamma) \sin(\vartheta - \gamma) \dot{\varphi} \dot{\vartheta} \\
& + M_B l \left(\begin{array}{c} \cos(\alpha) \cos(\psi - \theta) \cos(\vartheta - \gamma) \\ + \cos(\vartheta - \gamma) \sin(\alpha) \sin(\psi - \theta) \end{array} \right) \ddot{x} \\
& + M_B l \left(\begin{array}{c} \cos(\psi - \theta) \cos(\vartheta - \gamma) \sin(\alpha) \sin(\beta) \\ - \cos(\alpha) \cos(\vartheta - \gamma) \sin(\beta) \sin(\psi - \theta) \end{array} \right) \ddot{y} \\
& - M_B g l \cos(\vartheta - \gamma) \sin(\psi - \theta) = 0
\end{aligned} \tag{3.34}$$

and

$$\begin{aligned}
& M_B l^2 \ddot{\vartheta} + M_B l^2 \cos(\vartheta - \gamma) \sin(\vartheta - \gamma) \dot{\psi}^2 - M_B g l \cos(\psi - \theta) \sin(\vartheta - \gamma) \\
& + M_B l \left(\begin{array}{c} \cos(\psi - \theta) \sin(\alpha) \sin(\vartheta - \gamma) \\ - \cos(\alpha) \sin(\psi - \theta) \sin(\vartheta - \gamma) \end{array} \right) \ddot{x} \\
& + M_B l \left(\begin{array}{c} \cos(\beta) \cos(\vartheta - \gamma) - \cos(\alpha) \cos(\psi - \theta) \sin(\beta) \sin(\vartheta - \gamma) \\ - \sin(\alpha) \sin(\beta) \sin(\psi - \theta) \sin(\vartheta - \gamma) \end{array} \right) \ddot{y} = 0.
\end{aligned} \tag{3.35}$$

3.3 Modeling of Motor and Cart

The dynamic equations for the motor and cart were identified by [Bro06] and assumed that are the first-order systems with the transfer function between the motor input or voltage [volt] and the cart output or velocity [m/s]. The transfer function of the motor and cart can be given by

$$G_{Motor\&Cart}(s) = \frac{v(s)}{V(s)} = \frac{K}{\tau s + 1}. \tag{3.36}$$

where K is the DC (or steady-state) gain of the motor and cart, obtained from the final value theorem, and τ is the time constant of the motor and cart, obtained from the exponential form of the step response. And [Bro06] used the camera as sensor for measuring the position of the motor and cart. The dynamic equations for motor and cart, which were identified by [Bro06], are used for this research as follows:

$$\ddot{x} = -\left(\frac{1}{\tau_x}\right)\dot{x} + \left(\frac{K_x}{\tau_x}\right)V_x \tag{3.37}$$

$$\ddot{y} = -\left(\frac{1}{\tau_y}\right)\dot{y} + \left(\frac{K_y}{\tau_y}\right)V_y \tag{3.38}$$

where V_x and V_y are the voltage input given to the motor along x - and y -axes respectively, τ_x and τ_y are the time constants of the motor and cart along x - and y -axes: 0.0714 and 0.04 respectively and K_x and K_y are the DC gains of the motor and cart along x - and y -axes: 0.0241 and 0.0239 respectively.

Chapter 4

Control Design and Simulation

This chapter contains the essential background control theories, which are used to design the controllers for this research in Chapter 4.1. The control problems of 3D inverted pendulum are defined in two types; regulation and tracking. These control techniques in Chapter 4.1 are applied to design the controllers for 3D inverted pendulum and the simulations of each control technique in each problem are illustrated in Chapter 4.2.

4.1 Background Control Theory

4.1.1 Non-linear Control (Approximate feedback linearization)

[Yam02] proposed this approximate feedback linearization for non-linear systems that the exact linearization method [Isi95] is not applicable. Their method is an expansion of linear controller design and has a two-step procedure to solve the approximate linearization. First, the non-linear system (4.1) is transformed approximately into the controllable canonical form (4.10) with a state transformation matrix (4.7). Second, a standard non-linear linearization control law (4.4) is used to transform the non-linear system in the controllable canonical form (4.10) into a linear system in the controllable canonical form (4.17). The control structure of this method is shown in Figure 4.1.

Consider the SISO non-linear system of the form

$$\dot{x}(t) = f(x) + g(x)u(t) \quad (4.1)$$

where $x(t) \in \mathbb{R}^n$ is a state vector, $u(t) \in \mathbb{R}$ is a control vector and $f(x)$ and $g(x): \mathbb{R}^n \rightarrow \mathbb{R}^n$ are vector fields and assumed to be smooth. At the equilibrium point of system $x(t) = 0$, it is assumed that the element $\eta(x)$ of $f(x)$ satisfies

$$\frac{\partial \eta(x)}{\partial x_i} \neq \infty, i = 1, 2, \dots, n \quad (4.2)$$

where x_i is the i -th row of $x(t)$.

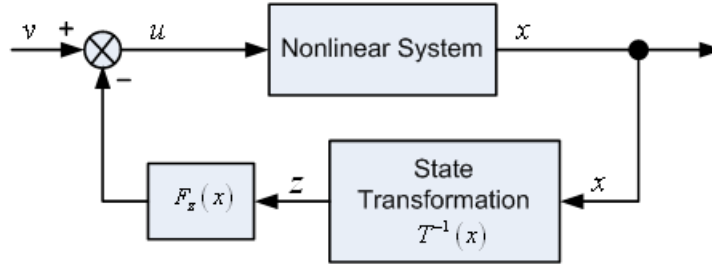


Figure 4.1 Structure of approximate feedback linearization control

Referring to the assumption (4.2), the non-linear system (4.1) can be rewritten in the state space form as follows

$$\dot{x}(t) = A(x)x(t) + b(x)u(t) \quad (4.3)$$

where $A(x) \in \mathbb{R}^{n \times n}$ is a state matrix, $b(x) \in \mathbb{R}^{n \times 1}$ is a input matrix and $(A(x), b(x))$ is controllable. Under these conditions, the control law is

$$u(t) = -F_z(x)z(t) + v(t) \quad (4.4)$$

such that the new state variable or linearizing state z and the new input v satisfy a linear time-invariant relation

$$\dot{z}(t) = A_z z(t) + B_z v(t) \quad (4.5)$$

where $A_z \in \mathbb{R}^{n \times n}$ is a new state matrix and $B_z \in \mathbb{R}^{n \times 1}$ is a new input matrix.

The state transformation matrix used to transform z into x can be written as follows

$$x(t) = T(x)z(t) \quad (4.6)$$

where $T(x)$ is the state transformation matrix and denoted by

$$T(x) = \begin{bmatrix} b(x) & A(x)b(x) & A(x)^2 b(x) & \cdots & A(x)^{n-1} b(x) \end{bmatrix} \begin{bmatrix} a_1(x) & a_2(x) & \cdots & a_{n-1}(x) & 1 \\ a_2(x) & a_3(x) & \cdots & 1 & 0 \\ \vdots & \vdots & \ddots & \vdots & \vdots \\ a_{n-1}(x) & 1 & \cdots & 0 & 0 \\ 1 & 0 & \cdots & 0 & 0 \end{bmatrix}. \quad (4.7)$$

The following approximation is written as follows

$$\frac{dT(x)}{dt} \approx 0, \quad \forall t, x. \quad (4.8)$$

Referring to the approximation (4.8), the coordinate transformation matrix (4.7) is applied to the non-linear system (4.3) in order to transform the non-linear system (4.3) into the controllable canonical form (4.10) using two following theorems.

Theorem 1 The state transformation matrix (4.7) will can transform the state of the non-linear system (4.3). If the state transformation matrix (4.7) is satisfied as follows

$$\det(T(x)) \neq 0. \quad (4.9)$$

When the state of the non-linear system (4.3) has been transformed by the state transformation matrix (4.7). The non-linear system with a new state vector in the controllable canonical form can be written as follows

$$\begin{aligned} \frac{dz(t)}{dt} &= T(x)^{-1} A(x)T(x)z(t) + T(x)^{-1} b(x)u(t) \\ \dot{z}(t) &\equiv A_z(x)z(t) + b_z(x)u(t) \end{aligned} \quad (4.10)$$

where $A_z(x)$ and $b_z(x)$ are denoted by

$$A_z(x) = \begin{bmatrix} 0 & 1 & 0 & \cdots & 0 \\ 0 & 0 & 1 & \cdots & 0 \\ \vdots & \vdots & \vdots & \ddots & \vdots \\ 0 & 0 & 0 & \cdots & 1 \\ -a_0(x) & -a_1(x) & -a_2(x) & \cdots & -a_{n-1}(x) \end{bmatrix} \quad (4.11)$$

and

$$b_z(x) = \begin{bmatrix} 0 \\ 0 \\ \vdots \\ 0 \\ 1 \end{bmatrix} \quad (4.12)$$

, respectively.

Theorem 2 Let the characteristic equation for $A(x)$,

$$\Phi(s) \equiv \det(sI - A(x)) = s^n + a_{n-1}(x)s^{n-1} + \dots + a_0(x) = 0 \quad (4.13)$$

be a x function equation that is satisfied by the eigenvalues of $A(x)$

$$\Phi(A) = A(x)^n + a_{n-1}(x)A(x)^{n-1} + \dots + a_0(x)I = 0. \quad (4.14)$$

Let the characteristic equation of the desired stable linear system be

$$s^n + \lambda_{n-1}s^{n-1} + \dots + \lambda_1s + \lambda_0 = 0. \quad (4.15)$$

And the non-linearities in the non-linear system (4.10) can be cancelled by the linearizing control law (4.4) and $F(x)$ can be obtained as follows

$$F(x) = \begin{bmatrix} -a_0(x) + \lambda_0 & -a_1(x) + \lambda_1 & \dots & -a_{n-2}(x) + \lambda_{n-2} & -a_{n-1}(x) + \lambda_{n-1} \end{bmatrix}. \quad (4.16)$$

Then the linearizing control law (4.4) applies to the non-linear system (4.10). The linear system is obtained as follows

$$\frac{dz(t)}{dt} = \begin{bmatrix} 0 & 1 & 0 & \dots & 0 \\ 0 & 0 & 1 & \dots & 0 \\ \vdots & \vdots & \vdots & \ddots & \vdots \\ 0 & 0 & 0 & \dots & 1 \\ -\lambda_0 & -\lambda_1 & -\lambda_2 & \dots & -\lambda_{n-1} \end{bmatrix} z(t) + \begin{bmatrix} 0 \\ 0 \\ \vdots \\ 0 \\ 1 \end{bmatrix} v(t). \quad (4.17)$$

When the linear system (4.17) is obtained, the new input $v(t)$ will be designed by using standard linear techniques such as pole placement or LQR.

4.1.2 Model Reference Adaptive Control (MRAC)

Model reference adaptive control can be called as direct adaptive control. It doesn't require the parameter identification of the system, which uses to compute the parameter adaptation mechanism or adaptive law. The parameter adaptation mechanism of MRAC can be made using three basic approaches: MIT rule [Mar89] [Hwa93], Lyapunov [Par66] [Win68] [Sob82] [Kau98] and Hyperstability approach [Lan69] [Lan79]. In this research MRAC using Lyapunov approach is used to determine the adaptive law to control 3D inverted pendulum.

4.1.2.1 MRAC using Full State Feedback

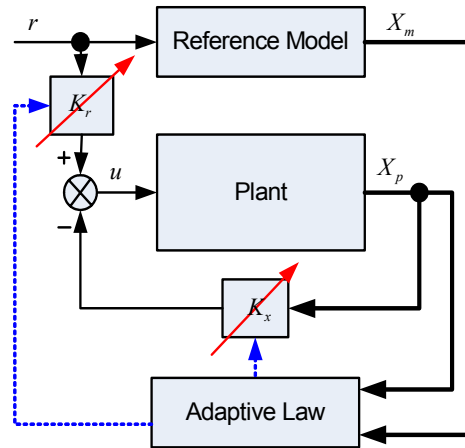


Figure 4.2 Structure of MRAC using full state feedback

MRAC using full state feedback is presented in [Win68] based on Lyapunov's second method suggested by [Par66]. The linear time-invariant system in controllable canonical form considered as a plant is represented by

$$\begin{aligned} \dot{x}_p(t) &= A_p x_p(t) + B_p u(t) \\ y_p(t) &= C_p x_p(t) \end{aligned} \quad (4.18)$$

where $x_p(t) \in \mathbb{R}^n$ is a state vector, $u(t) \in \mathbb{R}^m$ is a control vector, $y_p(t) \in \mathbb{R}$ is a output vector, $A_p \in \mathbb{R}^{n \times n}$ is a state matrix, $B_p \in \mathbb{R}^{n \times m}$ is a control input matrix and $C_p \in \mathbb{R}^{1 \times n}$ is an output matrix.

It is assumed that the reference system can be adequately modelled by the linear time-invariant system in controllable canonical form as follows

$$\begin{aligned} \dot{x}_m(t) &= A_m x_m(t) + B_m r(t) \\ y_m(t) &= C_m x_m(t) \end{aligned} \quad (4.19)$$

where $r(t) \in \mathbb{R}^m$ is a reference input vector and the dimensionality of the other vectors and matrixes of the reference system is the same as the plant.

An adaptive control law is given by

$$u = K_r(t)r(t) - K_x(t)x_p(t) \quad (4.20)$$

which the gain matrixes $K_r(t)$ and $K_x(t)$ can be adaptable. Substituting the adaptive control law (4.20) into the system (4.18). A new system is obtained as follows

$$\begin{aligned}\dot{x}_p(t) &= A_c x_p(t) + B_c r(t) \\ y_p(t) &= C_p x_p(t)\end{aligned}\quad (4.21)$$

where $A_c = A_p - B_p K_x(t)$ and $B_c = B_p K_r(t)$.

Define the state error vector by $e(t) = x_p(t) - x_m(t)$, then the state error equation is obtained as follows

$$\dot{e}(t) = A_m e(t) + A x_p(t) + B r(t) \quad (4.22)$$

where $A = A_c - A_m$ and $B = B_c - B_m$. And the state error equation (4.22) can be rewritten as follows

$$\dot{e}(t) = A_m e(t) + B_l \phi^T \omega \quad (4.23)$$

where $B_l = [0 \dots 0 \ 1]^T$, $\phi^T = [B \ A]$ and $\omega = [r \ x_p]^T$.

A Lyapunov function is chosen as a function of the error and parameter error to prove the stability of the adaptive system as follows

$$V = e^T(t) P e(t) + \phi^T \Gamma^{-1} \phi \quad (4.24)$$

where P and Γ^{-1} are symmetric positive definite matrixes which V is an acceptable Lyapunov function candidate. The time derivative of V is

$$\dot{V} = e^T(t) (A_m^T P + P A_m) e(t) + 2e^T(t) P B_l \phi^T \omega + 2\phi^T \Gamma^{-1} \dot{\phi}^T. \quad (4.25)$$

The time-invariant system is stable if there exist positive definite matrixes P and Q , such that the following Lyapunov equation is satisfied as follows

$$P A_m + A_m^T P = -Q. \quad (4.26)$$

Therefore the adaptive law is obtained as follows

$$\dot{K}(t) = -\Gamma e^T(t) P B_l \omega. \quad (4.27)$$

4.1.2.2 MRAC for Output Tracking

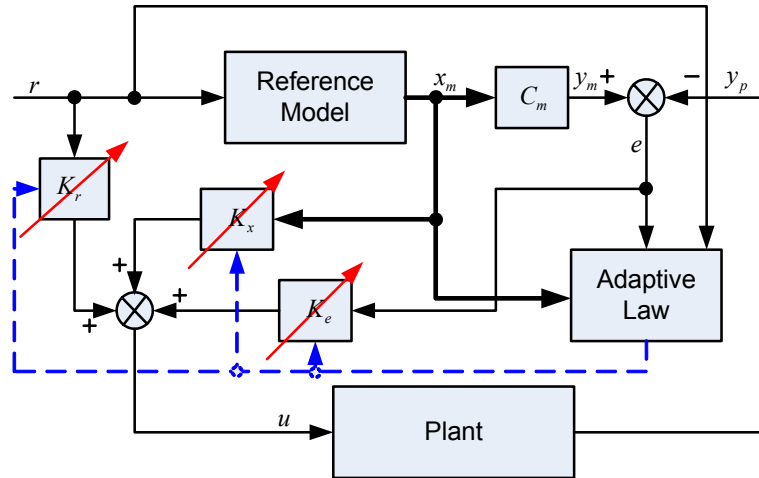


Figure 4.3 Structure of MRAC for output tracking

MRAC for output tracking was developed by [Sob82] and [Kau98] based on command generator tracker (CGT) as shown in Figure 4.3. It requires a system which satisfies almost strictly positive real (ASPR) condition. The dynamics of the controlled system are written in Equation (4.18) and a desired stable reference model is described by Equation (4.19). For this algorithm it doesn't require the order of the reference model to be the same as the controlled system. Therefore the adaptive control law is obtained and implemented based on output measurements as follows

$$u(t) = K_x(t)x_m(t) + K_r(t)r(t) + K_e(t)e_y(t) \quad (4.28)$$

or

$$u(t) = K(t)z(t) \quad (4.29)$$

where

$$\begin{aligned} e_y(t) &= y_m(t) - y_p(t) \\ z^T(t) &= [e^T, x_m^T, r^T]^T \\ K(t) &= [K_e(t), K_x(t), K_r(t)]. \end{aligned}$$

The adaptive law based on CGT approach is given as a combination of the proportional and integral terms

$$K(t) = K(t_0) + \int_{t_0}^t e_y(\tau) z^T(\tau) d\tau = K_p(t) + K_I(t). \quad (4.30)$$

The gain matrixes $K_p(t)$ and $K_I(t)$ are adaptive as follows:

$$K_p(t) = e_y(t)z^T(t)\bar{T} \quad (4.31)$$

and

$$\dot{K}_I(t) = e_y(t)z^T(t)T \quad (4.32)$$

where \bar{T} and T are positive semi-definite symmetric and positive definite symmetric matrixes, respectively.

4.1.3 Robust Tracking Control

This technique was proposed by Davison [Dav76] [Dav87] for a linear, time-invariant, multivariable system and it could be called “robust servomechanism control”. It contains two parts such as a servo-compensator and a stabilizing-compensator. This structure is shown in Figure 4.4.

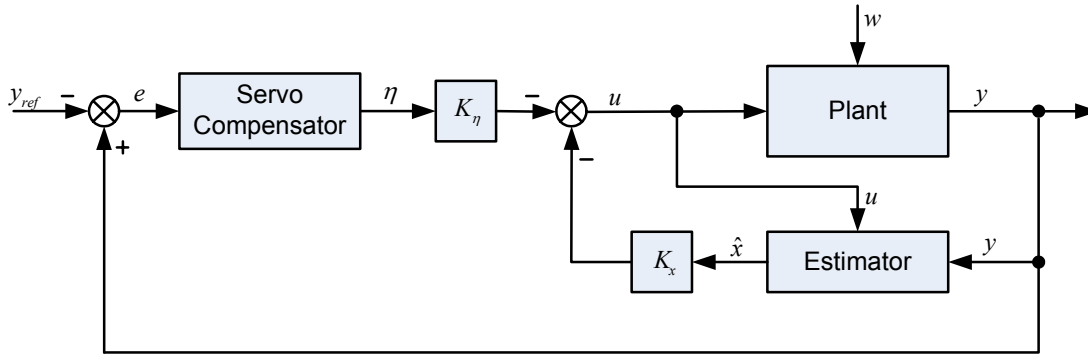


Figure 4.4 Structure of robust tracking control

Consider a system given by

$$\begin{aligned} \dot{x}(t) &= Ax(t) + Bu(t) + Ew(t) \\ y(t) &= Cx(t) + Du(t) + Fw(t) \\ e(t) &= y(t) - y_{ref}(t) \end{aligned} \quad (4.33)$$

where $x(t) \in \mathbb{R}^n$ is a state vector, $u(t) \in \mathbb{R}^m$ is a control vector, $y(t) \in \mathbb{R}^r$ is a plant output vector, $w(t) \in \mathbb{R}^q$ is a disturbance vector and $e(t) \in \mathbb{R}^r$ is a difference vector between the plant output $y(t)$ and the specified reference input $y_{ref}(t)$. The system is assumed that (A, B) is controllable, (A, C) is observable and $m \geq r$.

Let a servo-compensator be given by

$$\dot{\eta}(t) = \tilde{A}\eta(t) + \tilde{B}e(t) \quad (4.34)$$

where $\eta \in \mathbb{R}^p$ is a output vector of a servo-compensator, $\tilde{A} \in \mathbb{R}^{p \times p}$ is a state matrix of the servo-compensator, $\tilde{B} \in \mathbb{R}^p$ is an input matrix of the servo-compensator and the servo-compensator is assumed that (\tilde{A}, \tilde{B}) is controllable.

Remark The state and input matrixes of the servo-compensator are given in the controllable canonical form as follows

$$\tilde{A} = \begin{bmatrix} 0 & 1 & 0 & \cdots & 0 \\ 0 & 0 & 1 & \cdots & 0 \\ \vdots & \vdots & \vdots & \ddots & \vdots \\ -\alpha_1 & -\alpha_2 & -\alpha_3 & \cdots & -\alpha_p \end{bmatrix} \text{ and } \tilde{B} = \begin{bmatrix} 0 \\ 0 \\ \vdots \\ 1 \end{bmatrix}.$$

Combination the system (4.33) and servo-compensator (4.34), a new system is obtained as follows

$$\begin{aligned} \begin{bmatrix} \dot{\eta}(t) \\ \dot{x}(t) \end{bmatrix} &= \begin{bmatrix} \tilde{A} & \tilde{B}C \\ 0 & A \end{bmatrix} \begin{bmatrix} \eta(t) \\ x(t) \end{bmatrix} + \begin{bmatrix} \tilde{B}D \\ B \end{bmatrix} u(t) + \begin{bmatrix} \tilde{B}F \\ E \end{bmatrix} w(t) + \begin{bmatrix} \tilde{B} \\ 0 \end{bmatrix} y_{ref}(t) \\ \begin{bmatrix} \eta(t) \\ y(t) \end{bmatrix} &= \begin{bmatrix} I & 0 \\ 0 & C \end{bmatrix} \begin{bmatrix} \eta(t) \\ x(t) \end{bmatrix} + \begin{bmatrix} 0 \\ D \end{bmatrix} u(t) + \begin{bmatrix} 0 \\ F \end{bmatrix} w(t) \end{aligned} \quad (4.35)$$

or, alternatively as

$$\begin{aligned} \dot{\bar{x}}(t) &= \bar{A}\bar{x}(t) + \bar{B}u(t) + \bar{E}\bar{w}(t) \\ y(t) &= \bar{C}\bar{x}(t) + \bar{D}u(t) + \bar{F}\bar{w}(t) \end{aligned} \quad (4.36)$$

where $\bar{x}(t) = [\eta(t) \ x(t)]^T$, $\bar{y}(t) = [\eta(t) \ y(t)]^T$, $\bar{w}(t) = [y_{ref}(t)^T \ w(t)^T]^T$,

$\bar{A} = \begin{bmatrix} \tilde{A} & \tilde{B}C \\ 0 & A \end{bmatrix}$, $\bar{B} = \begin{bmatrix} \tilde{B}D \\ B \end{bmatrix}$, $\bar{C} = \begin{bmatrix} I & 0 \\ 0 & C \end{bmatrix}$, $\bar{D} = \begin{bmatrix} 0 \\ D \end{bmatrix}$, $\bar{E} = \begin{bmatrix} \tilde{B} & \tilde{B}F \\ 0 & E \end{bmatrix}$, $\bar{F} = \begin{bmatrix} 0 & 0 \\ 0 & F \end{bmatrix}$, (\bar{A}, \bar{B}) is controllable and (\bar{A}, \bar{C}) is observable.

Then the robust control law has the following structure.

$$u(t) = -K\bar{x}(t) = -K_x\hat{x}(t) - K_\eta\eta(t). \quad (4.37)$$

The control gain K will be designed by using standard linear techniques such as pole placement or LQR.

4.2 Control Design

For this research two types of the control problems such as regulation and tracking are defined. In the regulation problem of 3D inverted pendulum the control system will be designed in order that the state of closed-loop system will be stabilized around an equilibrium point. Therefore, its task is to control the position of the cart to maintain at the middle of the table while the pendulum is balanced in upright position. For tracking problem the control object is to design the controller that the system output tracks a path. That is to control the position of the cart to track a path while the pendulum is balanced in upright position. The path used in this research is specified as a circle.

4.2.1 Regulation Problem

The controller of 3D inverted pendulum for the regulation problem is firstly designed based on the linear model although the dynamics model of 3D inverted pendulum in Equations (3.34) and (3.35) are the non-linear model. Consequently, Equations (3.34) and (3.35) will be linearized using the first-order Taylor series expansion about an operating point. The desired operating point of 3D inverted pendulum is defined as $\left[\vartheta \ \psi \ \dot{\vartheta} \ \dot{\psi} \ \ddot{x} \ \ddot{y} \right]^T = [0 \ 0 \ 0 \ 0 \ 0 \ 0]^T$ and the inclination angle of the camera and table are eliminated. The linearized equations are obtained as follows

$$\ddot{\psi} = \left(\frac{g}{l} \right) \psi + \left(\frac{-1}{l} \right) \ddot{x} \quad (4.38)$$

$$\ddot{\vartheta} = \left(\frac{g}{l} \right) \vartheta + \left(\frac{-1}{l} \right) \ddot{y} . \quad (4.39)$$

In addition, the system has not only the inverted pendulum but also the motor and cart. So the dynamic models of the motor and cart (3.37) and (3.38) are substituted into the linearized dynamic models of the pendulum (4.38) and (4.39) as follows

$$\ddot{\psi} = \left(\frac{g}{l} \right) \psi + \left(\frac{1}{l\tau_x} \right) \dot{x} - \left(\frac{K_x}{l\tau_x} \right) V_x \quad (4.40)$$

$$\ddot{\vartheta} = \left(\frac{g}{l} \right) \vartheta + \left(\frac{1}{l\tau_y} \right) \dot{y} - \left(\frac{K_y}{l\tau_y} \right) V_y . \quad (4.41)$$

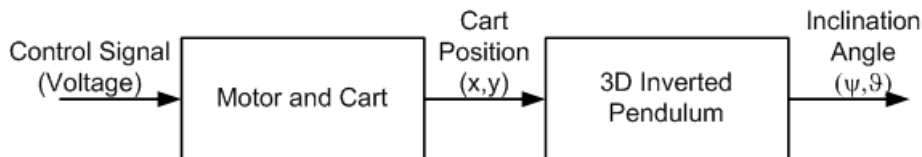


Figure 4.5 Block diagram of pendulum, motor and cart

For Equations (3.37), (3.38), (4.40) and (4.41) the state vector X and input vector U are chosen as $\left[\psi \ \dot{\psi} \ x \ \dot{x} \ \vartheta \ \dot{\vartheta} \ y \ \dot{y} \right]^T$ and $\left[V_x \ V_y \right]^T$ respectively. Thus Equations (3.37), (3.38), (4.40) and (4.41) can be written in state form as follows

$$\begin{aligned} \dot{X} &= AX + BU \\ Y &= CX + DU \end{aligned} \quad (4.42)$$

where the matrixes A , B , C and D are denoted by

$$A = \begin{bmatrix} 0 & 1 & 0 & 0 & 0 & 0 & 0 & 0 \\ \frac{g}{l} & 0 & 0 & \frac{1}{l\tau_x} & 0 & 0 & 0 & 0 \\ 0 & 0 & 0 & 1 & 0 & 0 & 0 & 0 \\ 0 & 0 & 0 & -\frac{1}{\tau_x} & 0 & 0 & 0 & 0 \\ 0 & 0 & 0 & 0 & 0 & 1 & 0 & 0 \\ 0 & 0 & 0 & 0 & \frac{g}{l} & 0 & 0 & \frac{1}{l\tau_y} \\ 0 & 0 & 0 & 0 & 0 & 0 & 0 & 1 \\ 0 & 0 & 0 & 0 & 0 & 0 & 0 & -\frac{1}{\tau_y} \end{bmatrix}, \quad B = \begin{bmatrix} 0 & 0 \\ -\frac{K_x}{l\tau_x} & 0 \\ 0 & 0 \\ \frac{K_x}{\tau_x} & 0 \\ 0 & 0 \\ 0 & -\frac{K_y}{l\tau_y} \\ 0 & 0 \\ 0 & \frac{K_y}{\tau_y} \end{bmatrix},$$

$$C = \begin{bmatrix} 1 & 0 & 0 & 0 & 0 & 0 & 0 & 0 \\ 0 & 0 & 1 & 0 & 0 & 0 & 0 & 0 \\ 0 & 0 & 0 & 0 & 1 & 0 & 0 & 0 \\ 0 & 0 & 0 & 0 & 0 & 0 & 1 & 0 \end{bmatrix} \quad \text{and} \quad D = \begin{bmatrix} 0 & 0 \\ 0 & 0 \\ 0 & 0 \\ 0 & 0 \end{bmatrix}.$$

And the system can be written in the following transfer functions

$$\frac{\psi(s)}{V_x(s)} = \frac{-K_x s^2}{(ls^2 - g)(\tau_x s^2 + s)} \quad (4.43)$$

$$\frac{\vartheta(s)}{V_y(s)} = \frac{-K_y s^2}{(ls^2 - g)(\tau_y s^2 + s)}. \quad (4.44)$$

After the linearization process, the dynamic model of 3D inverted pendulum is decoupled as two planar inverted pendulums. The controller can be developed individually by x - and y -axes, respectively. Two stabilization controllers will be designed for each planar inverted pendulum based on various control theories to solve this problem as following.

4.2.1.1 PID Controller

[Bro06] had designed PID controller with compensator to test his system. This research has taken his design as a reference controller for developing the next controllers and comparing the performance of each controller. The control structure is shown in Figure 4.6.

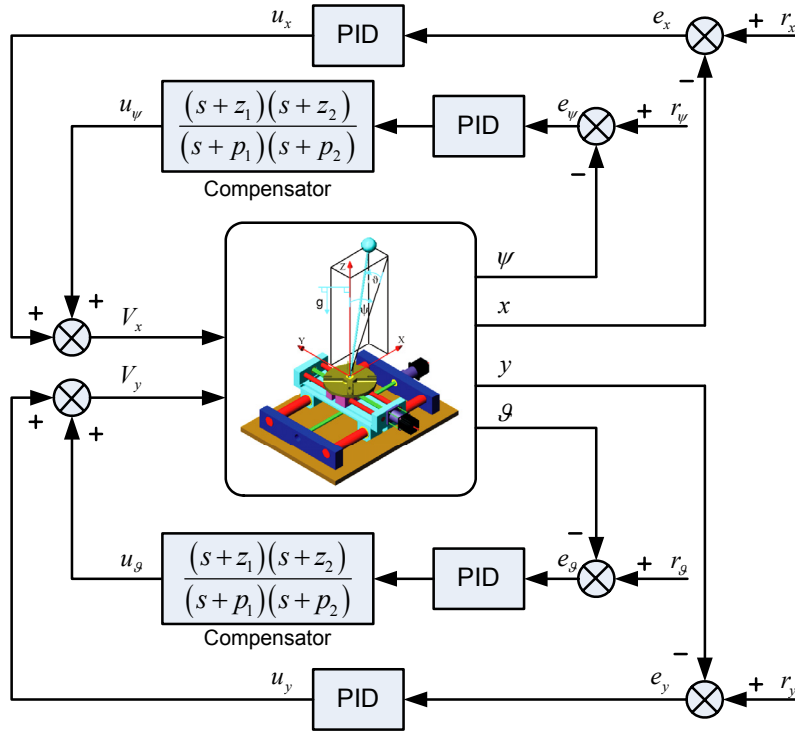


Figure 4.6 PID controller and compensator for regulation problem

4.2.1.2 State Feedback

The dynamic equations of 3D inverted pendulum in state form (4.42) are used to design the feedback gain matrix K by linear quadratic regulator (LQR). This method was designed for 3D inverted pendulum by [Bro06]. It has an advantage over the pole placement method because it allows the feedback gain matrix to be determined that will result in the minimum amount of energy being required to stabilize the system. The state feedback control law is given by

$$U = -K\hat{X} \quad (4.45)$$

that minimizes the performance index

$$J = \int_0^{\infty} (X^T Q X + U^T R U) dt. \quad (4.46)$$

where Q is a positive semi-definite real matrix and R is a positive definite real matrix.

By adjusting the value of the matrix R , the amount of control input can be varied. Increasing R will result in less energy being used to control the system. The matrix Q determines the amount of weighting or importance assigned to each of the state variables. A larger value puts more emphasis on that particular variable.

For computing the feedback gain matrix, the matrixes Q and R are specified as $\text{diag}\{30, 0, 1000, 0, 30, 0, 1000, 0\}$ and $\text{diag}\{0.0038, 0.0038\}$ [Bro06], respectively. The control structure is shown in Figure 4.7 and the feedback gain matrix K is obtained as follows

$$K = - \begin{bmatrix} 873.46 & 194.30 & 500.00 & 334.62 & 0 & 0 & 0 & 0 \\ 0 & 0 & 0 & 0 & 819.44 & 182.15 & 512.99 & 331.85 \end{bmatrix}. \quad (4.47)$$

The full-order estimator is constructed to estimate the state vector of the system. The selection of the estimator gain matrix L is also based on LQR. So the matrixes Q and R are specified as $\text{diag}\{10, 10, 1000, 10, 10, 10, 1000, 10\}$, $\text{diag}\{0.01, 0.01, 0.01, 0.01\}$ [Bro06] and the estimator gain matrix is obtained as follows

$$L = \begin{bmatrix} 34.44 & 92.87 & 0.006 & 1.734 & 0 & 0 & 0 & 0 \\ 0.006 & 0.261 & 316.23 & 0.132 & 0 & 0 & 0 & 0 \\ 0 & 0 & 0 & 0 & 34.42 & 92.20 & 0.002 & 0.642 \\ 0 & 0 & 0 & 0 & 0 & 0 & 316.23 & 0.586 \end{bmatrix}. \quad (4.48)$$

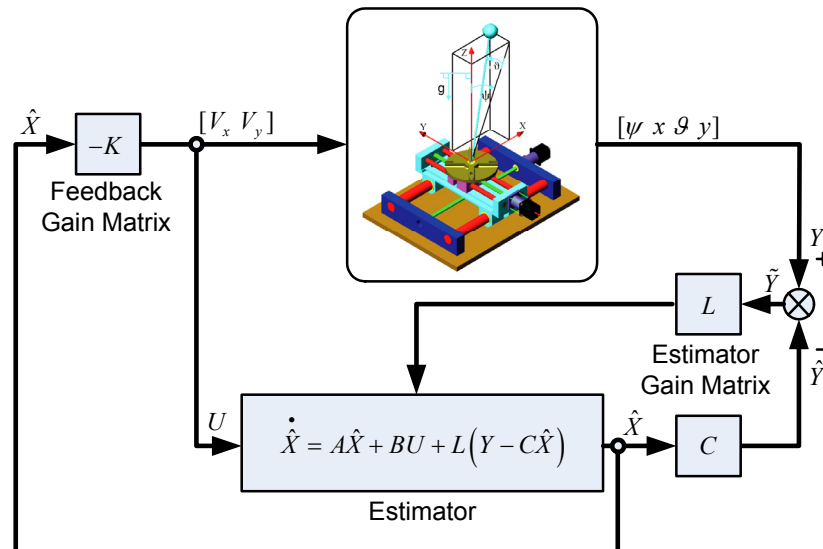


Figure 4.7 State feedback and estimator for regulation problem

4.2.1.3 Non-linear Controller

The control theory in Chapter 4.1.1 is applied to control 3D inverted pendulum and its control structure is shown in Figure 4.9. Unfortunately this theory can perform only a system that has only one input, then the non-linear system of 3D inverted pendulum will be separated into two non-linear systems of 2D inverted pendulum or planar inverted pendulum by projecting the pendulum onto xz - and yz -planes as shown in Figure 4.8 and each system on each plane can be controlled individually. These projections are considered as coupled pendulums inside two orthogonal planes. Their inertias J_{xz} and J_{yz} can be described as functions of their lengths l_{xz} and l_{yz} or their inclination angles ψ and ϑ with respect to the origin.

$$J_{xz} = J \left(\frac{l_{xz}^2}{l^2} \right) = J \cdot \frac{1}{\frac{\cos^2 \psi}{\sin^2 \vartheta} + \sin^2 \psi} \quad (4.49)$$

$$J_{yz} = J \left(\frac{l_{yz}^2}{l^2} \right) = J \cdot \frac{1}{\frac{\cos^2 \vartheta}{\sin^2 \psi} + \sin^2 \vartheta} \quad (4.50)$$

where J is the inertia of 3D inverted pendulum and l is the length of the pendulum. It is assumed that the inclination angles of the pendulum are within $\pm 5^\circ$, the variations of these lengths and inertias are less than 3.15%. Consequently, the variations of the following parameters are substitutable.

$$\begin{aligned} l_{xz} &\cong l_{yz} \cong l \\ J_{xz} &\cong J_{yz} \cong J \end{aligned} \quad (4.51)$$

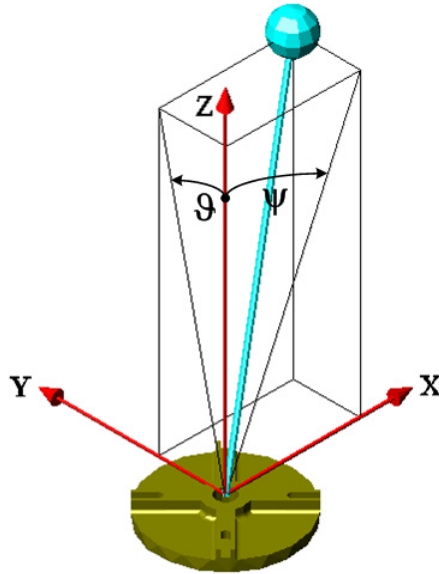


Figure 4.8 Projection of the pendulum onto xz - and yz -planes

After this simplification, the projections are considered as two uncoupled pendulums onto xz - and yz -planes which can be controlled individually. Therefore, the non-linear dynamic equation of the pendulum for each plane can be described with non-linear dynamic equation of 2D inverted pendulum (3.14), which can be written without the inclination angles of the table and camera as follows

$$M_B l^2 \ddot{\psi} + M_B l \cos(\psi) \ddot{x} - M_B g l \sin(\psi) = 0 \quad (4.52)$$

$$M_B l^2 \ddot{\vartheta} + M_B l \cos(\vartheta) \ddot{y} - M_B g l \sin(\vartheta) = 0. \quad (4.53)$$

Since the control strategy of the pendulum for each plane should be the same, except for some different parameters, to simplify the description. The control strategy will be derived only one of these two planes, which the control strategy for xz -plane will be explained as follows.

Substituting the dynamic equations of the motor and cart (3.37) into the non-linear dynamic equation of 2D inverted pendulum on xz -plane (4.52).

$$M_B l^2 \ddot{\psi} - M_B g l \sin(\psi) - M_B l \cos(\psi) \left(\frac{1}{\tau_x} \right) \dot{x} + M_B l \cos(\psi) \left(\frac{K_x}{\tau_x} \right) V_x = 0 \quad (4.54)$$

So the whole dynamic equations on xz -plane consist of 2 equations (3.37) and (4.54) and let the state vector X and input vector U_x be $[\psi \ \dot{\psi} \ x \ \dot{x}]^T$ and V_x respectively, then the dynamic equations on xz -plane (3.37) and (4.54) can be expressed in form (4.1) as follows

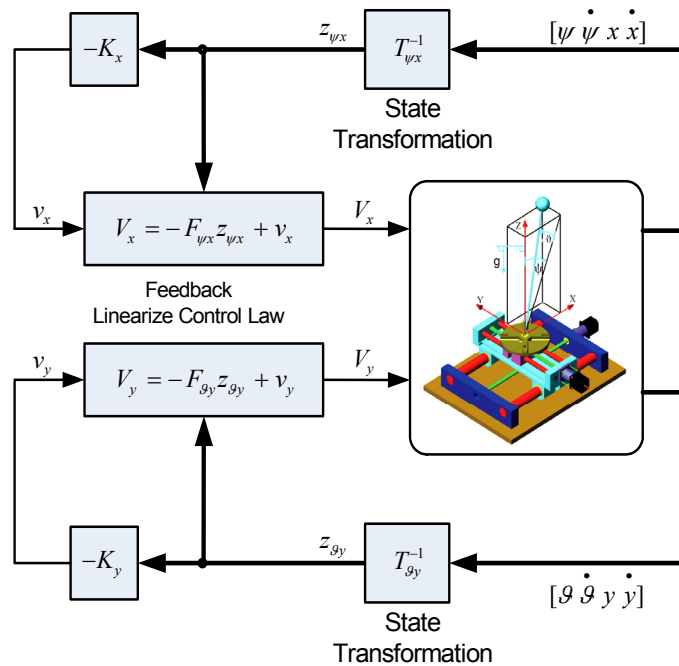


Figure 4.9 Approximate feedback linearization for regulation problem

$$\begin{bmatrix} \dot{\psi} \\ \psi \\ \ddot{x} \\ \dot{x} \\ x \\ \ddot{x} \\ x \end{bmatrix} = \begin{bmatrix} \dot{\psi} \\ \frac{g \sin(\psi)}{l} - \frac{\cos(\psi) \dot{x}}{l\tau_x} \\ \dot{x} \\ -\left(\frac{1}{\tau_x}\right) \dot{x} \\ x \\ \ddot{x} \\ x \end{bmatrix} + \begin{bmatrix} 0 \\ \frac{\cos(\psi) K_x}{l\tau_x} \\ 0 \\ \frac{K_x}{\tau_x} \end{bmatrix} U_x. \quad (4.55)$$

Equations (4.55) can be rewritten in form (4.3), where the matrixes $A(x)$ and $B(x)$ are denote by

$$A(x) = \begin{bmatrix} 0 & 1 & 0 & 0 \\ \frac{g \sin(\psi)}{l\psi} & 0 & 0 & \frac{\cos(\psi)}{l\tau_x} \\ 0 & 0 & 0 & 1 \\ 0 & 0 & 0 & -\frac{1}{\tau_x} \end{bmatrix} \text{ and } B(x) = \begin{bmatrix} 0 \\ -\frac{K_x \cos(\psi)}{l\tau_x} \\ 0 \\ \frac{K_x}{\tau_x} \end{bmatrix}.$$

The characteristic equation of $A(x)$ is obtained as follows

$$s^4 + \frac{1}{\tau_x} s^3 - \frac{g \sin(\psi)}{l\psi} s^2 - \frac{g \sin(\psi)}{l\tau_x \psi} s = 0. \quad (4.56)$$

Referring to Equation (4.7), the state transformation matrix $T_{\psi x}$ is obtained as follows

$$T_{\psi x} = \begin{bmatrix} 0 & 0 & -\frac{K_x \cos(\psi)}{l\tau_x} & 0 \\ 0 & 0 & 0 & -\frac{K_x \cos(\psi)}{l\tau_x} \\ -\frac{K_x g \sin(\psi)}{l\tau_x \psi} & 0 & \frac{K_x}{\tau_x} & 0 \\ 0 & -\frac{K_x g \sin(\psi)}{l\tau_x \psi} & 0 & \frac{K_x}{\tau_x} \end{bmatrix}. \quad (4.57)$$

The desired stable system is selected from the minimum ITAE standard forms for a zero steady-state step error with $\omega_n = 5.8 \text{ rad/sec}$ as given by

$$s^4 + 2.1\omega_n s^3 + 3.4\omega_n^2 s^2 + 2.7\omega_n^3 s + \omega_n^4 = 0. \quad (4.58)$$

The stable linear system can be computed from Equation (4.17) as follows

$$\frac{dz_{\psi x}}{dt} = \begin{bmatrix} 0 & 1 & 0 & 0 \\ 0 & 0 & 1 & 0 \\ 0 & 0 & 0 & 1 \\ -\omega_n^4 & -2.7\omega_n^3 & -3.4\omega_n^2 & -2.1\omega_n \end{bmatrix} z_{\psi x} + \begin{bmatrix} 0 \\ 0 \\ 0 \\ 1 \end{bmatrix} v_x. \quad (4.59)$$

Referring to Equations (4.4) and (4.16), the linearizing control law can be obtained as follows

$$U_x = -F_{\psi x} z_{\psi x} + v_x \quad (4.60)$$

$$\text{where } F_{\psi x} = \begin{bmatrix} \omega_n^4 & \frac{g \sin(\psi)}{l\tau_x \psi} + 2.7\omega_n^3 & \frac{g \sin(\psi)}{l\psi} + 3.4\omega_n^2 & -\frac{1}{\tau_x} + 2.1\omega_n \end{bmatrix}.$$

When the state transformation matrix (4.57), the linear system (4.59) and linearizing control law (4.60) are obtained. Then the new input v_x in Equation (4.60) is designed using LQR to find the feedback gain matrix K_x for the linear system (4.59). The matrixes Q and R are selected as $\text{diag}\{10,1,10,1\}$ and 1 respectively and the feedback gain matrix K_x is obtained as follows

$$K_x = [0.353 \quad 2.352 \quad 2.656 \quad 0.003]. \quad (4.61)$$

In the same way, the controller for 2D inverted pendulum on yz -plane can be determined in the same way on xz -plane. So the state transformation matrix $T_{\vartheta y}$, linearizing control law U_y and the feedback gain matrix K_y are obtained as follows

$$T_{\vartheta y} = \begin{bmatrix} 0 & 0 & -\frac{K_y \cos(\vartheta)}{l\tau_y} & 0 \\ 0 & 0 & 0 & -\frac{K_y \cos(\vartheta)}{l\tau_y} \\ -\frac{K_y g \sin(\vartheta)}{l\tau_y \vartheta} & 0 & \frac{K_y}{\tau_y} & 0 \\ 0 & -\frac{K_y g \sin(\vartheta)}{l\tau_y \vartheta} & 0 & \frac{K_y}{\tau_y} \end{bmatrix}, \quad (4.62)$$

$$U_y = - \begin{bmatrix} \omega_n^4 & \frac{g \sin(\vartheta)}{l\tau_y \vartheta} + 2.7\omega_n^3 & \frac{g \sin(\vartheta)}{l\vartheta} + 3.4\omega_n^2 & -\frac{1}{\tau_y} + 2.1\omega_n \end{bmatrix} z_{\vartheta y} + v_y, \quad (4.63)$$

$$\text{and } K_y = [0.353 \quad 2.352 \quad 2.656 \quad 0.003]. \quad (4.64)$$

4.2.1.4 MRAC using Full State Feedback

The control theory in Chapter 4.1.2.1 is applied to control 3D inverted pendulum and its control structure is shown in Figure 4.10. As all reference inputs are zero, then it's not necessary to have the gain matrix K_r in the control structure. The control design will be derived individually on each plane since the dynamic model of 3D inverted pendulum is decoupled as planar inverted pendulum after the linearization. Thus the control design along x -axis or on xz -plane will be illustrated as following.

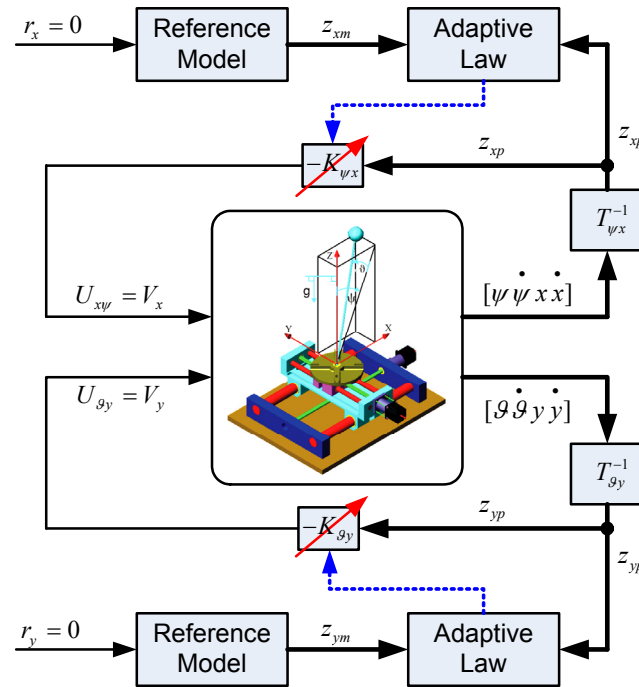


Figure 4.10 MRAC using full state feedback for regulation problem

The reference system (4.19) is selected from the minimum ITAE standard forms for a zero steady-state step error as follows

$$\begin{aligned} \dot{z}_{xm}(t) &= A_{xm}z_{xm}(t) + B_{xm}r_x(t) \\ y_{xm}(t) &= C_{xm}z_{xm}(t) + D_{xm}r_x(t) \end{aligned} \quad (4.65)$$

where the matrixes A_{xm} , B_{xm} , C_{xm} and D_{xm} are denoted by

$$A_{xm} = \begin{bmatrix} 0 & 1 & 0 & 0 \\ 0 & 0 & 1 & 0 \\ 0 & 0 & 0 & 1 \\ -\omega_n^4 & -2.7\omega_n^3 & -3.4\omega_n^2 & -2.1\omega_n \end{bmatrix}, \quad B_{xm} = \begin{bmatrix} 0 \\ 0 \\ 0 \\ 1 \end{bmatrix}$$

$$C_{xm} = \begin{bmatrix} 1 & 0 & 0 & 0 \\ 0 & 1 & 0 & 0 \\ 0 & 0 & 1 & 0 \\ 0 & 0 & 0 & 1 \end{bmatrix} \quad \text{and} \quad D_{xm} = \begin{bmatrix} 0 \\ 0 \\ 0 \\ 0 \end{bmatrix}.$$

And the matrix Q is defined as

$$Q = \begin{bmatrix} -q_1 & 0 & 0 & 0 \\ 0 & -q_2 & 0 & 0 \\ 0 & 0 & -q_3 & 0 \\ 0 & 0 & 0 & -q_4 \end{bmatrix}. \quad (4.66)$$

Then the matrix P can be obtained from Equation (4.26) as follows

$$P = \begin{bmatrix} p_{11} & p_{12} & p_{13} & p_{14} \\ p_{12} & p_{22} & p_{23} & p_{p24} \\ p_{13} & p_{23} & p_{33} & p_{34} \\ p_{14} & p_{p24} & p_{34} & p_{44} \end{bmatrix} \quad (4.67)$$

where

$$\begin{aligned} p_{11} &= \frac{18587q_1}{8420\omega_n} + \frac{370\omega_n q_2}{1263} + \frac{175\omega_n^3 q_3}{1263} + \frac{75\omega_n^5 q_4}{421} \\ p_{12} &= \frac{9747q_1}{4210\omega_n^2} + \frac{245q_2}{842} + \frac{315\omega_n^2 q_3}{842} + \frac{405\omega_n^4 q_4}{842} \\ p_{13} &= \frac{33923q_1}{25260\omega_n^3} + \frac{175q_2}{1263\omega_n} + \frac{75\omega_n q_3}{421} + \frac{590\omega_n^3 q_4}{1263} \\ p_{14} &= \frac{q_1}{2\omega_n^4} \\ p_{22} &= \frac{81679q_1}{25260\omega_n^3} + \frac{2767q_2}{1684\omega_n} + \frac{6583\omega_n q_3}{5052} + \frac{7261\omega_n^3 q_4}{5052} \\ p_{23} &= \frac{4403q_1}{2105\omega_n^4} + \frac{833q_2}{842\omega_n^2} + \frac{325q_3}{421} + \frac{1377\omega_n^2 q_4}{842} \\ p_{24} &= \frac{361q_1}{421\omega_n^5} + \frac{370q_2}{1263\omega_n^3} + \frac{175q_3}{1263\omega_n} + \frac{75\omega_n q_4}{421} \\ p_{33} &= \frac{18067q_1}{12630\omega_n^5} + \frac{1329q_2}{1684\omega_n^3} + \frac{6329q_3}{5052\omega_n} + \frac{12227\omega_n q_4}{5052} \\ p_{34} &= \frac{259q_1}{421\omega_n^6} + \frac{245q_2}{842\omega_n^4} + \frac{315q_3}{842\omega_n^2} + \frac{405q_4}{842} \\ p_{44} &= \frac{370q_1}{1263\omega_n^7} + \frac{175q_2}{1263\omega_n^5} + \frac{75q_3}{421\omega_n^3} + \frac{590q_4}{1263\omega_n} \end{aligned}$$

Referring to Equation (4.27), therefore the adaptive law can be obtained as follows

$$\dot{K}_{\psi x}(t) = - \left[p_{14} e_x(t) + p_{24} \dot{e}_x(t) + p_{34} \ddot{e}_x(t) + p_{44} \dddot{e}_x(t) \right] \begin{bmatrix} \gamma_1 & 0 & 0 & 0 \\ 0 & \gamma_2 & 0 & 0 \\ 0 & 0 & \gamma_3 & 0 \\ 0 & 0 & 0 & \gamma_4 \end{bmatrix} z_{xp}(t) \quad (4.68)$$

where $e_x(t) = z_{xm}(t) - z_{xp}(t)$.

And the control law is

$$U_{\psi x}(t) = -K_{\psi x}(t) z_{xp}(t) \quad (4.69)$$

where z_{xp} is a new state vector transformed from the state vector $\begin{bmatrix} \psi & \dot{\psi} & x & \dot{x} \end{bmatrix}^T$ of the pendulum on xz -plane, which can be determined by $z_{xp} = T_{\psi x}^{-1} \begin{bmatrix} \psi & \dot{\psi} & x & \dot{x} \end{bmatrix}^T$, $T_{\psi x}$ is the transformation matrix and $K_{\psi x}$ is the feedback gain matrix.

To determinate the initial gain matrix $K_{\psi x}$, the dynamic model of 2D inverted pendulum on xz -plane will be transformed into controllable canonical form because this control theory can apply only the system in the controllable canonical form. Therefore, the dynamic model of 2D inverted pendulum on xz -plane transformed into controllable canonical form is

$$\begin{aligned} \dot{z}_{xp}(t) &= A_{xp} z_{xp}(t) + B_{xp} u_{xp}(t) \\ y_{xp}(t) &= C_{xp} z_{xp}(t) \end{aligned} \quad (4.70)$$

where the matrixes A_{xp} , B_{xp} and C_{xp} are denoted by

$$A_{xp} = \begin{bmatrix} 0 & 1 & 0 & 0 \\ 0 & 0 & 1 & 0 \\ 0 & 0 & 0 & 1 \\ 0 & \frac{g}{l\tau_x} & \frac{g}{l} & \frac{-1}{\tau_x} \end{bmatrix}, \quad B_{xp} = \begin{bmatrix} 0 \\ 0 \\ 0 \\ 1 \end{bmatrix} \quad \text{and} \quad C_{xp} = \begin{bmatrix} 0 & 0 & \frac{-K_x}{l\tau_x} & 0 \\ \frac{-gK_x}{l\tau_x} & 0 & \frac{K_x}{\tau_x} & 0 \end{bmatrix}.$$

And the transformation matrix used to transform the dynamic model of 2D inverted pendulum on xz -plane into controllable canonical form is

$$T_{\psi_x} = \begin{bmatrix} 0 & 0 & \frac{-K_x}{l\tau_x} & 0 \\ 0 & 0 & 0 & \frac{-K_x}{l\tau_x} \\ \frac{-gK_x}{l\tau_x} & 0 & \frac{-K_x}{\tau_x} & 0 \\ 0 & \frac{-gK_x}{l\tau_x} & 0 & \frac{K_x}{\tau_x} \end{bmatrix}. \quad (4.71)$$

Then the initial gain matrix K_{ψ_x} can be designed using LQR technique with the system in controllable canonical form (4.70) and the matrixes Q and R are $diag\{5000,0,1,0\}$ and 0.0038 respectively. The initial gain matrix K_{ψ_x} is obtained as follows

$$K_{\psi_x} = [1147.10 \quad 940.75 \quad 213.19 \quad 12.14]. \quad (4.72)$$

To determinate the adaptive laws on yz -plane, it is the same as on xz -plane. So the adaptive laws on yz -plane can be obtained as follows

$$\dot{K}_{g_y}(t) = - \left[p_{14}e_y(t) + p_{24}\dot{e}_y(t) + p_{34}\ddot{e}_y(t) + p_{44}\dddot{e}_y(t) \right] \begin{bmatrix} \gamma_1 & 0 & 0 & 0 \\ 0 & \gamma_2 & 0 & 0 \\ 0 & 0 & \gamma_3 & 0 \\ 0 & 0 & 0 & \gamma_4 \end{bmatrix} z_{yp}(t) \quad (4.73)$$

where $e_y(t) = z_{ym}(t) - z_{yp}(t)$ and all term of p is the same as in Equation (4.67).

And the control law on yz -plane is

$$U_{g_y}(t) = -K_{g_y}(t)z_{yp}(t). \quad (4.74)$$

The transformation matrix on yz -plane is

$$T_{g_y} = \begin{bmatrix} 0 & 0 & \frac{-K_y}{l\tau_y} & 0 \\ 0 & 0 & 0 & \frac{-K_y}{l\tau_y} \\ \frac{-gK_y}{l\tau_y} & 0 & \frac{-K_y}{\tau_y} & 0 \\ 0 & \frac{-gK_y}{l\tau_y} & 0 & \frac{K_y}{\tau_y} \end{bmatrix}. \quad (4.75)$$

And the initial gain matrix K_{g_y} on yz -plane can be obtained as the initial gain matrix K_{ψ_x} with the matrixes $Q = \text{diag}\{5000, 0, 1, 0\}$ and $R = 0.0038$ as follows

$$K_{g_y} = [1147.10 \quad 1474.40 \quad 324.87 \quad 10.70]. \quad (4.76)$$

4.2.1.5 Simulation Results

In the simulation, MATLAB/Simulink is implemented to simulate the control algorithms of 3D inverted pendulum. The model block of 3D inverted pendulum and the motor and cart used to simulate in MATLAB/Simulink are created from Equations (3.34), (3.35), (3.37) and (3.38) and some dynamic equation parameters in Equations (3.34) and (3.35) are set to the following values: $M_B = 0.1 \text{ kg}$ and $l = 0.5 \text{ m}$. The sampling time is selected as 1 ms.

The controllers designed in Chapter 4.2.1 are simulated and compared their results. The initial condition of the simulation is specified as $[\psi \dot{\psi} x \dot{x} \vartheta \dot{\vartheta} y \dot{y}] = [1.72[\text{deg}] \ 0 \ 0 \ 0 \ 1.72[\text{deg}] \ 0 \ 0 \ 0]$.

For PID controller the parameters of the compensator and the gains of the inclination angle and position of the cart are selected as $[z_1 \ z_2 \ p_1 \ p_2] = [6 \ 6 \ 1 \ 15]$, $[K_p \ K_D \ K_I] = [-1100 \ -10 \ -100]$ and $[K_p \ K_D \ K_I] = [-360 \ 0 \ -20]$, respectively.

For the state feedback and estimator, the feedback gain matrix (4.47) and the estimator gain matrix (4.48) are used to simulate.

For non-linear controller the linearizing control laws (4.60) and (4.63) are used to linearize the non-linear model of 3D inverted pendulum to the linear model which is modelled from ITAE with $\omega_n = 5.8 \text{ rad/sec}$ and the state transformation matrixes (4.57) and (4.62) are used to transform the state of the non-linear system into the new state z_{ψ_x} and z_{g_y} . The feedback gain matrixes (4.61) and (4.64) are used to stabilize the linearized system of 3D inverted pendulum.

For MRAC using full state feedback the adaptive laws (4.68) and (4.73) and the control laws (4.69) and (4.74) are applied to simulate 3D inverted pendulum which ω_n of the reference model equals to 20 rad/sec and the value of $[\gamma_1 \ \gamma_2 \ \gamma_3 \ \gamma_4]$ of each adaptive law is $[1 \ 1 \ 1 \ 1] \times 10^3$.

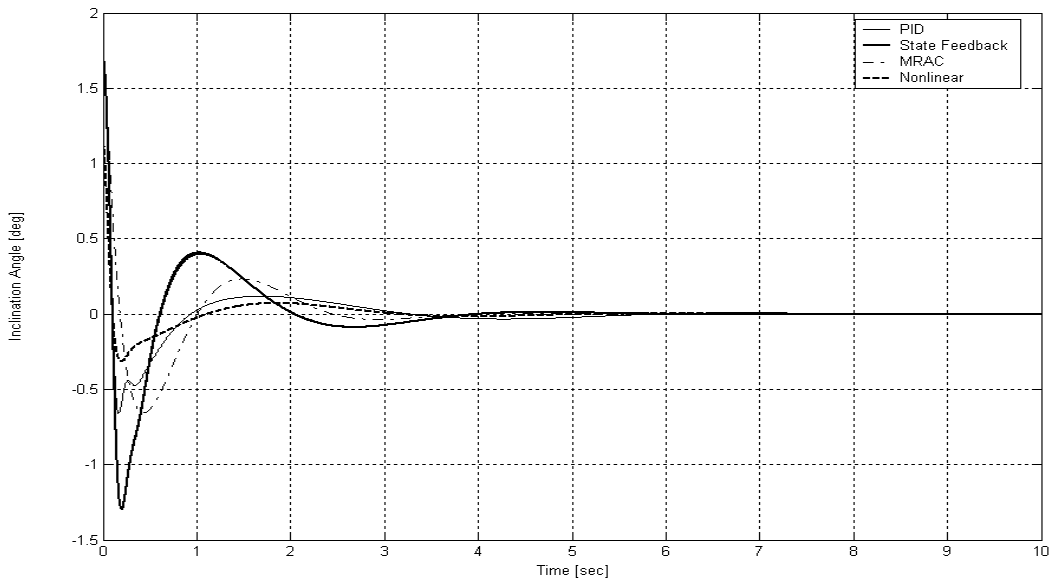


Figure 4.11 Comparison of the simulation responses of the inclination angle ψ for regulation problem

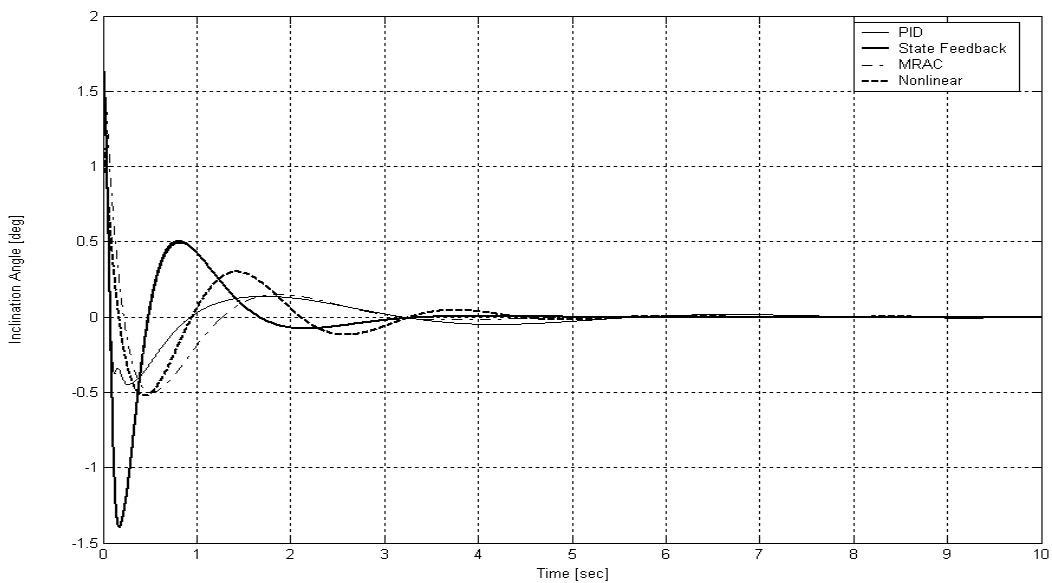


Figure 4.12 Comparison of the simulation responses of the inclination angle ϱ for regulation problem

Their simulation results are depicted in Figures 4.11-4.16. Figures 4.11-4.12 are the responses of the inclination angle versus time during the simulation operation. They show that all controllers designed in Chapters 4.2.1.1-4 can achieve to stabilize 3D inverted pendulum or that means the pendulum can be balanced in upright position. Note that the overshoot, which is obtained by the non-linear controller, is less than the other.

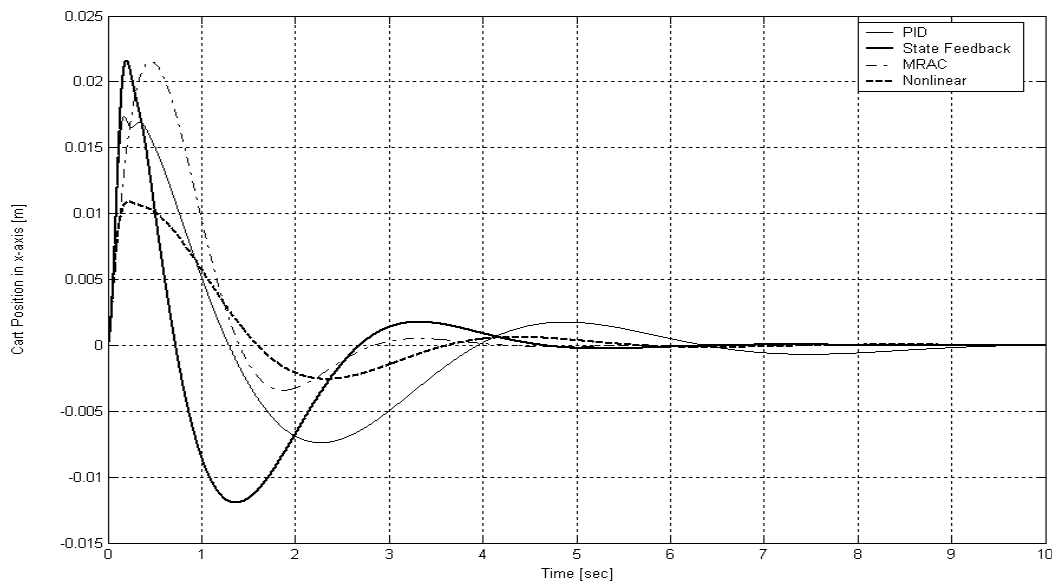


Figure 4.13 Comparison of the simulation responses of the cart position x for regulation problem

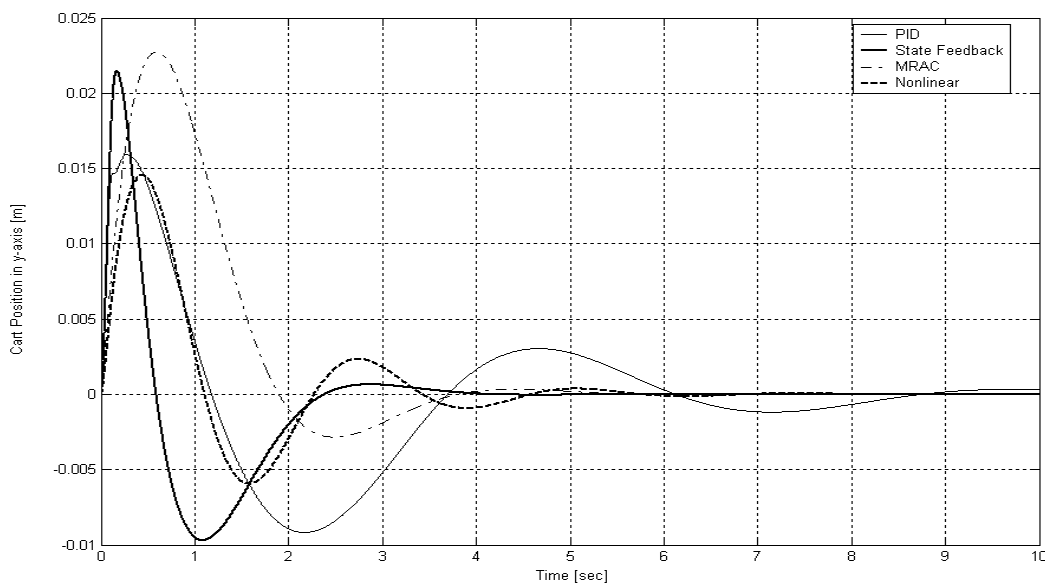


Figure 4.14 Comparison of the simulation responses of the cart position y for regulation problem

Figures 4.13-4.14 show the responses of the cart position versus time and their responses can converge toward zero. That means, the cart can be maintained at the middle of the table. Note that the non-linear controller gives the least overshoot but its settling time is a bit more than the state feedback and MRAC controller for the position of the cart along x - and y -axes.

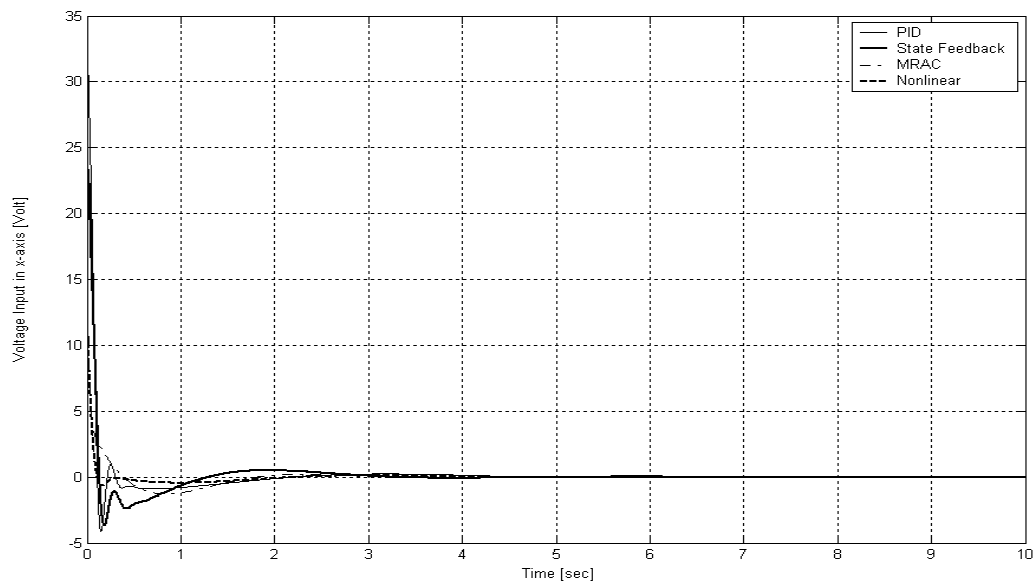


Figure 4.15 Comparison of the simulation responses of the control signal along x -axis for regulation problem

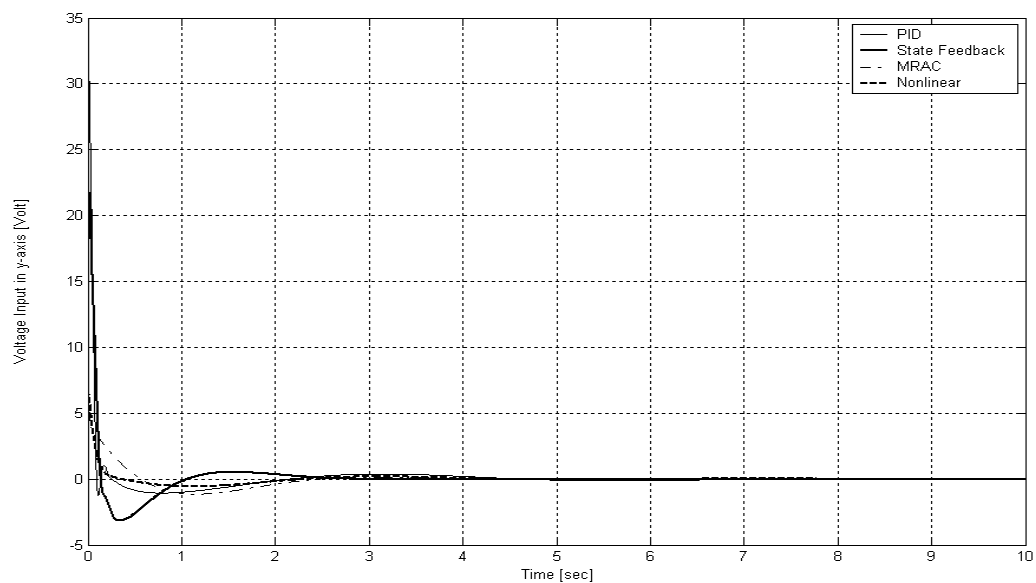


Figure 4.16 Comparison of the simulation responses of the control signal along y -axis for regulation problem

The control inputs in each axis are given in Figure 4.15-4.16 which the controller that gives the least value of the control inputs along x - and y -axes is the non-linear controller about 11.766 and 6.925 volt respectively.

4.2.2 Tracking Problem

In this section the various control laws, which force the position of the cart to track a desired reference path over the specified time interval, will be investigated. For this research, the circular path is specified as a reference input of the cart.

4.2.2.1 State Feedback

This technique is a tracker design that is developed from designing a regulator by adding a gain matrix K_r to guarantee tracking behaviour. Its control structure is shown in Figure 4.17. Its control law can be written as follows

$$U = K_r R - K_x \hat{X} \tag{4.77}$$

where K_x can be found in state feedback of the regulator. And K_r can be determined as follows

$$K_r = -\left(C[A - BK]^{-1} B\right)^{-1} \tag{4.78}$$

where A and B are the system matrixes of 3D inverted pendulum as in Equation (4.42) while the matrixes C and D are denoted by

$$C = \begin{bmatrix} 0 & 0 & 1 & 0 & 0 & 0 & 0 & 0 \\ 0 & 0 & 0 & 0 & 0 & 0 & 1 & 0 \end{bmatrix} \text{ and } D = \begin{bmatrix} 0 & 0 \\ 0 & 0 \end{bmatrix}$$

, respectively.

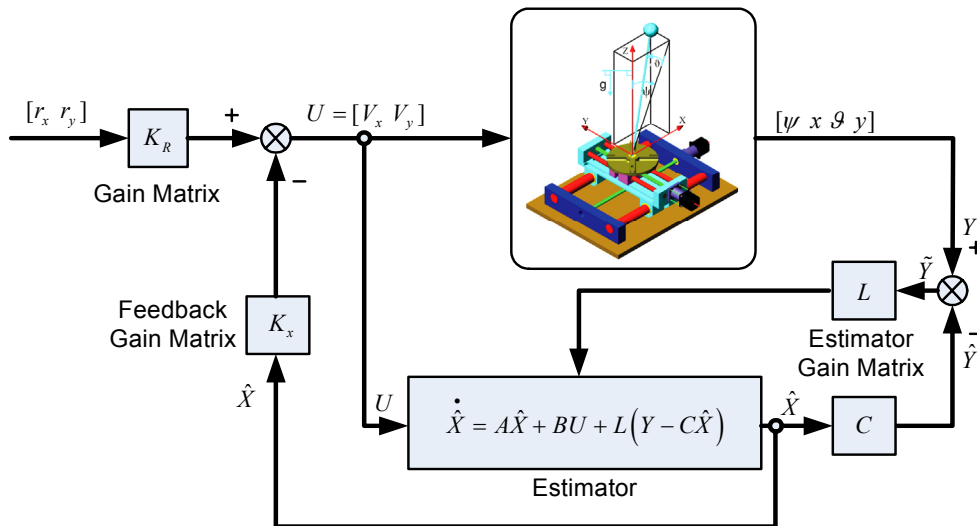


Figure 4.17 State feedback for tracking problem

4.2.2.2 MRAC using Full State Feedback

The control theory in Chapter 4.1.2.1 is applied to control 3D inverted pendulum and its control structure shown in Figure 4.18. This control design will be derived individually in each axis because as mentioned before, the dynamic model of 3D inverted pendulum is decoupled as 2 planar inverted pendulums, on xz - and yz -planes, after the linearization. The control design on xz -plane is firstly considered and assumed that the second-order reference model on xz -plane consists of 2 decouples parts such as (1) pendulum (2) motor and cart as follows

$$\dot{x}_m(t) = A_{xm}x_m(t) + B_{xm}r_x(t) \quad (4.79)$$

$$\dot{\psi}_m(t) = A_{\psi m}\psi_m(t) + B_{\psi m}r_\psi(t) \quad (4.80)$$

where x_m and ψ_m are the state vectors of the cart position and inclination angle respectively, r_x and r_ψ are the reference input vectors of the cart position and pendulum respectively, A_{xm} and $A_{\psi m}$ are the system matrixes of the reference model of the cart and pendulum in the controllable canonical form respectively and B_{xm} and $B_{\psi m}$ are the input matrixes of the reference model of the cart and pendulum respectively.

The control law for the inverted pendulum on xz -plane can be given as follows

$$V_x(t) = K_{rx}(t)r_x(t) + K_{r\psi}(t)r_\psi(t) + K_x(t)\left[x(t) \quad \dot{x}(t)\right]^T + K_\psi(t)\left[\psi(t) \quad \dot{\psi}(t)\right]^T. \quad (4.81)$$

The matrixes A_{xm} and $A_{\psi m}$ of the reference model are specified to be the same matrix. Therefore, the adaptive laws for the cart and pendulum are also the same. The determination of the adaptive law of the cart will be shown as following.

The reference system (4.19) is selected from the minimum ITAE standard forms for a zero steady-state ramp error and given by

$$\begin{aligned} \dot{x}_m(t) &= A_{xm}x_m(t) + B_{xm}r_x(t) \\ y_x(t) &= C_{xm}x_m(t) \end{aligned} \quad (4.82)$$

where the matrixes A_{xm} , B_{xm} and C_{xm} are denoted by

$$A_{xm} = \begin{bmatrix} 0 & 1 \\ -\omega_n^2 & -3.2\omega_n \end{bmatrix}, \quad B_{xm} = \begin{bmatrix} 0 \\ 1 \end{bmatrix} \quad \text{and} \quad C_{xm} = [1 \quad 0].$$

And the matrix Q is defined as follows

$$Q = \begin{bmatrix} -q_1 & 0 \\ 0 & -q_2 \end{bmatrix}. \quad (4.83)$$

The matrix P then can be found from Lyapunov equation (4.26) as follows

$$P = \begin{bmatrix} p_{11} & p_{12} \\ p_{12} & p_{22} \end{bmatrix} \quad (4.84)$$

where

$$p_{11} = \frac{281q_1}{160\omega_n} + \frac{5\omega_n q_2}{32}$$

$$p_{12} = \frac{q_1}{2\omega_n^2}$$

$$p_{22} = \frac{5q_1}{32\omega_n^3} + \frac{5q_2}{32\omega_n}.$$

Referring to Equation (4.27), the adaptive law for the cart on xz -plane can be found as follows:

$$\dot{K}_x(t) = - \left[p_{12}e_x(t) + p_{22}\dot{e}_x(t) \right] \begin{bmatrix} \gamma_1 & 0 \\ 0 & \gamma_2 \end{bmatrix} \begin{bmatrix} x(t) \\ \dot{x}(t) \end{bmatrix} \quad (4.85)$$

and

$$\dot{K}_{rx}(t) = - \left[p_{12}e_x(t) + p_{22}\dot{e}_x(t) \right] \gamma r_x \quad (4.86)$$

where $e_x(t) = x_m(t) - x(t)$.

The adaptive law for the pendulum on xz -plane will be obtained as follows:

$$\dot{K}_\psi(t) = - \left[p_{12}e_\psi(t) + p_{22}\dot{e}_\psi(t) \right] \begin{bmatrix} \gamma_1 & 0 \\ 0 & \gamma_2 \end{bmatrix} \begin{bmatrix} \psi(t) \\ \dot{\psi}(t) \end{bmatrix} \quad (4.87)$$

and

$$\dot{K}_{r\psi}(t) = - \left[p_{12}e_\psi(t) + p_{22}\dot{e}_\psi(t) \right] \gamma r_\psi \quad (4.88)$$

where $e_\psi(t) = \psi_m(t) - \psi(t)$.

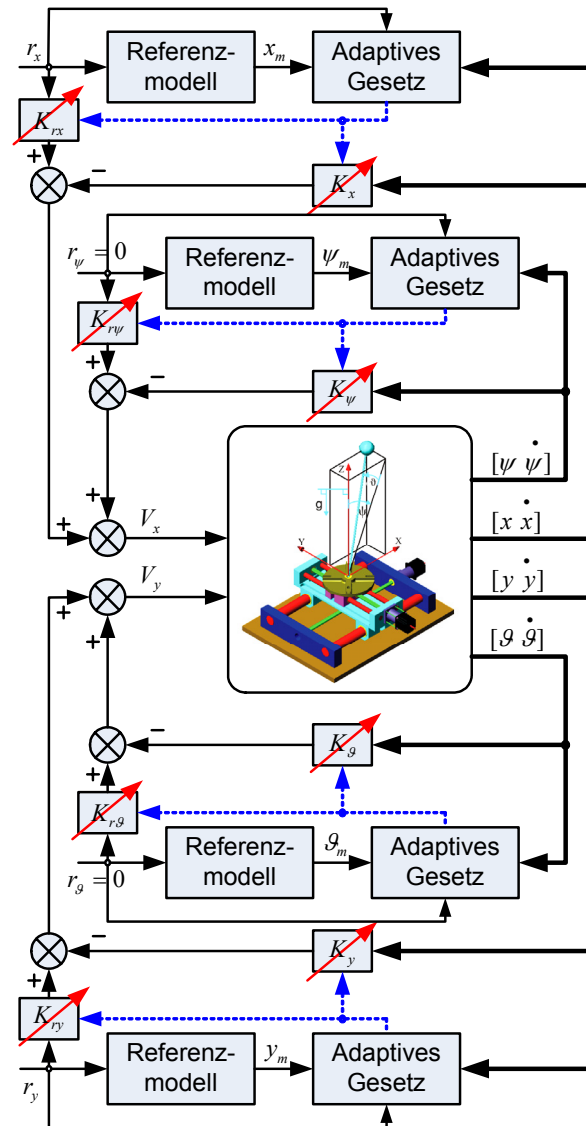


Figure 4.18 MRAC using full state feedback for tracking problem

For the control design on yz -plane, it is the same as on xz -plane. Therefore, the control law for the inverted pendulum on yz -plane can be given as follows

$$U_{y,g}(t) = K_{ry}(t)r_y(t) + K_{r,g}(t)r_g(t) + K_y(t) \begin{bmatrix} y(t) & \dot{y}(t) \end{bmatrix}^T + K_g(t) \begin{bmatrix} g(t) & \dot{g}(t) \end{bmatrix}^T. \quad (4.89)$$

The adaptive law for the cart on yz -plane is obtained as follows

$$\dot{K}_y(t) = - \begin{bmatrix} p_{12}e_y(t) + p_{22}\dot{e}_y(t) \end{bmatrix} \begin{bmatrix} \gamma_1 & 0 \\ 0 & \gamma_2 \end{bmatrix} \begin{bmatrix} y(t) \\ \dot{y}(t) \end{bmatrix} \quad (4.90)$$

and
$$\dot{K}_{r_y}(t) = -\left[p_{12}e_y(t) + p_{22}\dot{e}_y(t) \right] \gamma r_y \quad (4.91)$$

where $e_y(t) = y_m(t) - y(t)$.

And the adaptive law for the pendulum on yz -plane is obtained as follows

$$\dot{K}_g(t) = -\left[p_{12}e_g(t) + p_{22}\dot{e}_g(t) \right] \begin{bmatrix} \gamma_1 & 0 \\ 0 & \gamma_2 \end{bmatrix} \begin{bmatrix} \mathcal{G}(t) \\ \dot{\mathcal{G}}(t) \end{bmatrix} \quad (4.92)$$

and

$$\dot{K}_{r_g}(t) = -\left[p_{12}e_g(t) + p_{22}\dot{e}_g(t) \right] \gamma r_g \quad (4.93)$$

where $e_g(t) = \mathcal{G}_m(t) - \mathcal{G}(t)$ and all terms of p are as in Equation (4.84).

4.2.2.3 Robust Tracking Controller

The controller theory in Chapter 4.1.3 is applied to control the 3D inverted pendulum. The servo-compensator is firstly designed in order to be satisfied to the reference input. The reference input is a circle and can be given in equations as follows:

$$r_x = R \cos(\omega t) \quad (4.94)$$

and
$$r_y = R \sin(\omega t) \quad (4.95)$$

where r_x is the reference input of the cart position along x -axis, r_y is the reference input of the cart position along y -axis, t is the time [sec], ω is the angular velocity [rad/sec] and R is the radius of the circle [m].

After taking the second time derivatives of Equations (4.94) and (4.95), the matrix \tilde{A} of the servo-compensator can be obtained as follows:

$$\ddot{r}_x = -\omega^2 r_x \quad \text{or} \quad \tilde{A}_x = \begin{bmatrix} 0 & 1 \\ -\omega^2 & 0 \end{bmatrix} \quad (4.96)$$

and

$$\ddot{r}_y = -\omega^2 r_y \quad \text{or} \quad \tilde{A}_y = \begin{bmatrix} 0 & 1 \\ -\omega^2 & 0 \end{bmatrix}. \quad (4.97)$$

Then substituting the pendulum and cart system (4.42), the matrixes \tilde{A}_x (4.96) and \tilde{A}_y (4.97), into Equation (4.36). For this research the disturbance w is eliminated. Therefore the new system in state form will be obtained as follows

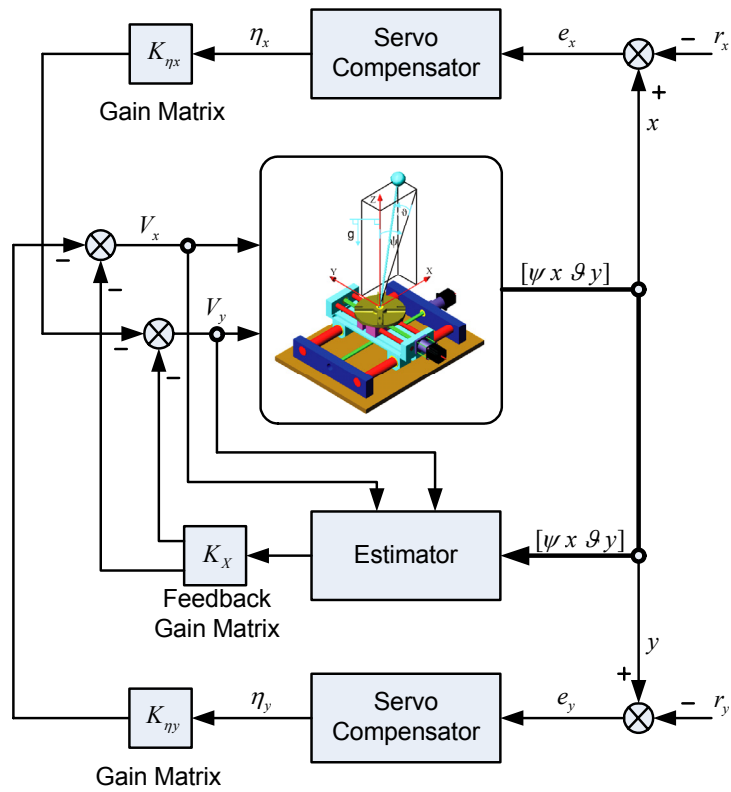


Figure 4.19 Robust tracking control for tracking problem

$$\begin{aligned} \dot{\bar{X}} &= \bar{A}\bar{X} + \bar{B}\bar{U} \\ \bar{Y} &= \bar{C}\bar{X} + \bar{D}\bar{U} \end{aligned} \tag{4.98}$$

where $\bar{X} = [\eta_x \dot{\eta}_x \eta_y \dot{\eta}_y \psi \dot{\psi} x \dot{x} \vartheta \dot{\vartheta} y \dot{y}]$, $\bar{U} = [V_x \ V_y]$ and the parameter matrix are given as follows

$$\bar{A} = \begin{bmatrix} 0 & 1 & 0 & 0 & 0 & 0 & 0 & 0 & 0 & 0 & 0 & 0 \\ -\omega^2 & 0 & 0 & 0 & 0 & 0 & 1 & 0 & 0 & 0 & 0 & 0 \\ 0 & 0 & 0 & 1 & 0 & 0 & 0 & 0 & 0 & 0 & 0 & 0 \\ 0 & 0 & -\omega^2 & 0 & 0 & 0 & 0 & 0 & 0 & 0 & 1 & 0 \\ 0 & 0 & 0 & 0 & 0 & 1 & 0 & 0 & 0 & 0 & 0 & 0 \\ 0 & 0 & 0 & 0 & \frac{g}{l} & 0 & 0 & \frac{1}{l\tau_x} & 0 & 0 & 0 & 0 \\ 0 & 0 & 0 & 0 & 0 & 0 & 0 & 1 & 0 & 0 & 0 & 0 \\ 0 & 0 & 0 & 0 & 0 & 0 & 0 & \frac{-1}{\tau_x} & 0 & 0 & 0 & 0 \\ 0 & 0 & 0 & 0 & 0 & 0 & 0 & 0 & 0 & 1 & 0 & 0 \\ 0 & 0 & 0 & 0 & 0 & 0 & 0 & 0 & \frac{g}{l} & 0 & 0 & \frac{1}{l\tau_y} \\ 0 & 0 & 0 & 0 & 0 & 0 & 0 & 0 & 0 & 0 & 0 & 1 \\ 0 & 0 & 0 & 0 & 0 & 0 & 0 & 0 & 0 & 0 & 0 & \frac{-1}{\tau_y} \end{bmatrix} \quad \bar{B} = \begin{bmatrix} 0 & 0 \\ 0 & 0 \\ 0 & 0 \\ 0 & 0 \\ 0 & 0 \\ \frac{-K_x}{l\tau_x} & 0 \\ 0 & 0 \\ \frac{K_x}{\tau_x} & 0 \\ 0 & 0 \\ 0 & 0 \\ 0 & \frac{-K_y}{l\tau_y} \\ 0 & 0 \\ 0 & \frac{K_y}{\tau_y} \end{bmatrix}$$

$$\bar{C} = \begin{bmatrix} 0 & 0 & 0 & 0 & 1 & 0 & 0 & 0 & 0 & 0 & 0 & 0 \\ 0 & 0 & 0 & 0 & 0 & 0 & 1 & 0 & 0 & 0 & 0 & 0 \\ 0 & 0 & 0 & 0 & 0 & 0 & 0 & 0 & 1 & 0 & 0 & 0 \\ 0 & 0 & 0 & 0 & 0 & 0 & 0 & 0 & 0 & 0 & 1 & 0 \end{bmatrix} \quad \text{and} \quad \bar{D} = \begin{bmatrix} 0 & 0 \\ 0 & 0 \\ 0 & 0 \\ 0 & 0 \end{bmatrix}.$$

When the new system (4.98) is obtained, the LQR method is applied to calculate the gain matrixes K_{η_x} , K_{η_y} and K_x . For computing the gain matrixes, the matrixes Q and R are specified as $\text{diag}\{10, 0, 10, 0, 1, 0, 1, 0, 1, 0, 1, 0\} \times 10^3$ and $\text{diag}\{0.0038, 0.0038\}$ respectively. The control structure is shown in Figure 4.19. And the gain matrixes are obtained as follows

$$K_x = \begin{bmatrix} -1429 & -298.24 & -972.34 & -524.4 & 0 & 0 & 0 & 0 \\ 0 & 0 & 0 & 0 & -1343.3 & -277.6 & -964.18 & -510.34 \end{bmatrix},$$

$$K_{\eta_x} = [1273.6 \quad -502.36] \quad \text{and} \quad K_{\eta_y} = [1241 \quad -522.4]. \quad (4.99)$$

4.2.2.4 Non-linear Controller & MRAC for Output Tracking

This control design is the combination between non-linear control in Chapter 4.1.1 and MRAC for output tracking in Chapter 4.1.2.2. Like the MRAC for output tracking design, the controlled system or plant has to satisfy the strictly positive real (ASPR) condition. But the system of 3D inverted pendulum doesn't content ASTR condition. For this reason the non-linear control will be used to cancel the non-linearity of 3D inverted pendulum and transform

the non-linear system into the new equivalent linear system that satisfies ASPR condition. Then MRAC for output tracking is designed in order that the position of the cart is controlled to follow the output of the reference model. Its control structure is shown in Figure 4.20.

For the non-linear control design for the regulation problem in Chapter 4.2.1.3 is referred. Then the new inputs v_x and v_y in Equations (4.60) and (4.63) are designed using MRAC for output tracking. The reference systems of both xz - and yz -planes are selected from the minimum ITAE standard forms for a zero steady-state ramp error with below system matrixes as follows

$$A_m = \begin{bmatrix} 0 & 1 \\ -\omega_n^2 & -3.2\omega_n \end{bmatrix}, B_m = \begin{bmatrix} 0 \\ 1 \end{bmatrix}, C_m = [1 \ 0] \text{ and } D_m = 0. \quad (4.100)$$

Referring to Equation (4.28), thus the control law along x -axis is obtained as follows

$$v_x(t) = K_x(t) \begin{bmatrix} x_m(t) \\ \dot{x}_m(t) \\ x_m(t) \end{bmatrix} + K_{rx}(t)r_x(t) + K_{ex}(t)e_x(t) \quad (4.101)$$

where $e_x(t) = x_m(t) - x(t)$.

Referring to Equation (4.30), the adaptive law is obtained as follows

$$\begin{bmatrix} K_x(t) \\ K_{rx}(t) \\ K_{ex}(t) \end{bmatrix} = e_x(t) \begin{bmatrix} x_m(t) \\ \dot{x}_m(t) \\ x_m(t) \\ r_x(t) \\ e_x(t) \end{bmatrix} \bar{T} + \int_{t_0}^t e(t) \begin{bmatrix} x_m(t) \\ \dot{x}_m(t) \\ r_x(t) \\ e_x(t) \end{bmatrix} T d\tau. \quad (4.102)$$

Therefore the control law along y -axis is obtained as follows

$$v_y(t) = K_y(t) \begin{bmatrix} y_m(t) \\ \dot{y}_m(t) \\ y_m(t) \end{bmatrix} + K_{ry}(t)r_y(t) + K_{ey}(t)e_y(t) \quad (4.103)$$

where $e_y(t) = y_m(t) - y(t)$.

And the adaptive law along y -axis is obtained as follows

$$\begin{bmatrix} K_y(t) \\ K_{ry}(t) \\ K_{ey}(t) \end{bmatrix} = e_y(t) \begin{bmatrix} y_m(t) \\ \dot{y}_m(t) \\ r_y(t) \\ e_y(t) \end{bmatrix} \bar{T} + \int_{t_0}^t e_y(\tau) \begin{bmatrix} y_m(\tau) \\ \dot{y}_m(\tau) \\ r_y(\tau) \\ e_y(\tau) \end{bmatrix} T d\tau. \quad (4.104)$$

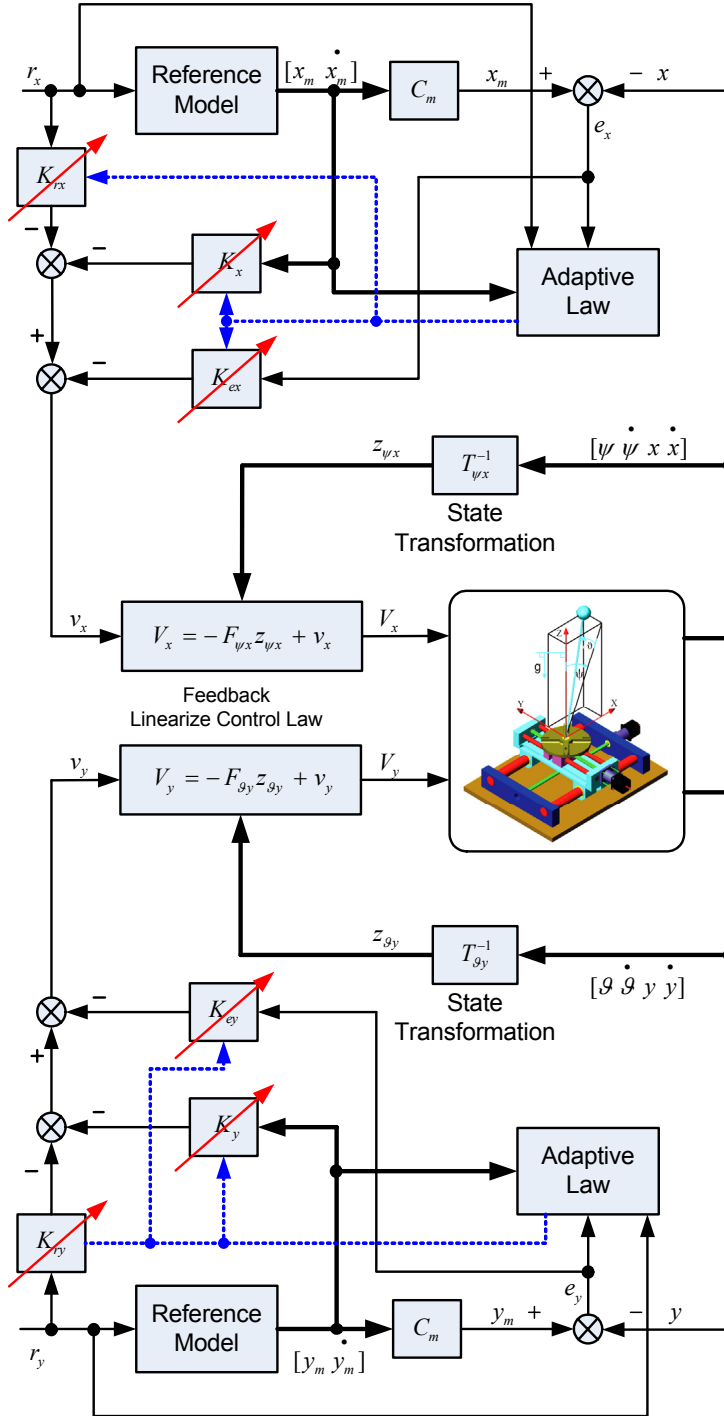


Figure 4.20 Non-linear control plus MRAC for output tracking for tracking problem

4.2.2.5 Simulation Results

For the simulation of tracking problem, the circular path is specified as the reference input for the cart which is given in Equations (4.94) and (4.95). The radius of the circle is specified to be a constant, 0.05 m . For the angular velocity ω , it is divided into two cases as follows: (1) constant angular velocity, $\omega = 2 \text{ rad/sec}$ (2) inconstant angular velocity, $\omega = 0.01(t-30) + 0.5 \text{ rad/sec}$. For the first case the constant angular velocity means that the cart will track the circular path with the constant velocity and for the inconstant angular velocity the cart follows the circular path with the various velocity. Therefore, the simulation of this problem will be divided into two cases as the angular velocity. The reference inputs along x - and y -axes can be divided into 3 intervals as shown in Table 4.1.

Time [sec]	r_x [m]	r_y [m]
$0 \leq t \leq 10$	0	0
$10 < t \leq 30$	$0.01(t-10) \leq R$	0
$t > 30$	$R \cos(\omega(t-30))$	$R \sin(\omega(t-30))$

Table 4.1 Reference inputs along x - and y -axes

At $0 \leq t \leq 10 \text{ sec}$, the pendulum will be stabilized and the cart will be maintained at the middle of the table. After that at $10 < t \leq 30 \text{ sec}$, the cart will move to a point which its coordinate is $(R, 0)$ in order to prepare the cart to track the circular path. When $t > 30 \text{ sec}$, the cart tracks the circular path while the pendulum is stabilized.

The controllers designed in Chapter 4.2.2.1-4 are provided to illustrate the performance of each controller which the initial conditions and some dynamic equation parameters of the system are the same as in Chapter 4.2.1.5.

For the state feedback the feedback gain matrix (4.47) and the estimator gain matrix (4.48) and the gain matrix K_r computed from Equation (4.78), $K_r = [K_x(1,3) \ K_x(2,7)]$, are used to simulate.

For MRAC using full state feedback, the adaptive laws (4.85)-(4.88) and (4.90)-(4.93) and the control laws (4.81) and (4.89) are applied to simulate 3D inverted pendulum with ω_n of the reference model $= 20 \text{ rad/sec}$. The matrix $[\gamma \ \gamma_1 \ \gamma_2]$ for the cart position on xz - and yz -planes are $[3 \ 3 \ 3] \times 10^4$ and $[\gamma \ \gamma_1 \ \gamma_2]$ for the inclination angle are $[2 \ 2 \ 2] \times 10^4$.

For the robust tracking control, the gain matrixes (4.99) and the estimator gain matrix (4.48) are used to control the pendulum.

For the non-linear control plus MRAC using output tracking, the state transformation matrixes (4.57) and (4.62) are used to transform the state to the new states $z_{\psi x}$ and $z_{\psi y}$. The linearizing control laws (4.60) and (4.63) are used to linearize the non-linear model of 3D

inverted pendulum to the linear model with $\omega_n = 5.8 \text{ rad/sec}$ and stabilize 3D inverted pendulum. The adaptive laws (4.102) and (4.104) and the control laws (4.101) and (4.103) are used to adapt the gain matrixes in order that the cart position tracks the input reference with ω_n of the reference model = 20 rad/sec . For this case, the matrixes \bar{T} and T in the adaptive laws (4.102) and (4.104) are defined as $[2 \ 2 \ 2 \ 2] \times 10^4$ and $[3 \ 3 \ 3 \ 3] \times 10^4$ respectively.

Their simulation results are depicted in Figures 4.21-4.27 for the constant angular velocity case and Figures 4.28-4.34 for the inconstant angular velocity case.

For constant angular velocity case, Figures 4.21-4.22 illustrate the responses of the inclination angle versus time and it can be seen that every controllers can first stabilize the pendulum. The oscillation of the inclination angle ψ occurs at $10 \leq t \leq 22 \text{ sec}$ in Figure 4.21 because the cart is moving to the right of the table. And since $t > 30 \text{ sec}$ the both of the inclination angles ψ and ϑ can not be zero move as sinusoidal curve because of the movement of the cart as a circle. Consequencely, the centrifugal force will occur and effect on the pendulum. If the cart moves as a circle with high speed, the effect of the centrifugal force to the inclination angle of the pendulum will be more than with low speed.

Figures 4.23-4.24 show the responses of the cart position versus time. From them, it can be observed that only the robust tracking controller can track a circular reference input. However the robust tracking controller is ineffective to track the other reference input as shown in Figure 4.23 at $10 \leq t \leq 30 \text{ sec}$ because its servo-compensators are designed for only the circular reference input. Since MRAC using full state feedback and non-linear control plus MRAC for output tracking are designed to follow the output of the reference model. Although they are ineffective to track the circular reference input, they are very successful to adapt the control gains in order to converge the position of the cart to the output of the reference model. For the state feedback controller, it can not achieve to track the circular reference input.

Figure 4.25 shows the responses of the cart position on xy -plane and the control inputs are presented in Figures 4.26-4.27.

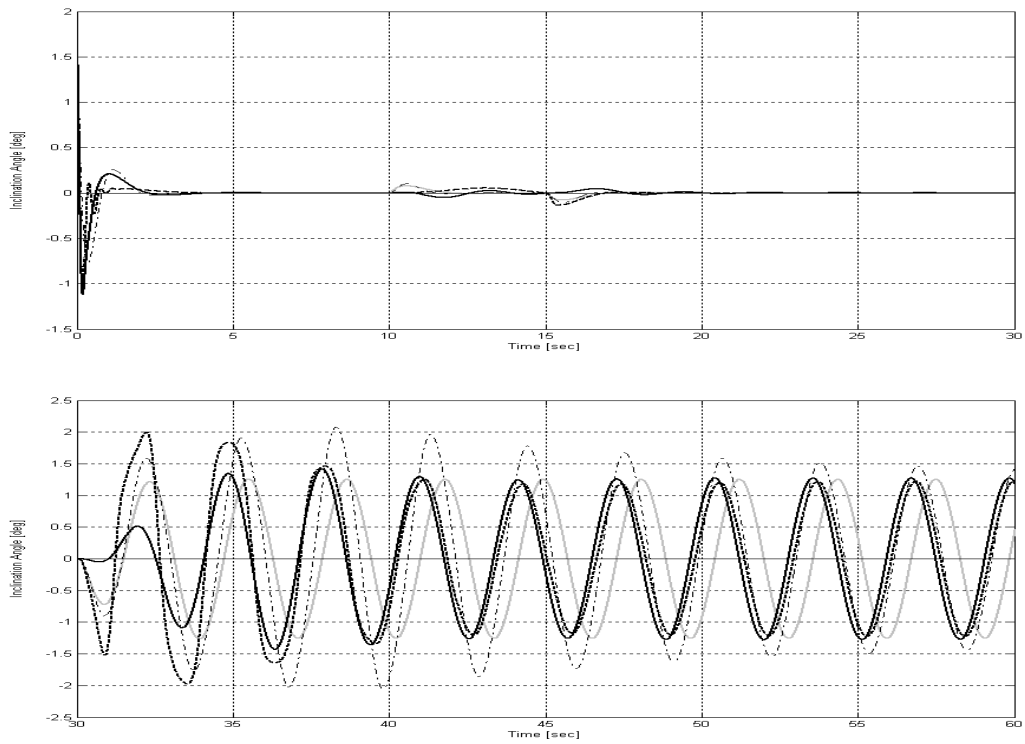


Figure 4.21 Comparison of the simulation responses of the inclination angle ψ for constant angular velocity case of tracking problem

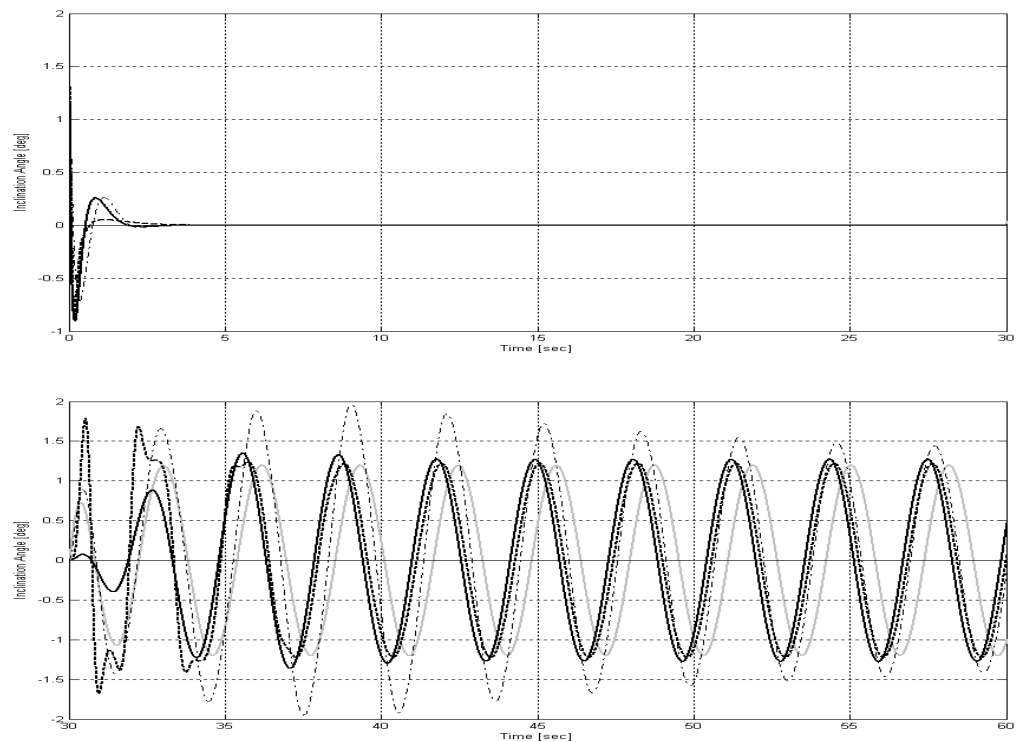


Figure 4.22 Comparison of the simulation responses of the inclination angle θ for constant angular velocity case of tracking problem
 (— : State Feedback, — : Robust Tracking, - - : MRAC, : Non-linear-MRAC and — : Reference Path)

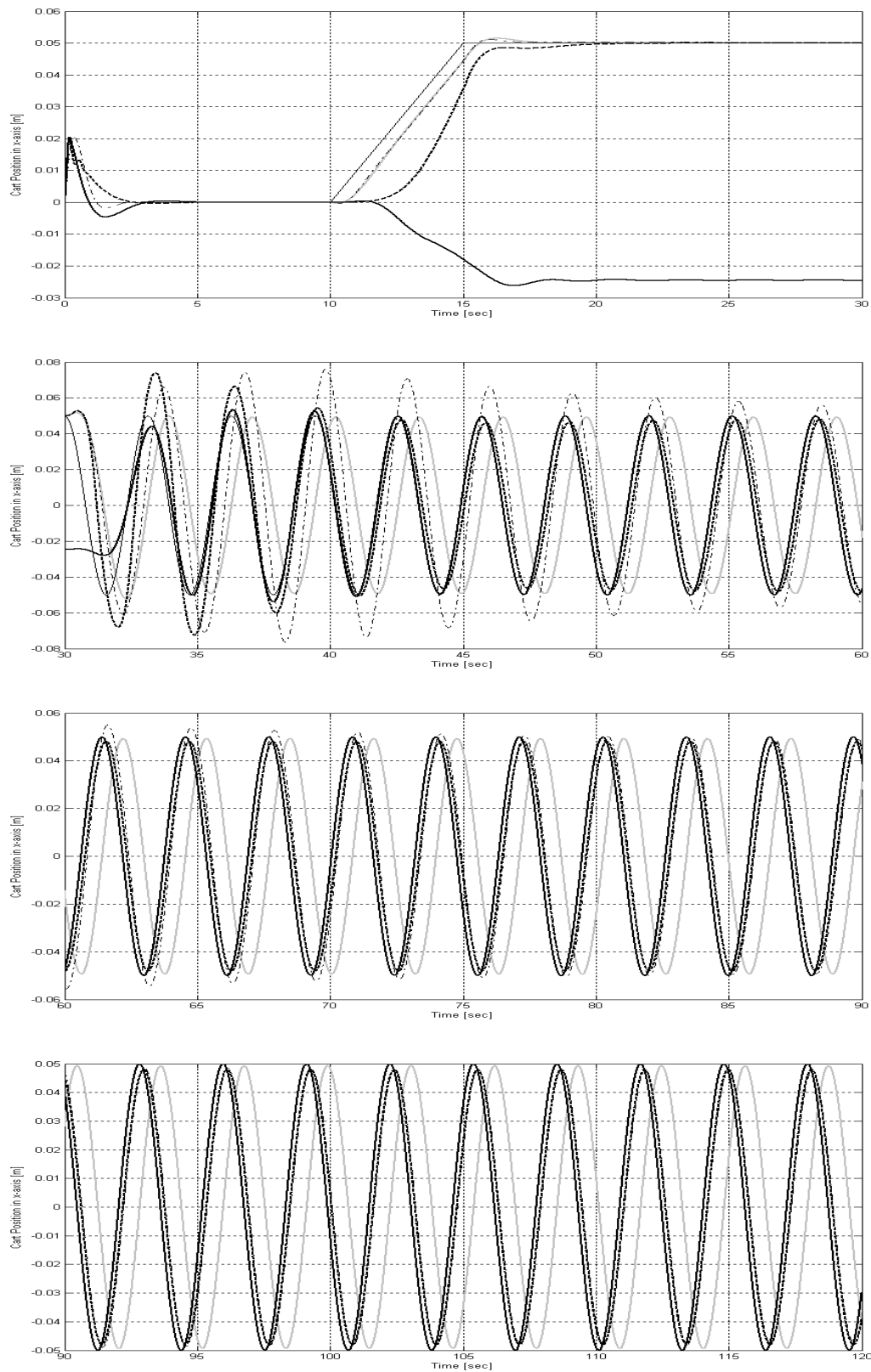


Figure 4.23 Comparison of the simulation responses of the cart position x for constant angular velocity case of tracking problem
 (— : State Feedback, — : Robust Tracking, - - : MRAC, ···· : Non-linear-MRAC and — : Reference Path)

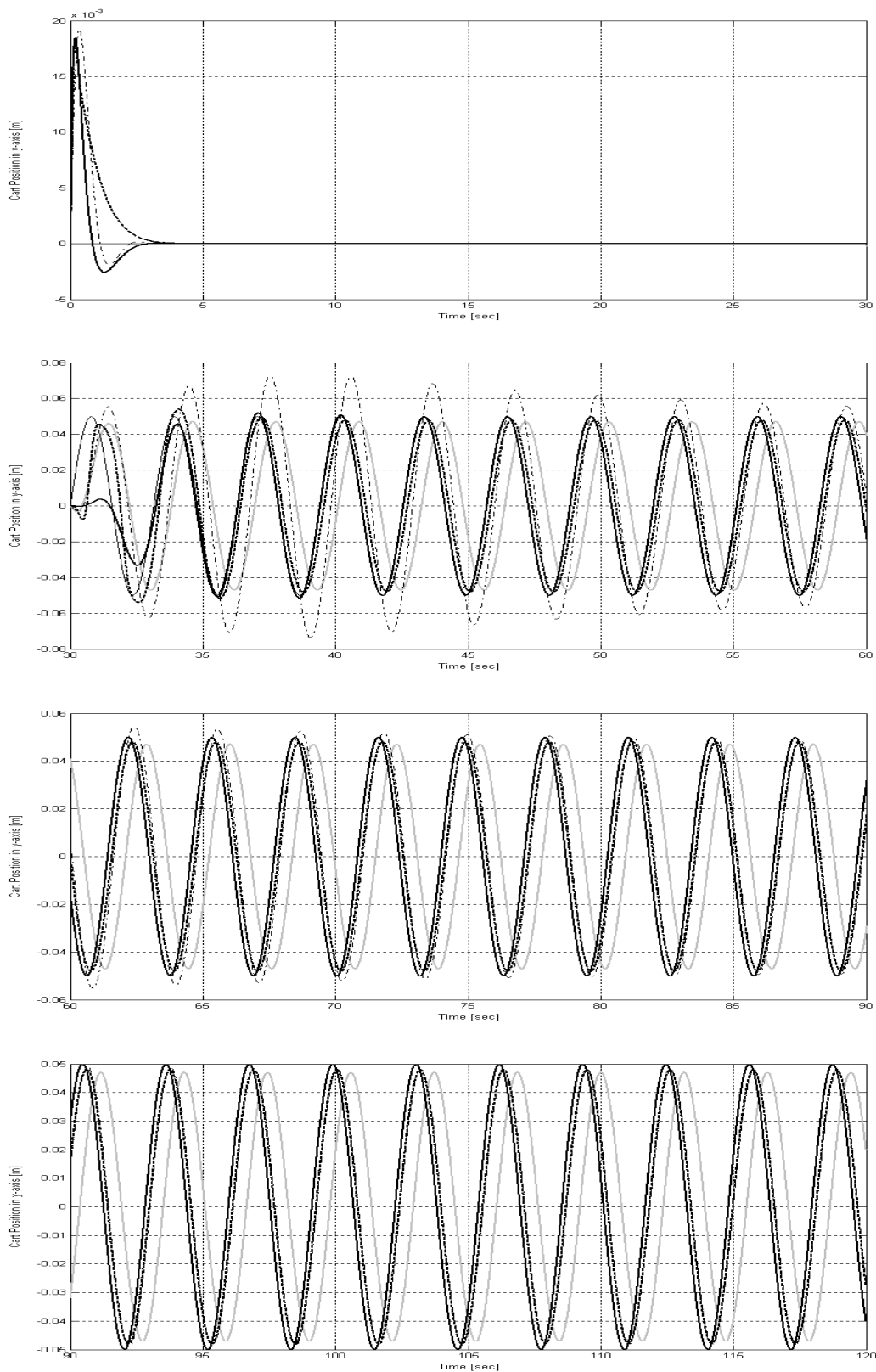


Figure 4.24 Comparison of the simulation responses of the cart position y for constant angular velocity case of tracking problem (— : State Feedback, — : Robust Tracking, - . - : MRAC, : Non-linear-MRAC and — : Reference Path)

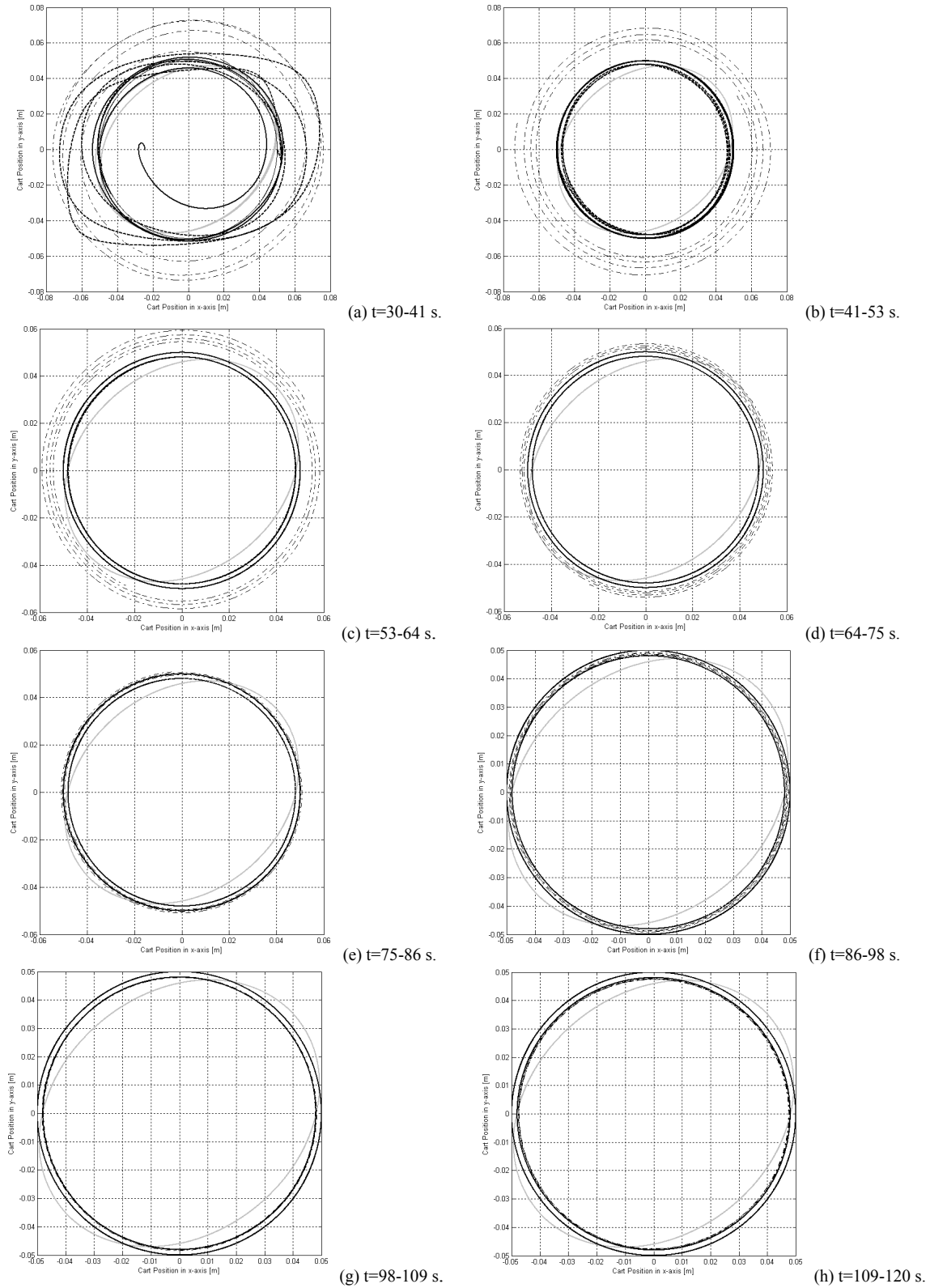


Figure 4.25 Comparison of the simulation responses of the cart position on xy -plane for constant angular velocity case of tracking problem
 (— : State Feedback, — : Robust Tracking, - - - : MRAC, : Non-linear-MRAC and : Reference Path)

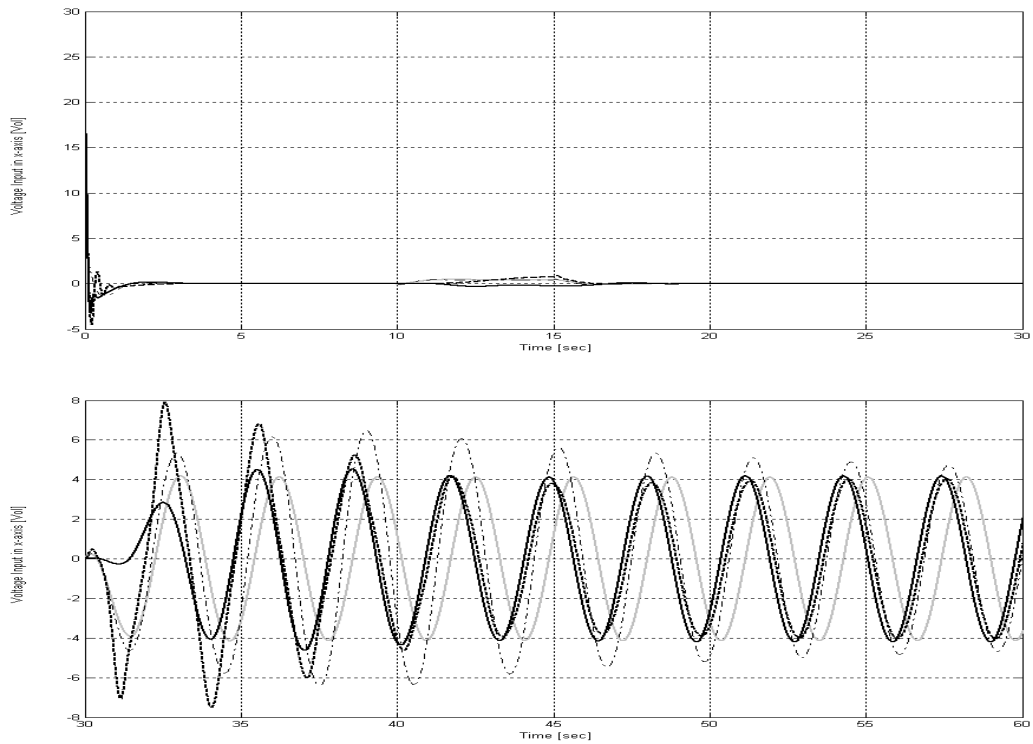


Figure 4.26 Comparison of the simulation responses of the control signal along x -axis for constant angular velocity case of tracking problem

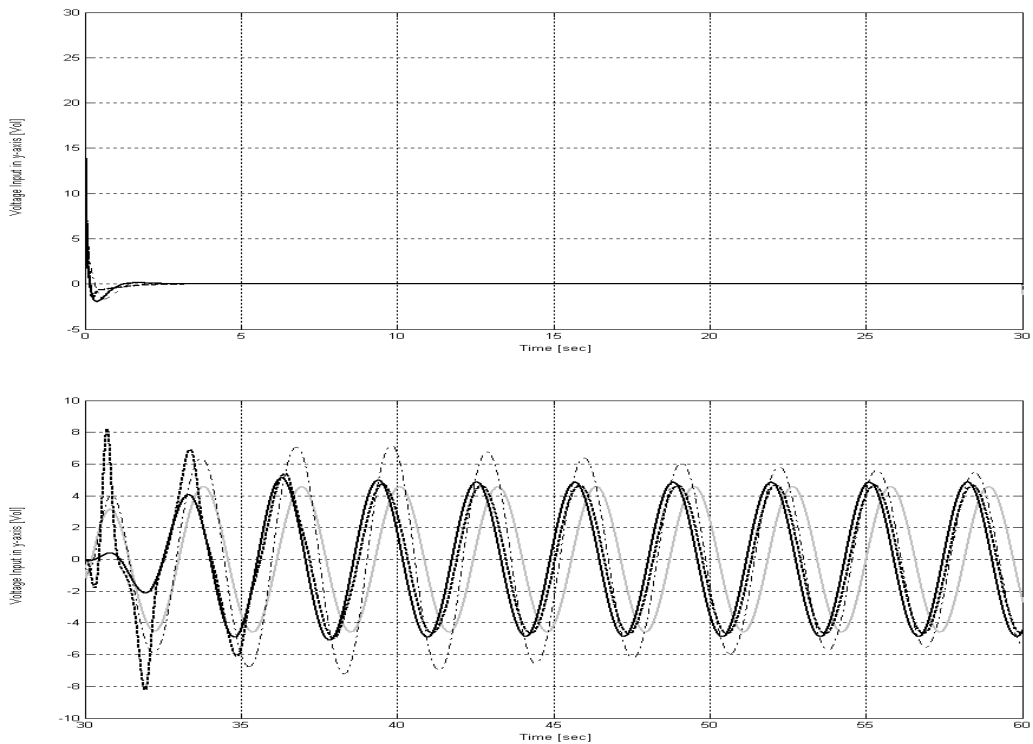


Figure 4.27 Comparison of the simulation responses of the control signal along y -axis for constant angular velocity case of tracking problem
 (— : State Feedback, - - - : Robust Tracking, . . . : MRAC and - . . . : Non-linear-MRAC)

In case of the inconstant angular velocity, the responses of the inclination angle and the position of the cart are represented in Figures 4.28-4.29 and Figures 4.30-4.31 respectively.

From Figures 4.28-4.29, it can be seen that the oscillation of both inclination angles will diverge from zero. That means, if 3D inverted pendulum is controlled longer than 120 sec. The pendulum is probably unstable.

From Figures 4.30-4.31, the robust tracking controller isn't successful to track the circular reference input since its servo-compensators are designed for only the constant angular velocity. But MRAC using full state feedback and non-linear control plus MRAC for output tracking can still achieve goal to adapt their control gains in order to converge the position of the cart to the output of the reference model. For the state feedback controller, it can not still achieve to track the circular reference input like the case of the constant angular velocity.

Figure 4.32 illustrates the cart position on xy -plane. The control inputs in each axis are given in Figures 4.33-4.34.

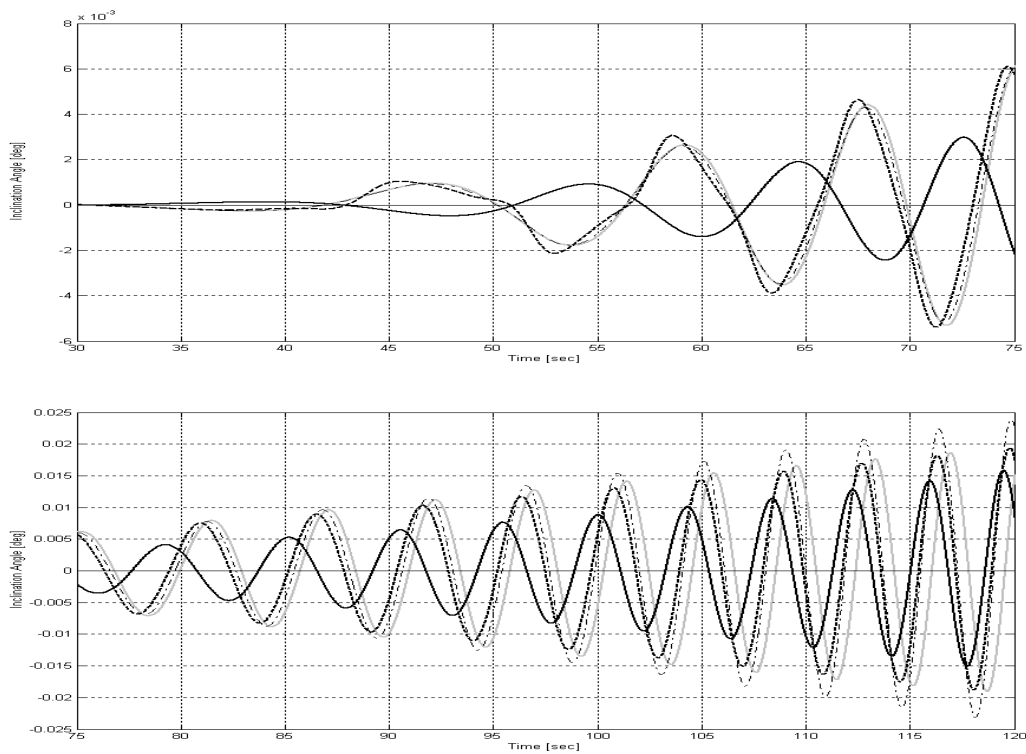


Figure 4.28 Comparison of the simulation responses of the inclination angle ψ for inconstant angular velocity case of tracking problem

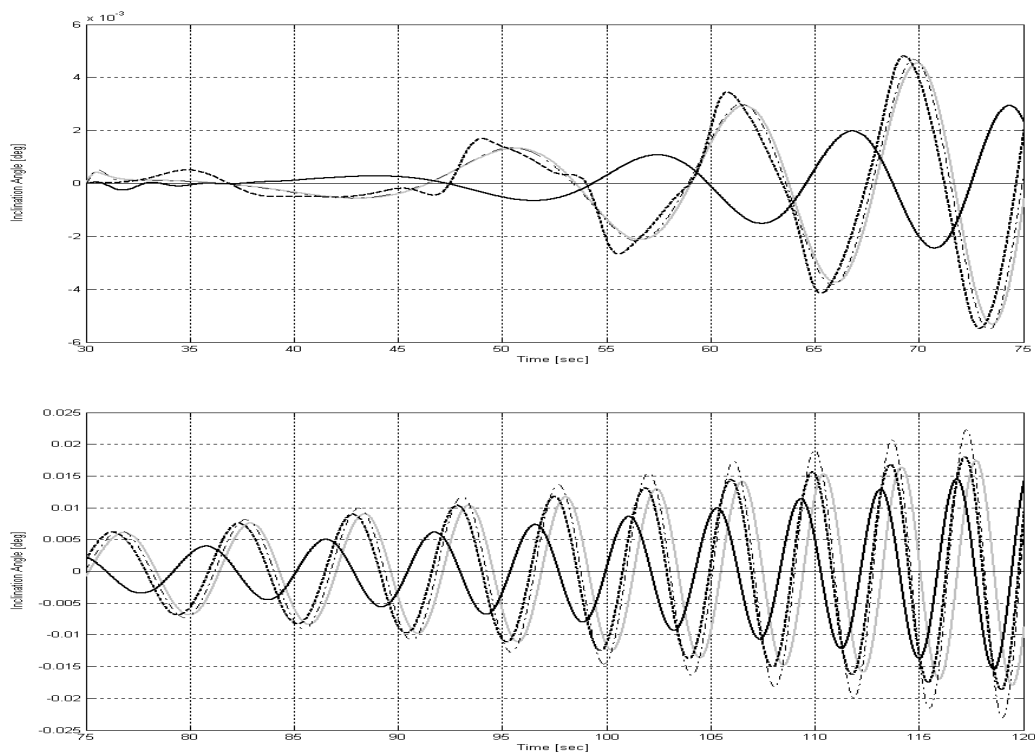


Figure 4.29 Comparison of the simulation responses of the inclination angle ϱ for inconstant angular velocity case of tracking problem
 (— : State Feedback, — : Robust Tracking, - - - : MRAC, : Non-linear-MRAC and — : Reference Path)

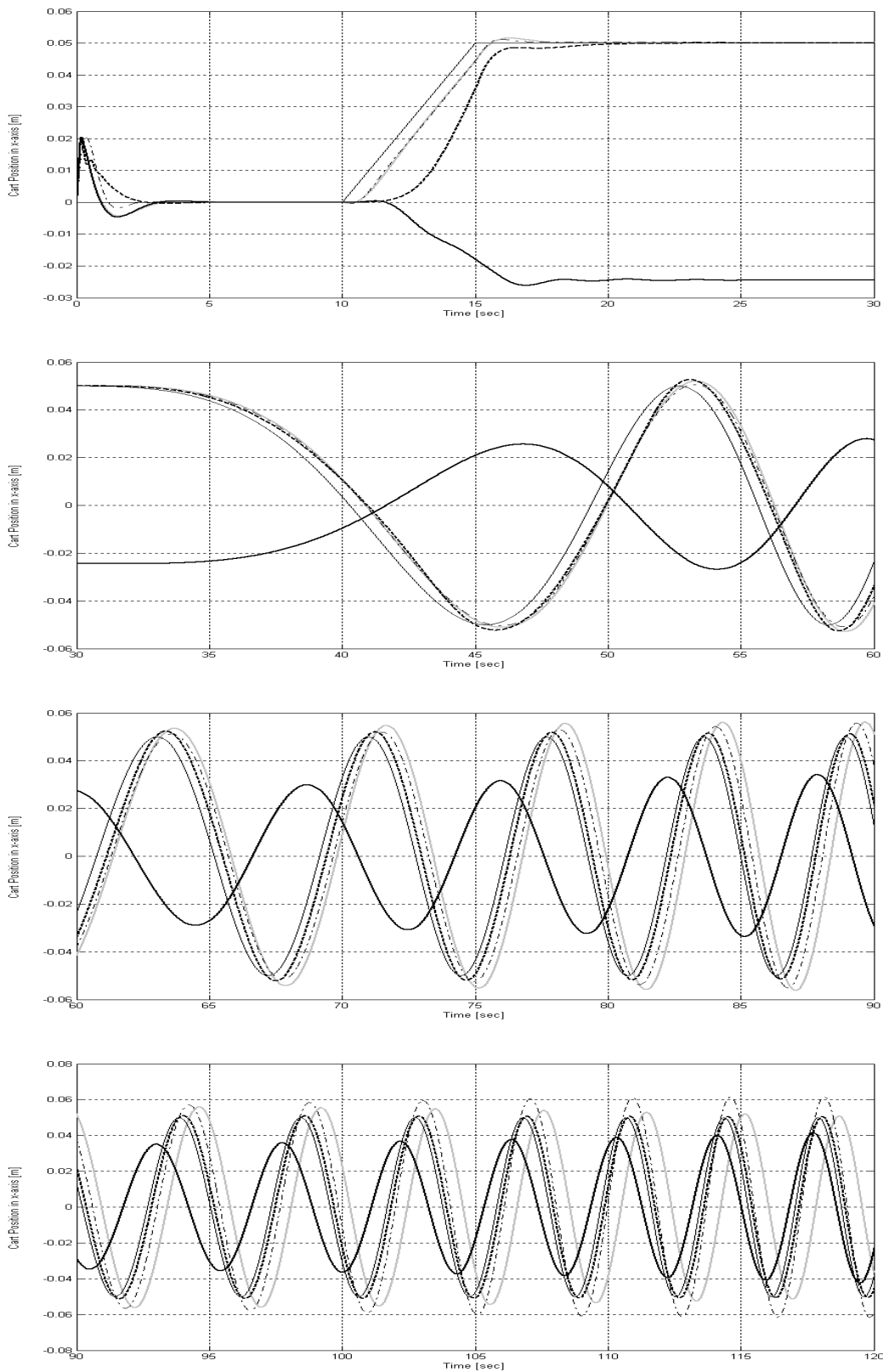


Figure 4.30 Comparison of the simulation responses of the cart position x for inconstant angular velocity case of tracking problem
 (— : State Feedback, — : Robust Tracking, - - - : MRAC, ···· : Non-linear-MRAC and — : Reference Path)

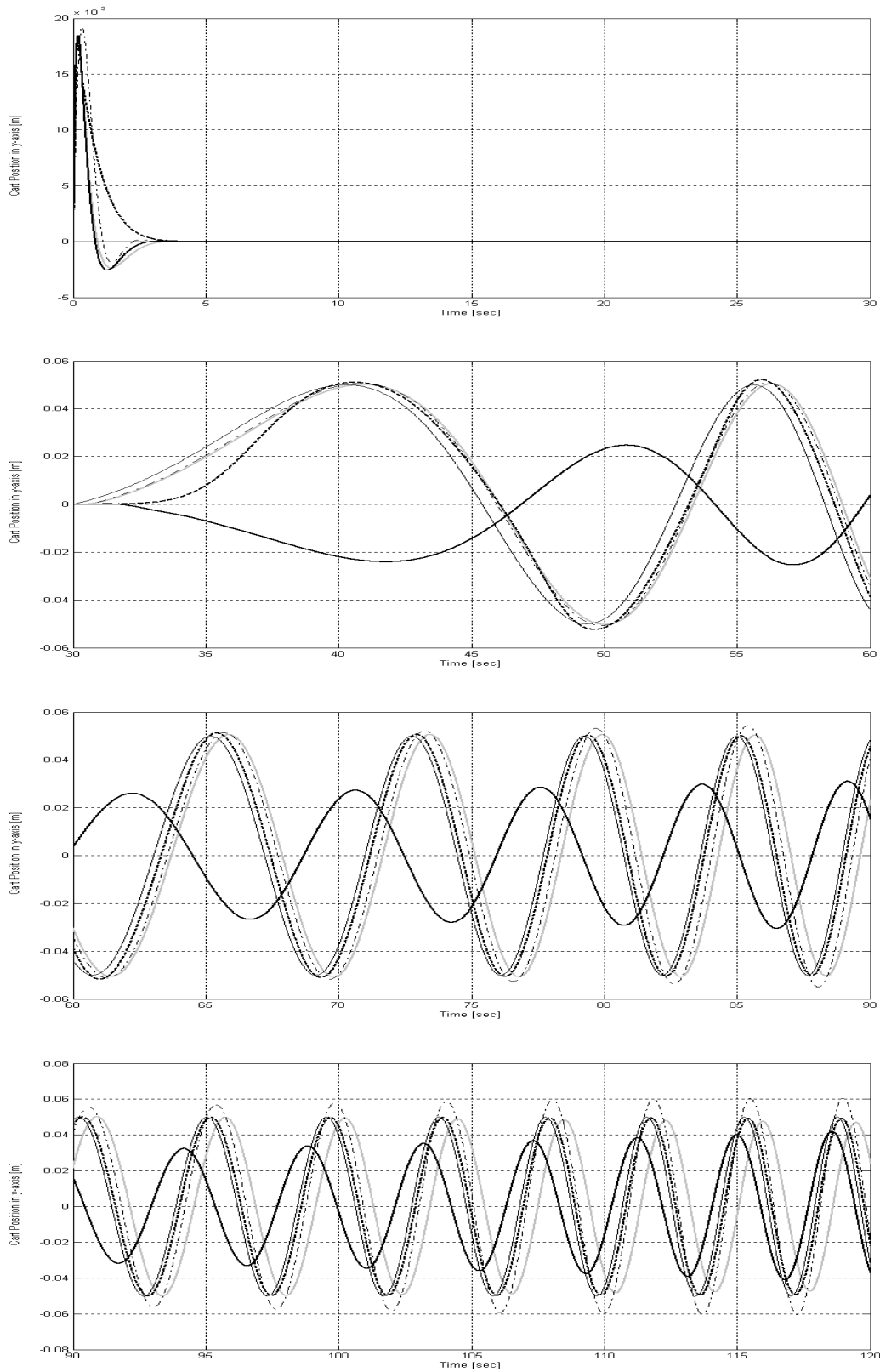


Figure 4.31 Comparison of the simulation responses of the cart position y for inconstant angular velocity case of tracking problem (— : State Feedback, — : Robust Tracking, - - - : MRAC,: Non-linear-MRAC and — : Reference Path)

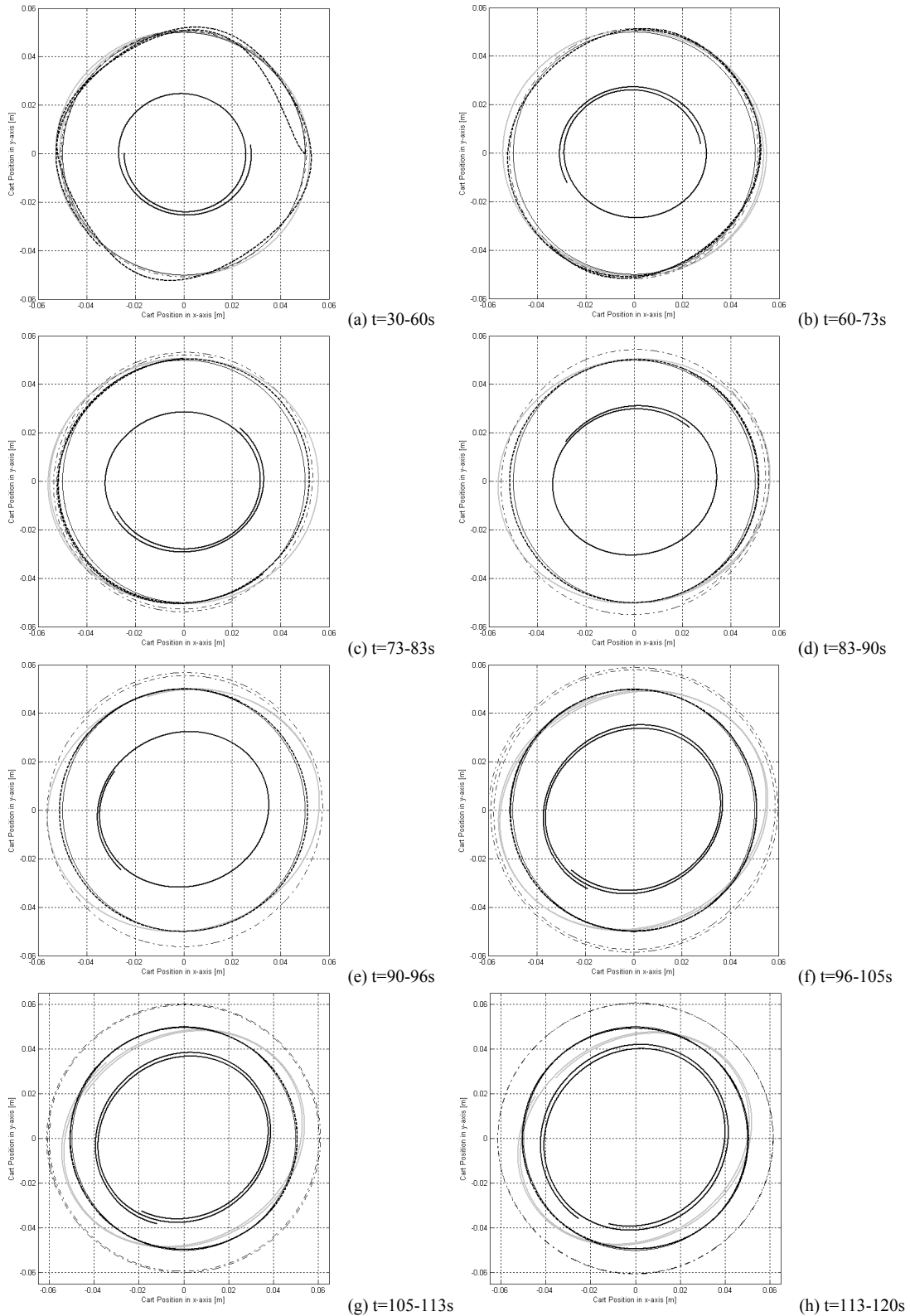


Figure 4.32 Comparison of the simulation responses of the cart position on xy -plane for inconstant angular velocity case of tracking problem
 (— : State Feedback, — : Robust Tracking, - - : MRAC, : Non-linear-MRAC and — : Reference Path)

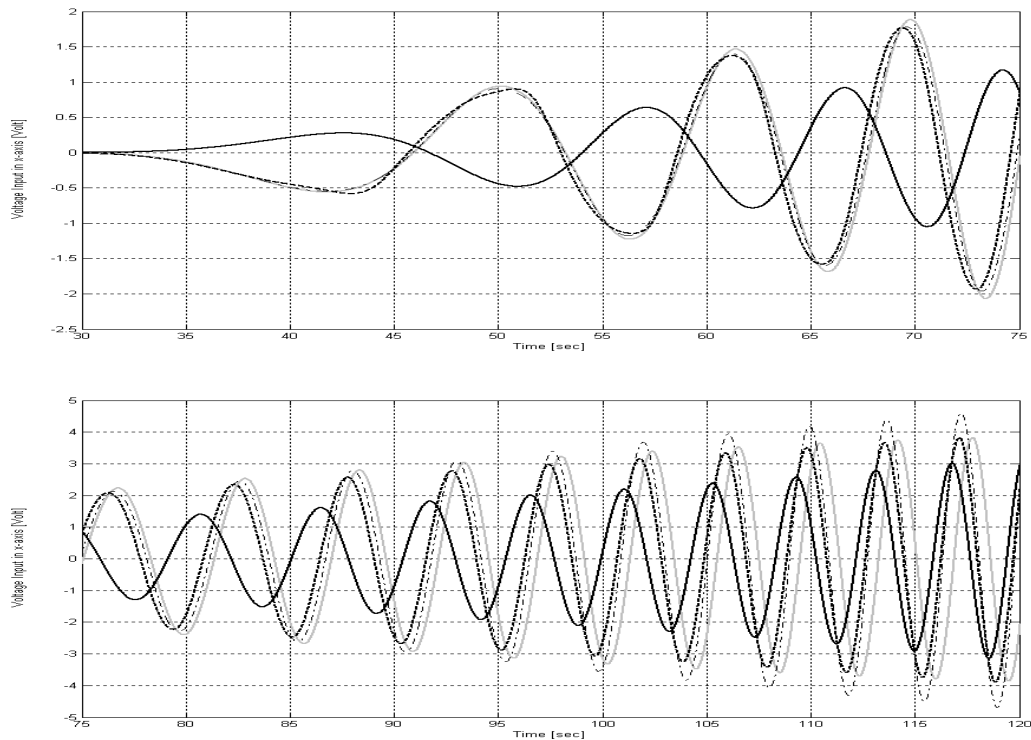


Figure 4.33 Comparison of the simulation responses of the control signal along x -axis for inconstant angular velocity case of tracking problem

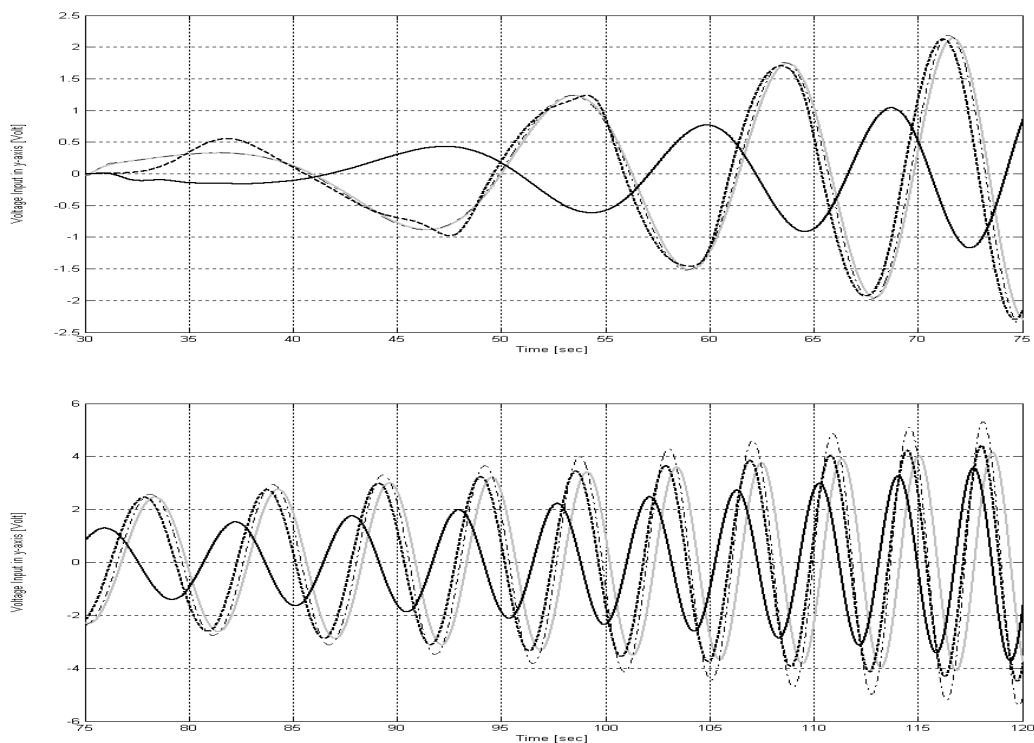


Figure 4.34 Comparison of the simulation responses of the control signal along y -axis for inconstant angular velocity case of tracking problem
 (— : State Feedback, - - - : Robust Tracking, . . . : MRAC and - . - . : Non-linear-MRAC)

Chapter 5

Experiments and Results

This chapter contains a process of the camera calibration, which the direction of the optical axis of the camera isn't parallel to the gravitation in Chapter 5.1. In Chapter 5.2, the controllers designed in Chapter 4.2 are coded in MATLAB/Simulink and integrated with a C-Mex file developed by Visual C++ in order to perform the experiments and their results will be also illustrated and discussed .

5.1 Camera Calibration

The previous research for 3D inverted pendulum at IMR [Bro06] had presented a process for calibrating the camera. In this process the direction of the optical axis of the camera must be exactly parallel to the gravitation. In this research a calibration of the camera, which the direction of the optical axis of the camera isn't parallel to the gravitation, will be proposed. This calibration of a camera will establish a relationship between 2D image coordinates and 3D world coordinates. This relationship between the 2D image coordinates and 3D world coordinates is determined by solving the unknown parameters of a camera model. The camera model used in this research is the pin-hole model [Hor96]. The pin-hole model is described by the following equations.

$$U = \frac{N_{UX}X + N_{UY}Y + N_{UZ}Z + N_U}{D_XX + D_Y Y + D_Z Z + D} \quad (5.1)$$

$$V = \frac{N_{VX}X + N_{VY}Y + N_{VZ}Z + N_V}{D_XX + D_Y Y + D_Z Z + D} \quad (5.2)$$

where X , Y , and Z are the 3D world coordinates of a point, U and V are the 2D image coordinates of its projection onto the camera view and N_{UX} , N_{UY} , N_{UZ} , N_U , N_{VX} , N_{VY} , N_{VZ} , N_V , D_X , D_Y , D_Z and D are the unknown parameters of the pin-hole model.

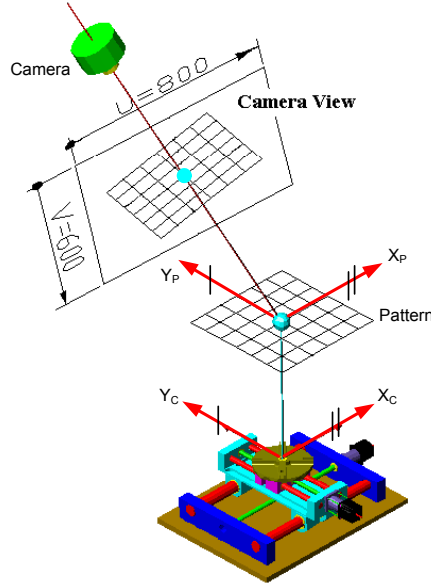


Figure 5.1 Camera Calibration

Equations (5.1) and (5.2) describe the projection of a point defined in 3D world coordinates onto an image. In this research these equations will be used to establish a relationship between the coordinates X , Y , and Z and the coordinates U and V of the ball at the end of the pendulum. Since it is necessary to use the position of the ball in 3D world coordinates to calculate the inclination angle of 3D inverted pendulum, the position of the ball in 3D world coordinates is computed by inverse mapping of Equations (5.1) and (5.2) as follows

$$X = \frac{N_{XU}U + N_{XV}V + N_X}{D_U U + D_V V + 1} \quad (5.3)$$

$$Y = \frac{N_{YU}U + N_{YV}V + N_Y}{D_U U + D_V V + 1} \quad (5.4)$$

$$Z = \frac{N_{ZU}U + N_{ZV}V + N_Z}{D_U U + D_V V + 1} \quad (5.5)$$

where N_{XU} , N_{YU} , N_{ZU} , N_{XV} , N_{YV} , N_{ZV} , N_X , N_Y , N_Z , D_U and D_V are the unknown parameters of inverse mapping of the pin-hole model.

Since the range of inclination angles ψ and ϑ of 3D inverted pendulum is $\pm 5^\circ$ near the steady balanced position, the variation of the coordinate Z of 3D inverted pendulum is less than 0.5%. Therefore, it can be assumed that the coordinate Z of 3D inverted pendulum is kept constant and set to be zero in this research. The equations used to compute the position of 3D inverted pendulum are only Equations (5.3) and (5.4).

In Equations (5.3) and (5.4) there are 8 unknown parameters: N_{XU} , N_{XV} , N_X , N_{YU} , N_{YV} , N_Y , D_U and D_V . The problem is how to determine these unknown parameters. So the non-linear least squares are used to estimate these unknown parameters with helping of the optimization toolbox of MATLAB software that minimize the sum of the squared differences between the measured and estimated data.

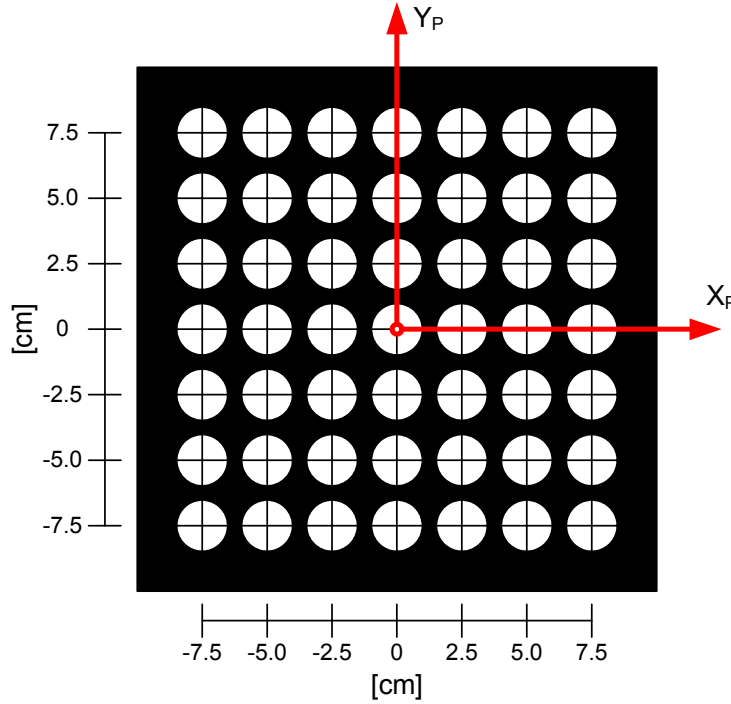


Figure 5.2 A planar model object or pattern

Because of 8 unknown parameters, it needs at least 8 sets of the measured data of the coordinates X , Y , U and V in order to estimate these unknown parameters. However in this research 49 sets of the measured data, which the range in 3D world coordinates is ± 7.5 cm. of x - and y -axes, are used to estimate these unknown parameters by capturing 49 circles on a planar model object or pattern, which is placed on the top of the case of the cart or the level of the ball, the x -axis of the pattern has to parallel to the x -axis of the cart and the center of the pattern must be the same center of the case of the cart, and calculating their centers as the measured data. This pattern is shown in Figure 5.2.

The mathematical models of 3D inverted pendulum in Chapter 3 have some parameters that influence to 3D inverted pendulum such as the inclination angles θ and γ of the camera and the inclination angles α and β of the table. The inclination angles θ and γ of the camera can be eliminated in the camera calibration process. The coordinates U_i and V_i used to estimate the unknown parameters are given by

$$U_i = u_i - u_p + u_b \quad (5.6)$$

$$V_i = v_i - v_p + v_b \quad ; i = 1, 2, \dots 49. \quad (5.7)$$

where u_i and v_i are the measured data of the center of 49 circles on the pattern. u_p and v_p are the measured data of the ball which is perpendicular to the table. u_b and v_b are the measured data of the ball which is parallel to the gravity. And U_i and V_i are the data used to estimate the unknown parameters in Equations (5.3) and (5.4).

Equations (5.6) and (5.7) are the translation of the pattern to a location that the coordinates X and Y of the circle, which is at the middle of the pattern, are the same as the coordinates X and Y of the table in 3D world coordinates in order to eliminate the inclination angle θ and γ of the camera from the system. The Figure 5.3 shows the description of the coordinates U and V in camera calibration process. The camera calibration will be performed every time when the position of the camera or the inclination angle of the camera and table is changed. The algorithm for camera calibration is shown as following.

1. Move the cart to the middle of the table.
2. Measure u_p, v_p, u_b, v_b, u_i and v_i .
3. Calculate U_i and V_i with Equation 5.6 and 5.7.
4. Find 8 unknown parameters: $N_{XU}, N_{XV}, N_X, N_{YU}, N_{YV}, N_Y, D_U$ and D_V in Equations (5.3) and (5.4).

From the experiment, the comparison results of the measured and estimated the coordinates X and Y of the pattern are shown in Table 5.1. It shows that the mean square errors of the coordinates X and Y are 5.53×10^{-8} and 6.77×10^{-8} respectively and both of estimated coordinates X and Y have enough accuracy to be possible to control 3D inverted pendulum.

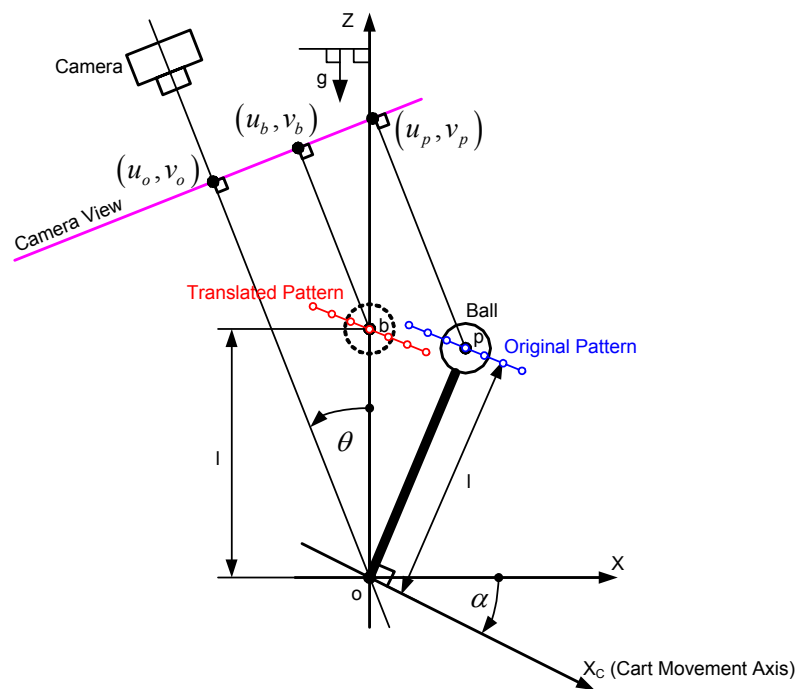


Figure 5.3 Description of the coordinates U and V in camera calibration process

No.	Measured Data X_i [m]	Estimated Data \hat{X}_i [m]	$\hat{X}_i - X_i$ [m]	Measured Data Y_i [m]	Estimated Data \hat{Y}_i [m]	$\hat{Y}_i - Y_i$ [m]
1	-0.075	-0.074946	0.000054	0.075	0.075163	0.000163
2	-0.050	-0.049788	0.000212	0.075	0.075304	0.000304
3	-0.025	-0.025099	-0.000099	0.075	0.074917	-0.000083
4	0.000	0.000172	0.000172	0.075	0.074532	-0.000468
5	0.025	0.025499	0.000499	0.075	0.074672	-0.000328
6	0.050	0.050354	0.000354	0.075	0.074809	-0.000191
7	0.075	0.075267	0.000267	0.075	0.074420	-0.000580
8	-0.075	-0.075014	-0.000014	0.050	0.049998	-0.000002
9	-0.050	-0.049814	0.000186	0.050	0.050111	0.000111
10	-0.025	-0.025084	-0.000084	0.050	0.050221	0.000221
11	0.000	-0.000300	-0.000300	0.050	0.050332	0.000332
12	0.025	0.024540	-0.000460	0.050	0.049915	-0.000085
13	0.050	0.049964	-0.000036	0.050	0.050028	0.000028
14	0.075	0.074381	-0.000619	0.050	0.050136	0.000136
15	-0.075	-0.075081	-0.000081	0.025	0.025275	0.000275
16	-0.050	-0.049839	0.000161	0.025	0.025360	0.000360
17	-0.025	-0.025068	-0.000068	0.025	0.025444	0.000444
18	0.000	-0.000242	-0.000242	0.025	0.024999	-0.000001
19	0.025	0.024637	-0.000363	0.025	0.025082	0.000082
20	0.050	0.050103	0.000103	0.025	0.025168	0.000168
21	0.075	0.074561	-0.000439	0.025	0.025249	0.000249
22	-0.075	-0.075149	-0.000149	0.000	-0.000058	-0.000058
23	-0.050	-0.049865	0.000135	0.000	-0.000001	-0.000001
24	-0.025	-0.025053	-0.000053	0.000	0.000055	0.000055
25	0.000	-0.000186	-0.000186	0.000	0.000111	0.000111
26	0.025	0.025266	0.000266	0.000	0.000169	0.000169
27	0.050	0.050243	0.000243	0.000	0.000225	0.000225
28	0.075	0.075279	0.000279	0.000	-0.000251	-0.000251
29	-0.075	-0.075216	-0.000216	-0.025	-0.024946	0.000054
30	-0.050	-0.050419	-0.000419	-0.025	-0.025448	-0.000448
31	-0.025	-0.025037	-0.000037	-0.025	-0.025419	-0.000419
32	0.000	-0.000128	-0.000128	-0.025	-0.025391	-0.000391
33	0.025	0.025367	0.000367	-0.025	-0.025362	-0.000362
34	0.050	0.050387	0.000387	-0.025	-0.025334	-0.000334
35	0.075	0.074923	-0.000077	-0.025	-0.024772	-0.000228
36	-0.075	-0.074756	0.000244	-0.050	-0.049916	0.000084
37	-0.050	-0.049916	0.000084	-0.050	-0.050447	-0.000447
38	-0.025	-0.025021	-0.000021	-0.050	-0.050447	-0.000447
39	0.000	-0.000072	-0.000072	-0.050	-0.049912	0.000088
40	0.025	0.024932	-0.000068	-0.050	-0.049911	0.000089
41	0.050	0.049991	-0.000009	-0.050	-0.049909	0.000091
42	0.075	0.075105	0.000105	-0.050	-0.049908	0.000092
43	-0.075	-0.074822	0.000178	-0.075	-0.074969	0.000031
44	-0.050	-0.049942	0.000058	-0.075	-0.074995	0.000005
45	-0.025	-0.025006	-0.000006	-0.075	-0.075022	-0.000022
46	0.000	-0.000015	-0.000015	-0.075	-0.075048	-0.000048
47	0.025	0.025030	0.000030	-0.075	-0.075075	-0.000075
48	0.050	0.050128	0.000128	-0.075	-0.074564	0.000436
49	0.075	0.074748	-0.000252	-0.075	-0.074590	0.000410

Table 5.1 Comparison of the measured and estimated results of the pattern

5.2 Control Experiments and Results

This section shows the experimental results of the proposed controllers in Chapter 4 on 3D inverted pendulum at the control laboratory of Institut für Mess- u. Regelungstechnik (IMR), Universität Hannover. For the equipments used in the practical experiments are represented in [Bro06]. The practical experiments will follow the simulations in Chapters 4.2.1.5 and 4.2.2.5 which all designed controllers will be performed in the experiments. Thus the practical experiments are divided into two parts such as regulation and tracking problem, as the simulations in Chapters 4.2.1.5 and 4.2.2.5.

5.2.1 Regulation Problem

For this problem, all simulated controllers, control gains and some parameters in Chapter 4.2.1.5 are performed in the experiment in order to stabilize 3D inverted pendulum and maintain the cart position at the middle of the table.

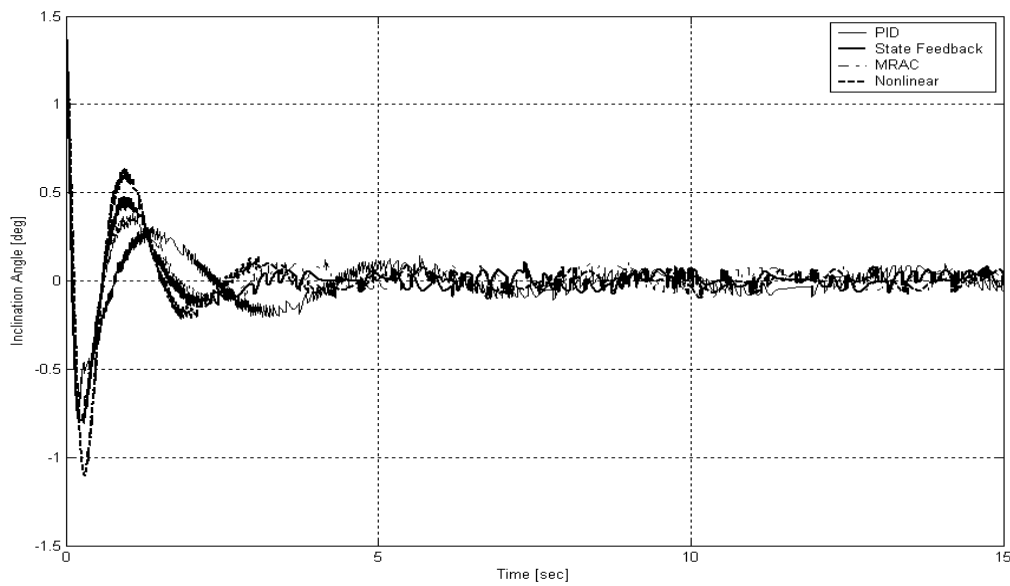


Figure 5.4 Comparison of the experimental responses of the inclination angle ψ for regulation problem

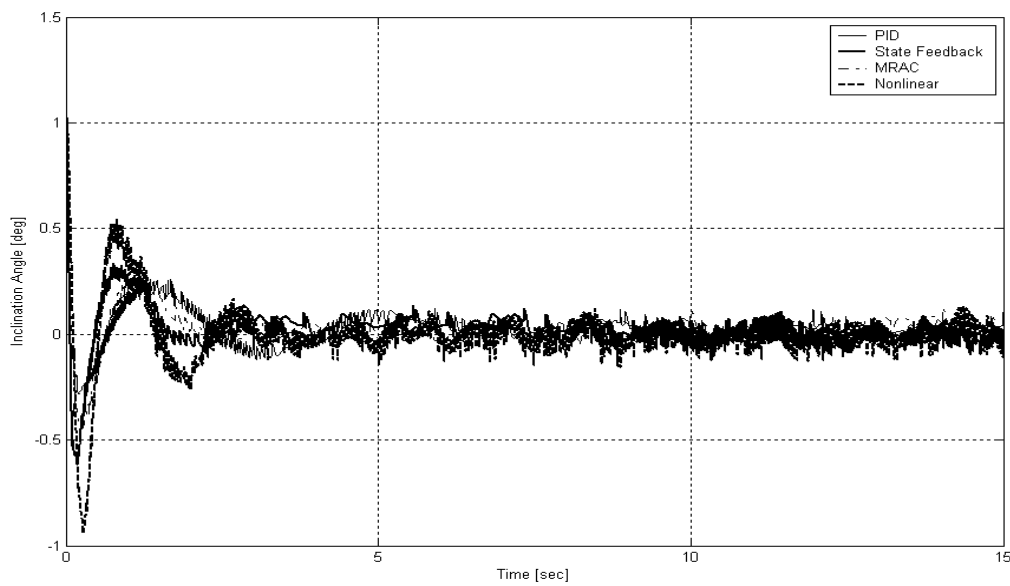


Figure 5.5 Comparison of the experimental responses of the inclination angle ϱ for regulation problem

Their experimental results are shown in Figures 5.4-5.9. Figures 5.4-5.5 are the responses of the inclination angles ψ and ϱ versus time during the experiment operation respectively. It can be seen that all proposed controllers can stabilize the pendulum. Note that the controller that gives the highest overshoot in the experiment is the non-linear control which it is different from the simulation.

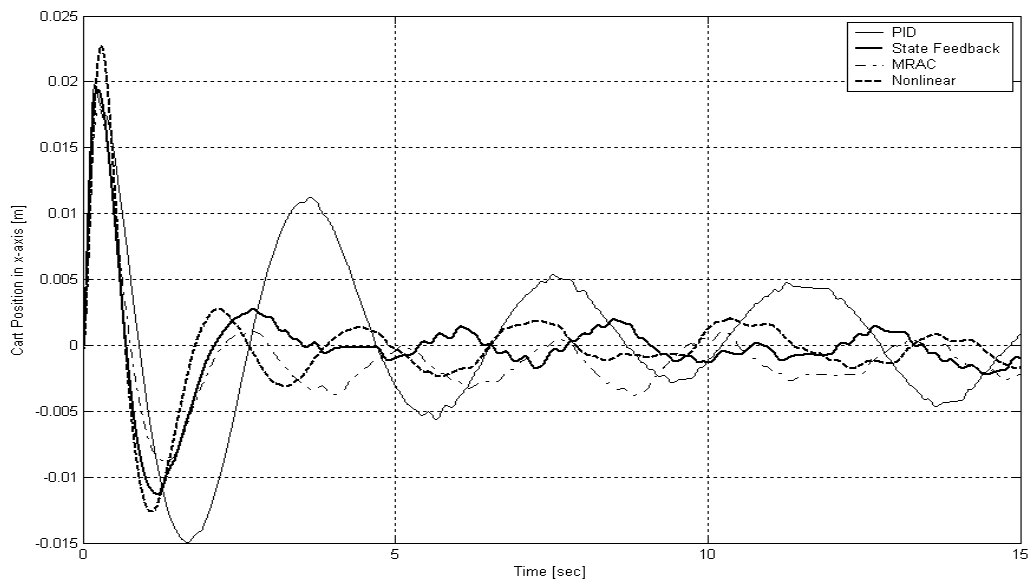


Figure 5.6 Comparison of the experimental responses of the cart position x for regulation problem

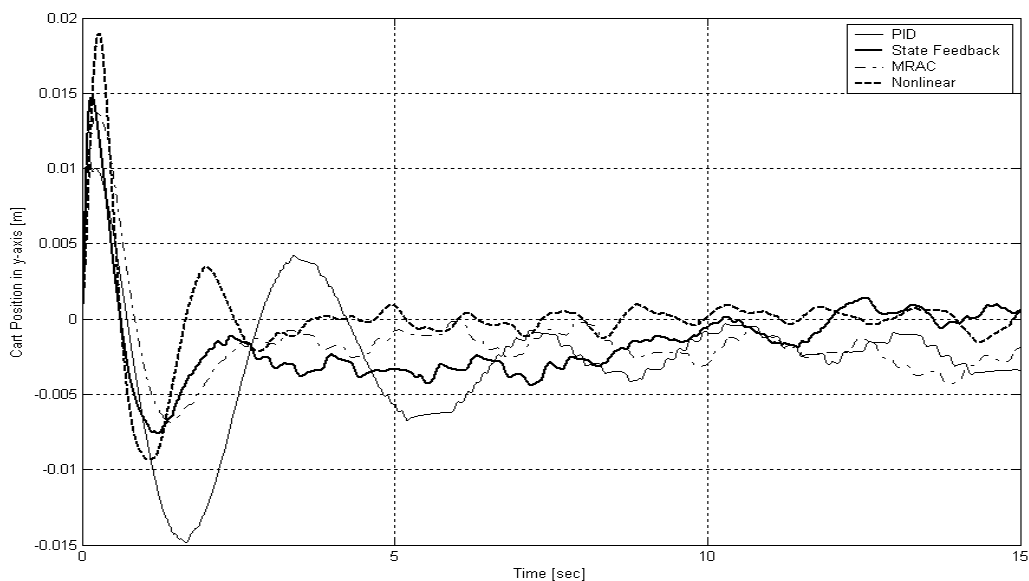


Figure 5.7 Comparison of the experimental responses of the cart position y for regulation problem

Figures 5.6-5.7 show the responses of the cart position along x - and y -axes versus time respectively. The results from Figures 5.6-5.7 show that all controllers can maintain the cart around the middle of the table which the responses obtained from PID controller oscillate more than the other.

The control inputs along each axis are given in Figure 5.8-5.9 which the controller that gives the least of the control inputs along x - and y -axes is the non-linear controller.

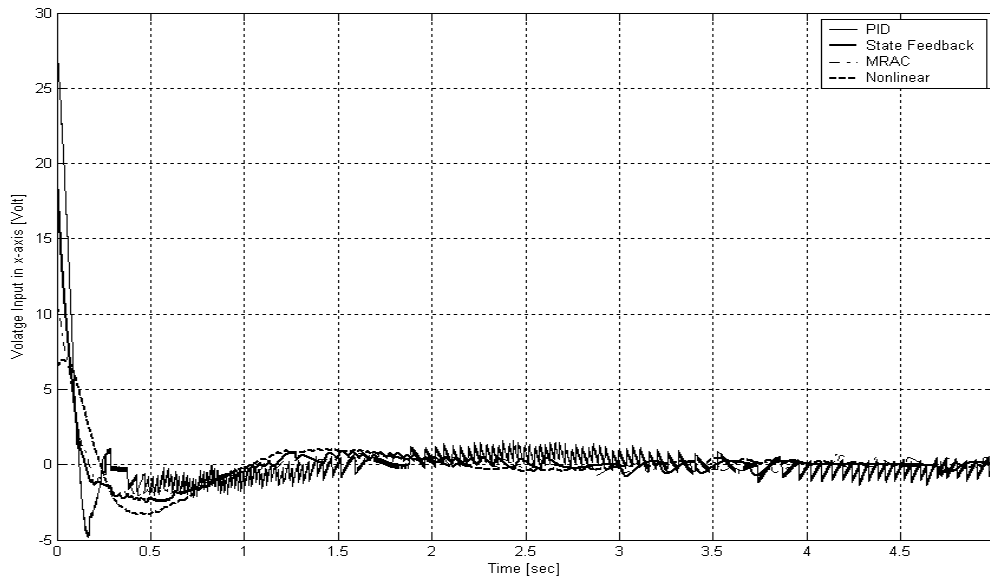


Figure 5.8 Comparison of the experimental responses of the control signal along x -axis for regulation problem

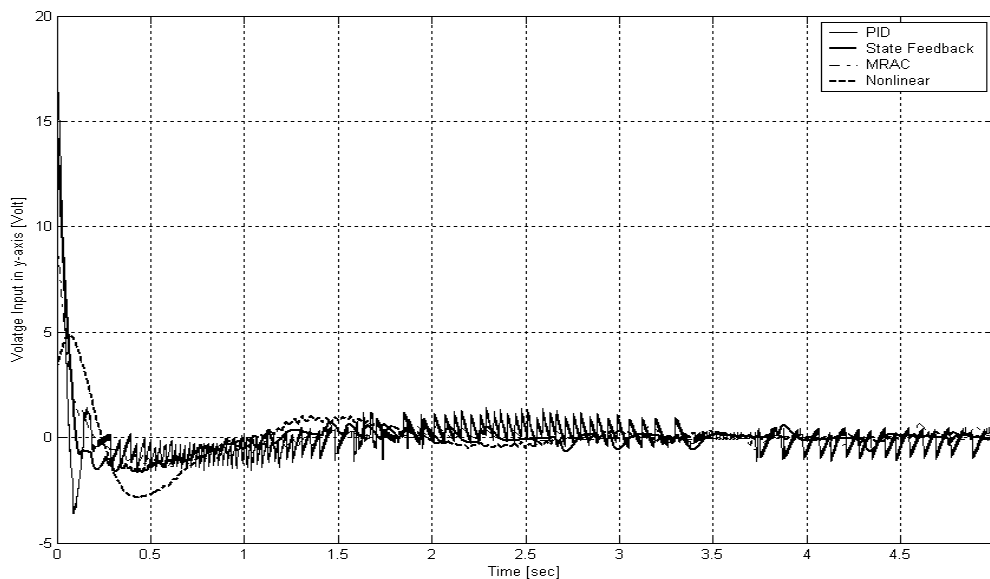


Figure 5.9 Comparison of the experimental responses of the control signal along y -axis for regulation problem

By comparing the experimental results to the simulation results it follows that the experimental results correspond well with the simulation results. However the main difference is the overshoot of the inclination angles ψ and ϑ given by the non-linear controller. It is observed that it gives the least overshoot in the simulation but it gives the highest overshoot in the experiment. Since the non-linear controller is designed from the simulation model. Therefore, when it is used to control the pendulum in the simulation, it can eliminate all non-linear terms in the simulation model but the real construction of 3D inverted pendulum has probably some terms of the non-linearity that aren't considered in the simulation non-linear

model of 3D inverted pendulum such as the friction term. Therefore, when the real construction of 3D inverted pendulum is controlled by the non-linear controller that is designed from the simulation non-linear model, it can't eliminate all non-linear terms in the real construction as in the simulation model. It is, therefore, the cause of the difference of the responses between the simulation and experiment.

5.2.2 Tracking Problem

For this problem all simulated controllers, controller gains and parameters in Chapter 4.2.2.5 are performed to control 3D inverted pendulum for the practical experiments.

Their experimental results are depicted in Figures 5.10-5.16 for the constant angular velocity case and Figures 5.17-5.23 for the inconstant angular velocity case.

In case of the constant angular velocity, Figures 5.10-5.11 illustrate the responses of the inclination angle ψ and ϑ versus time. It is observed that all controller can stabilize the pendulum while the cart is tracking the circular reference input. However the oscillation occurs when the cart tracks the circular reference input which it is in the vicinity of the valid value of the inclination angle. It means that the system is marginally stable.

Figures 5.12-5.13 show the responses of the cart position along x - and y -axes versus time. It is obvious that the robust tracking controller can track nicely the circular reference input for this case. However MRAC using full state feedback and the non-linear controller plus MRAC for output tracking can track quite well the circular reference input. Since they are designed for tracking the output of the reference model. For the state feedback controller, its results are not satisfactory to track the circular reference input.

The cart position on xy -plane is displayed in Figure 5.14 and the control inputs are presented in Figures 5.15-5.16.

By comparing the experimental results to the simulation results it follows that the experimental results correspond well with the simulation results. The main difference is the radius of the circle in Figure 5.14 that is obtained by the state feedback controller. It can be seen that the radius in the experiment is higher than the simulation. This is caused by the gain matrix K_r . Since the gain matrix K_r depends on knowing the DC gain or matrix B of the system exactly. If it is not exactly known, its performance deteriorates.

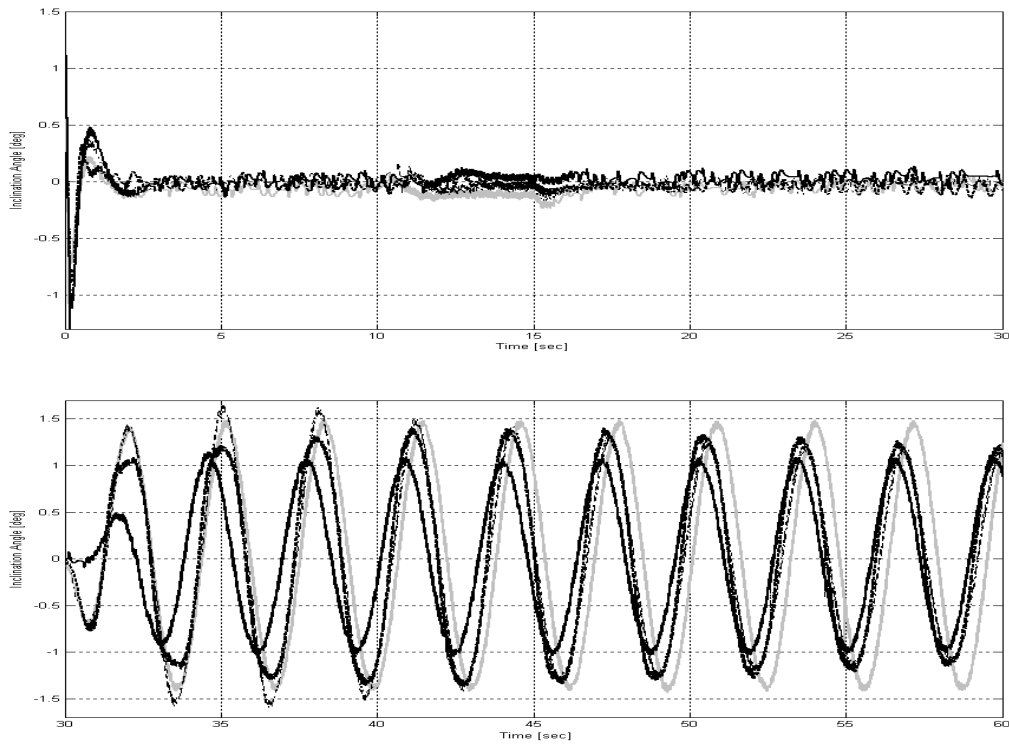


Figure 5.10 Comparison of the experimental responses of the inclination angle ψ for constant angular velocity case of tracking problem

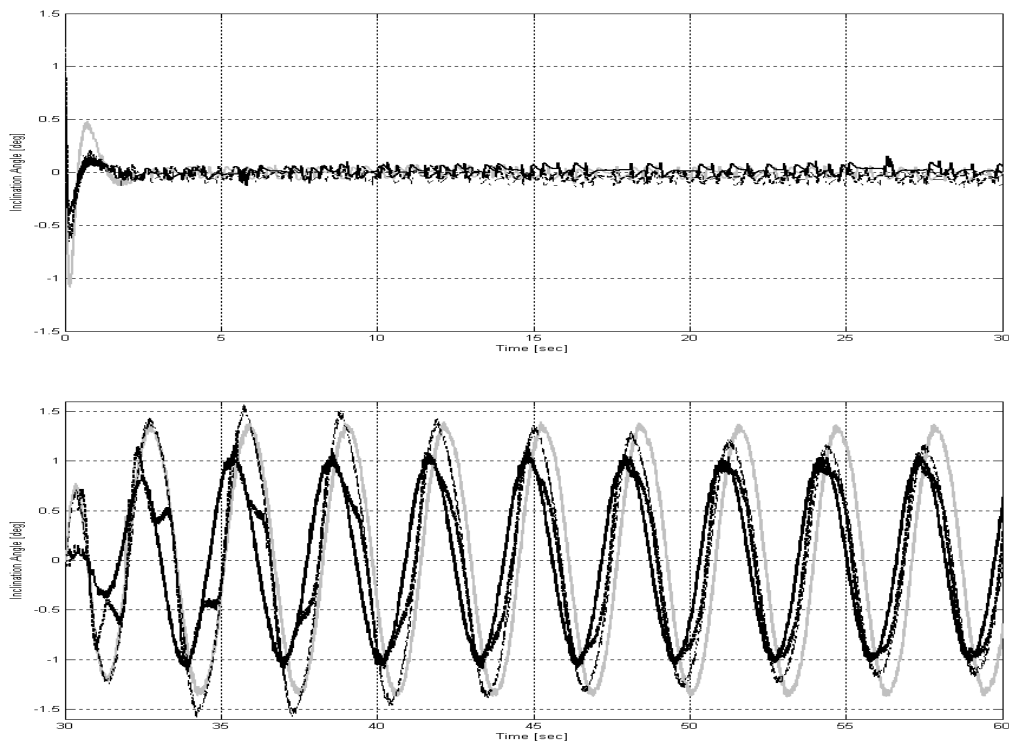


Figure 5.11 Comparison of the experimental responses of the inclination angle ϱ for constant angular velocity case of tracking problem
(— : State Feedback, — : Robust Tracking, - - - : MRAC and : Non-linear-MRAC)

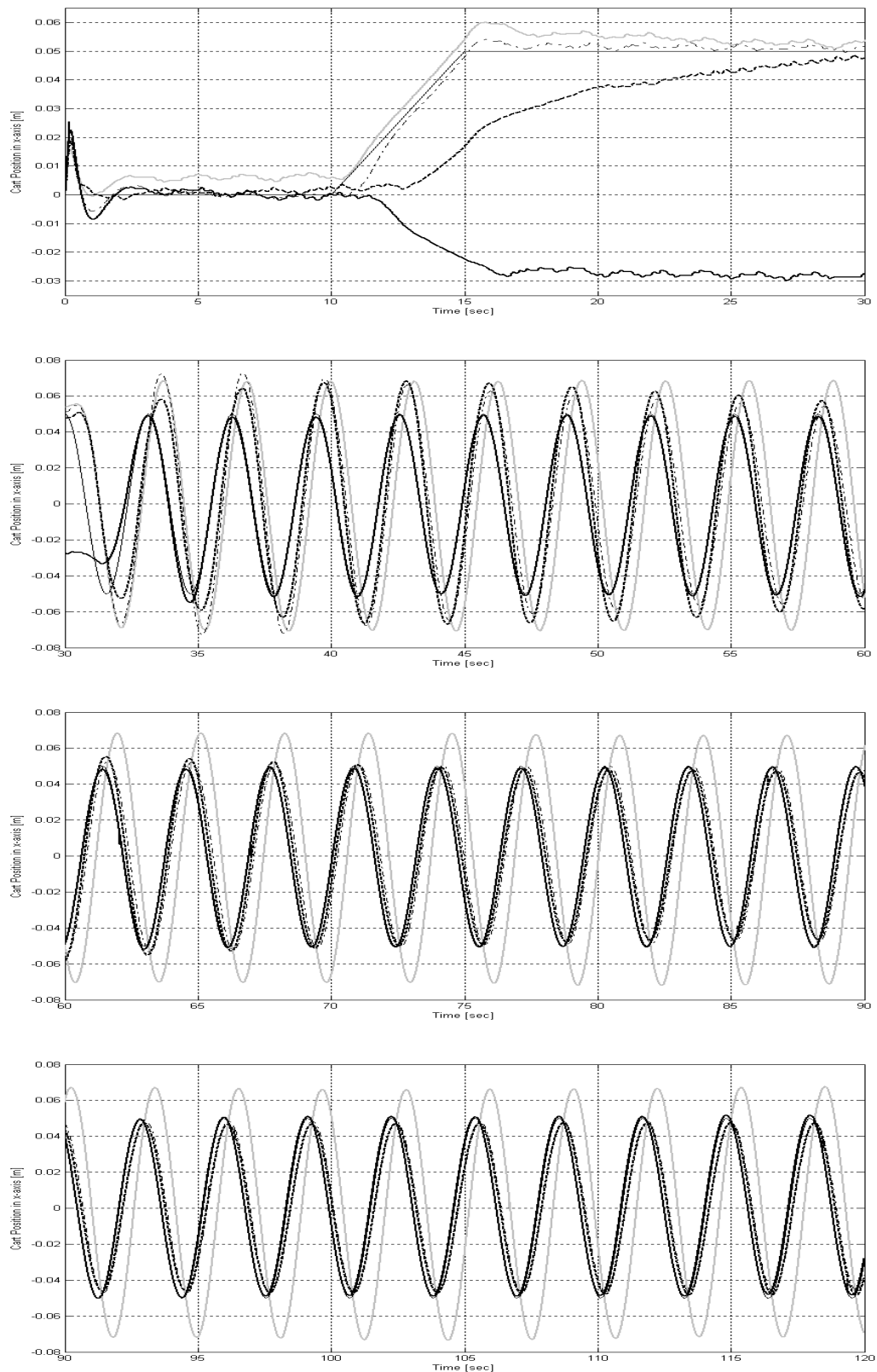


Figure 5.12 Comparison of the experimental responses of the cart position x for constant angular velocity case of tracking problem
 (— : State Feedback, — : Robust Tracking, - - - : MRAC, : Non-linear-MRAC and — : Reference Path)

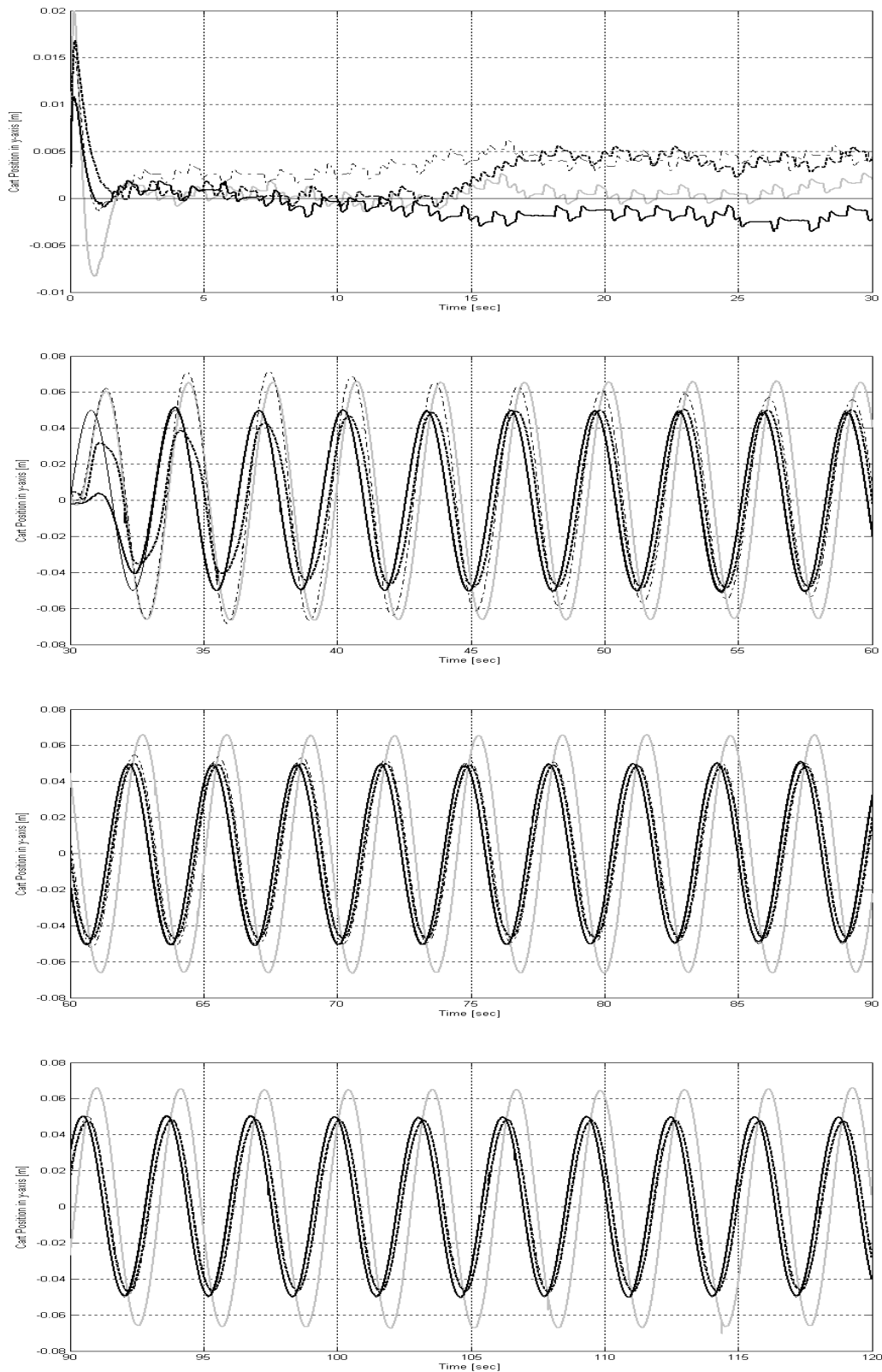


Figure 5.13 Comparison of the experimental responses of the cart position y for constant angular velocity case of tracking problem
 (— : State Feedback, — : Robust Tracking, - - - : MRAC, ···· : Non-linear-MRAC and — : Reference Path)

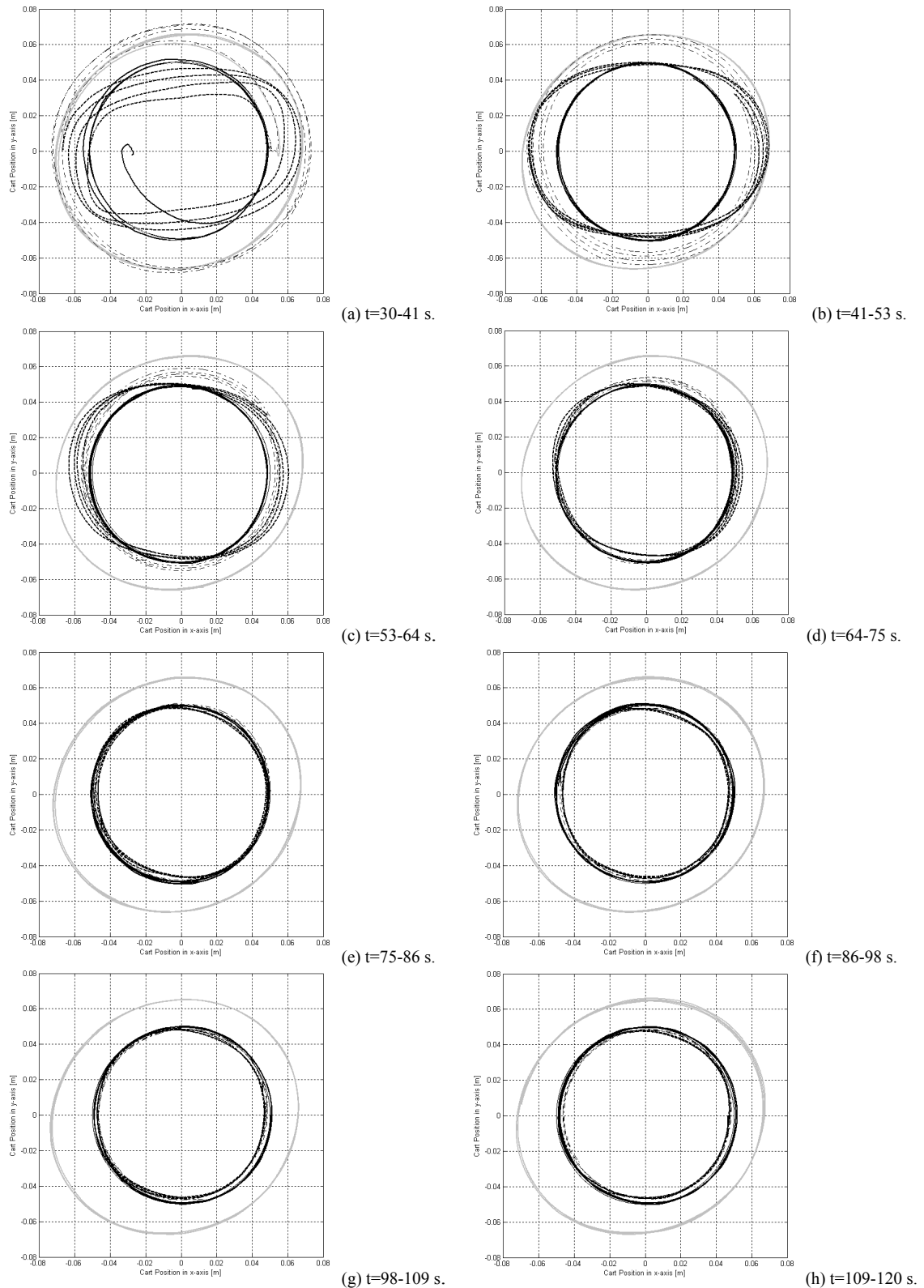


Figure 5.14 Comparison of the experimental responses of the cart position on xy -plane for constant angular velocity case of tracking problem
 (— : State Feedback, — : Robust Tracking, - - - : MRAC, : Non-linear-MRAC and — : Reference Path)

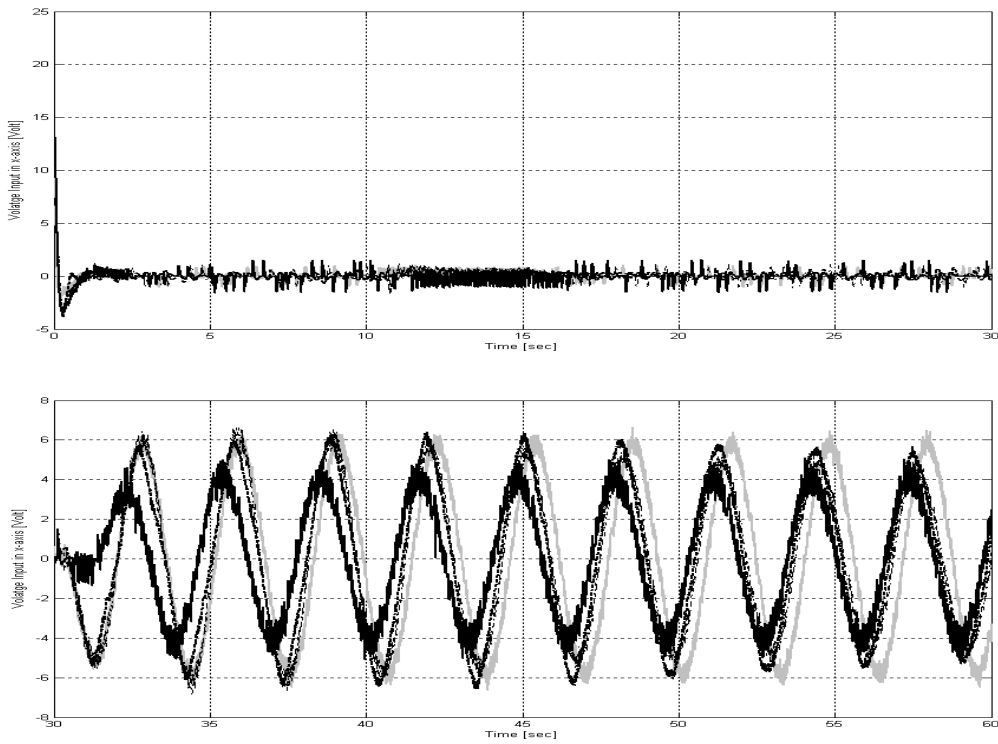


Figure 5.15 Comparison of the experimental responses of the control signal along x -axis for constant angular velocity case of tracking problem

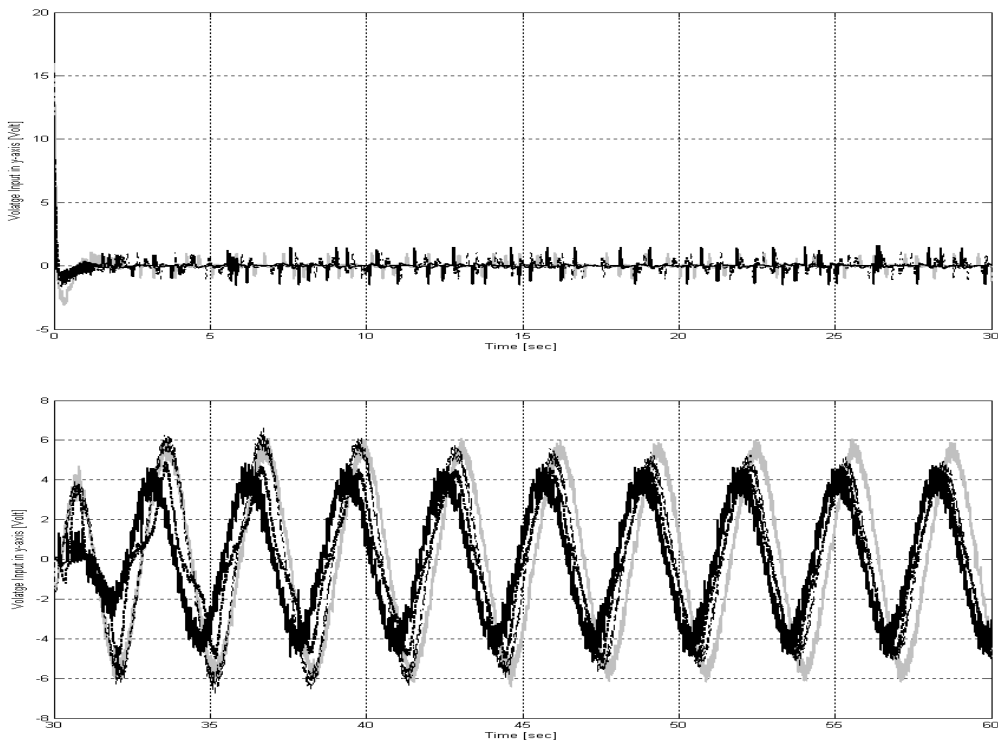


Figure 5.16 Comparison of the experimental responses of the control signal along y -axis for constant angular velocity case of tracking problem
 (— : State Feedback, — : Robust Tracking, - - - : MRAC and : Non-linear-MRAC)

In case of the inconstant angular velocity, the responses of the inclination angles ψ and ϑ are represented in Figures 5.17-5.18. It can be seen that the oscillation occurs when the cart tracks the circular reference input and it has the enlargement of the amplitude when the angular velocity of the circular reference input increases but it is still in the vicinity of the valid value of the inclination angle until the end of the experiment. This is caused by the centrifugal force which applies to the pendulum while the cart is tracking and the enlargement of the amplitude occurs by increasing the centrifugal force. Since the centrifugal force is obtained from $F_c = m_b \omega^2 R$ where m_b is the mass of the ball [kg], ω is the angular velocity [rad/sec] and R is the radius [m]. It can be seen that in this case the centrifugal force depends on the angular velocity. Therefore, when the angular velocity increases, the centrifugal force also increases. It can be concluded that the pendulum will incline to the center of the circle of the movement of the cart which it is the cause of the oscillation of the inclination angles ψ and ϑ . However the system of the pendulum will be probably unstable, if the experimental time is more than 120 sec. Since the pendulum will incline until it collides with the case of the cart.

Figures 5.19-5.20 show the position of the cart along x - and y -axes. For the robust tracking controller, when the cart starts to track the circular reference input, its response can't converge to the circular reference input. After that its response will converge slowly to the circular reference input. Because the angular velocity of the circular reference input is firstly 0.5 rad/sec then it will be increased with $\omega = 0.01(t - 30) + 0.5 \text{ rad/sec}$. When it closes to 2 rad/sec , the response of the robust tracking control will converge to the circular reference input. The non-linear controller plus MRAC for output tracking can be regarded as the best controller, which can converge well the position of the cart toward the circular reference input. For MRAC using full state feedback, it isn't satisfactory to adapt the control gains to track the circular reference input but it is better than the state feedback controller.

Figure 5.21 illustrates the cart position on xy -plane. The control inputs along each axis are shown in Figures 5.22-5.23.

By comparing the experimental results to the simulation results it follows that the experimental results correspond well with the simulation results. The radius of the circle in Figure 5.21 that is obtained by the state feedback controller is the main difference. It is observed that the radius in the experiment is more than the simulation. It is caused by the gain matrix K_r , which its reason is the same as in the case of the constant angular velocity.

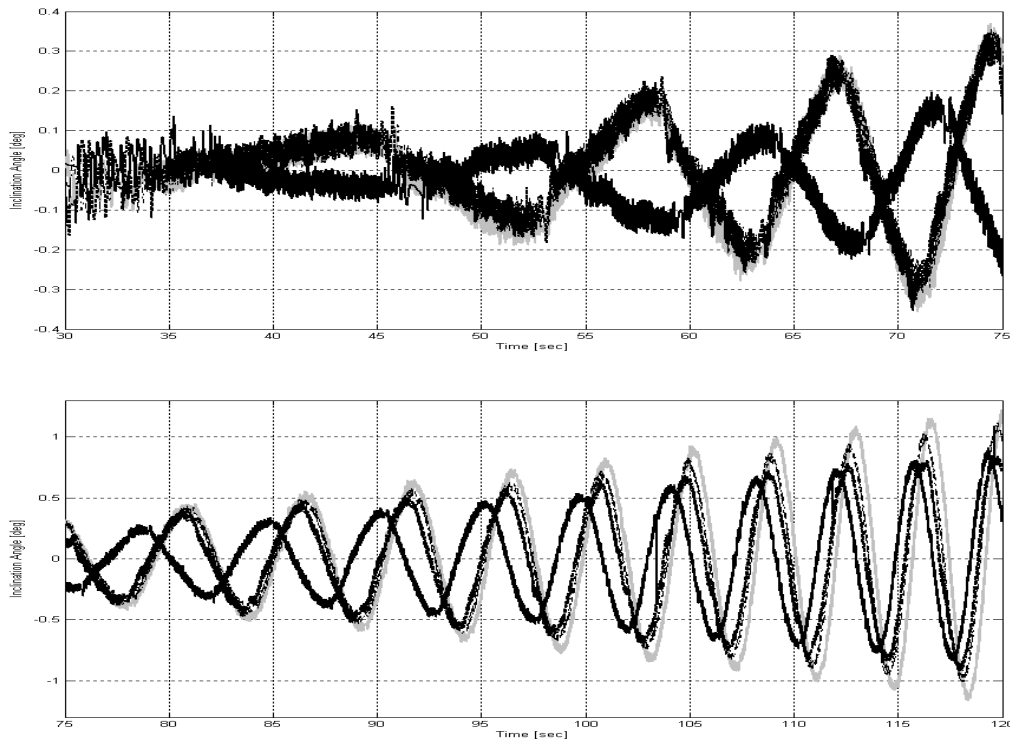


Figure 5.17 Comparison of the experimental responses of the inclination angle ψ for inconstant angular velocity case of tracking problem

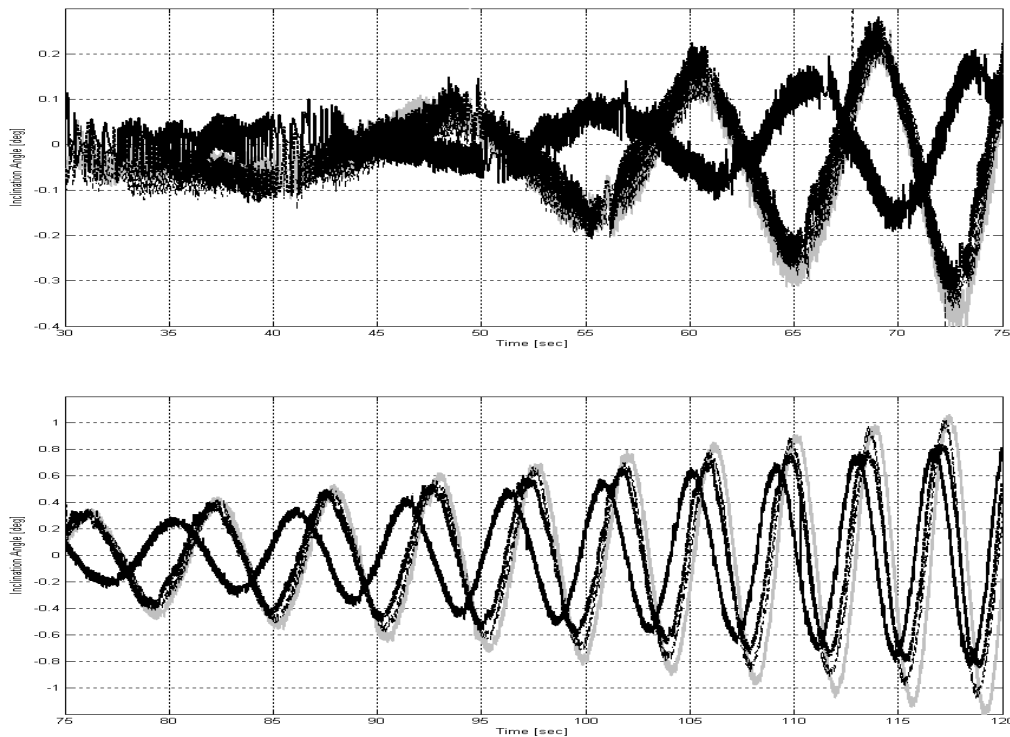


Figure 5.18 Comparison of the experimental responses of the inclination angle ϱ for inconstant angular velocity case of tracking problem
(— : State Feedback, — : Robust Tracking, - - - : MRAC and : Non-linear-MRAC)

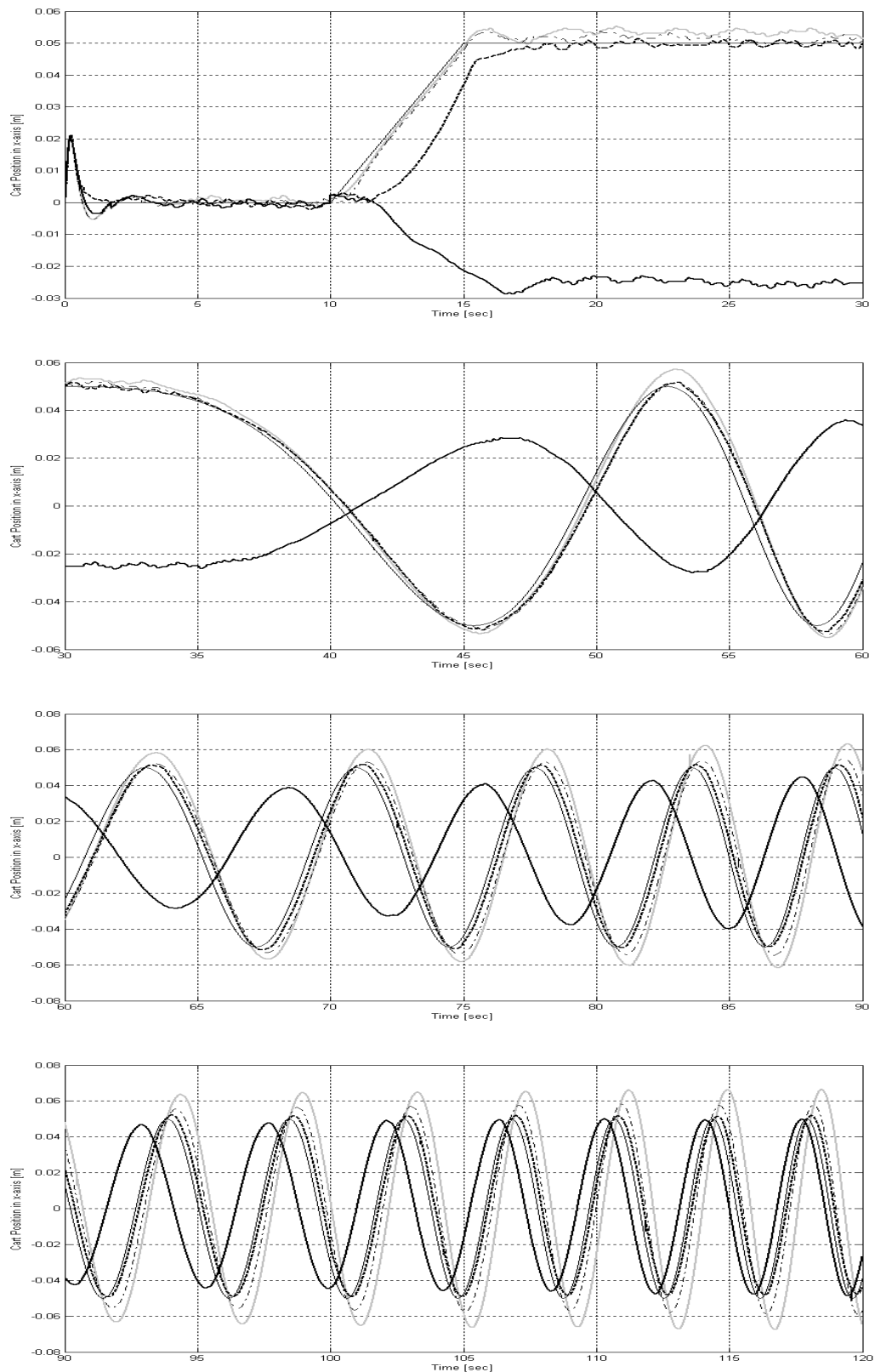


Figure 5.19 Comparison of the experimental responses of the cart position x for inconstant angular velocity case of tracking problem
 (— : State Feedback, — : Robust Tracking, - - - : MRAC, ···· : Non-linear-MRAC and — : Reference Path)

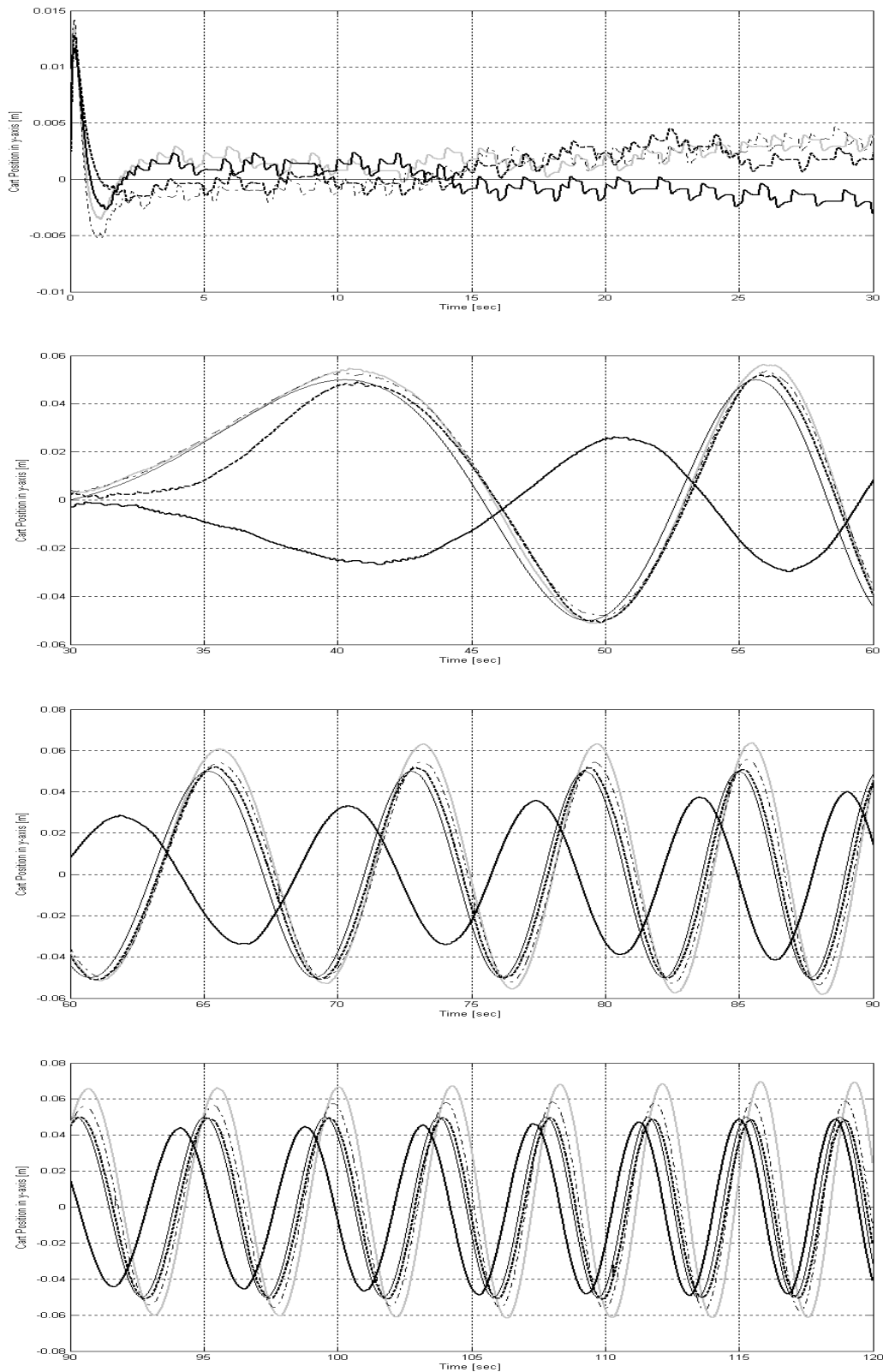


Figure 5.20 Comparison of the experimental responses of the cart position y for inconstant angular velocity case of tracking problem
 (— : State Feedback, — : Robust Tracking, - - : MRAC, : Non-linear-MRAC and — : Reference Path)

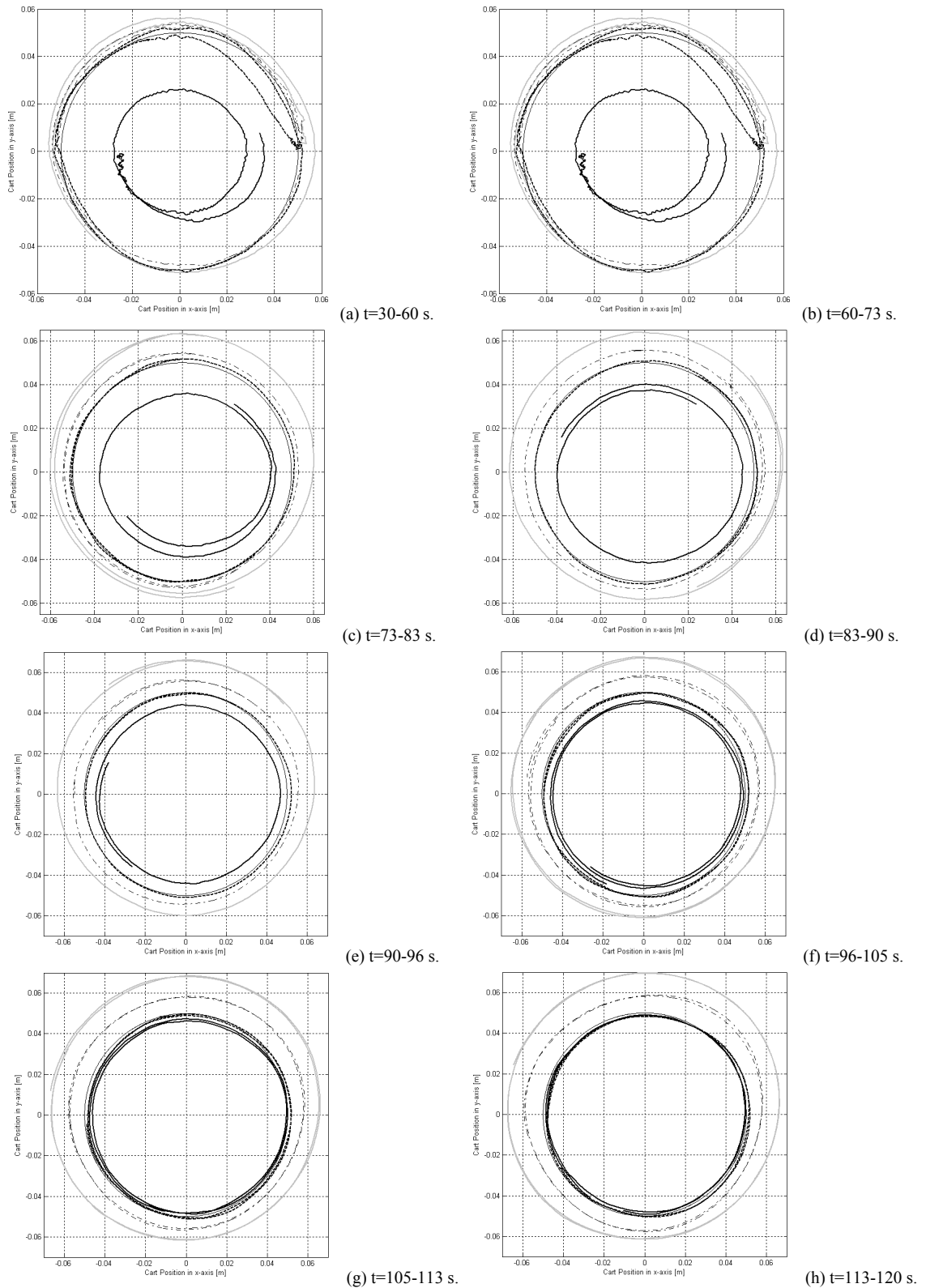


Figure 5.21 Comparison of the experimental responses of the cart position on xy -plane for inconstant angular velocity case of tracking problem
 (— : State Feedback, — : Robust Tracking, ···· : MRAC, ···· : Non-linear-MRAC and - - - : Reference Path)

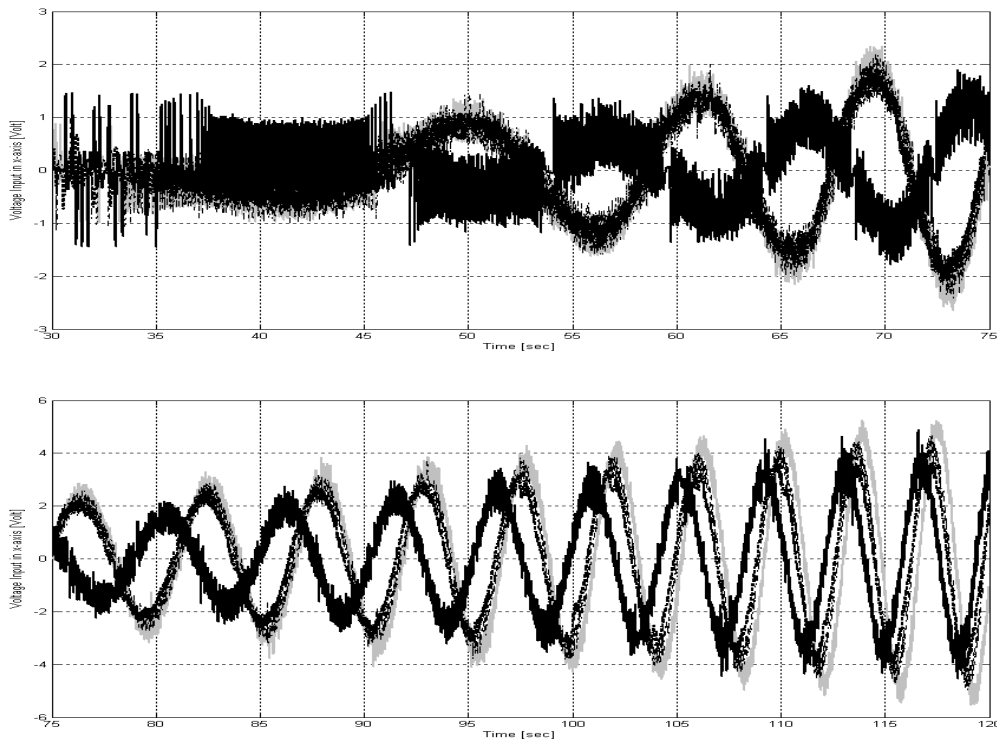


Figure 5.22 Comparison of the experimental responses of the control signal along x -axis for inconstant angular velocity case of tracking problem

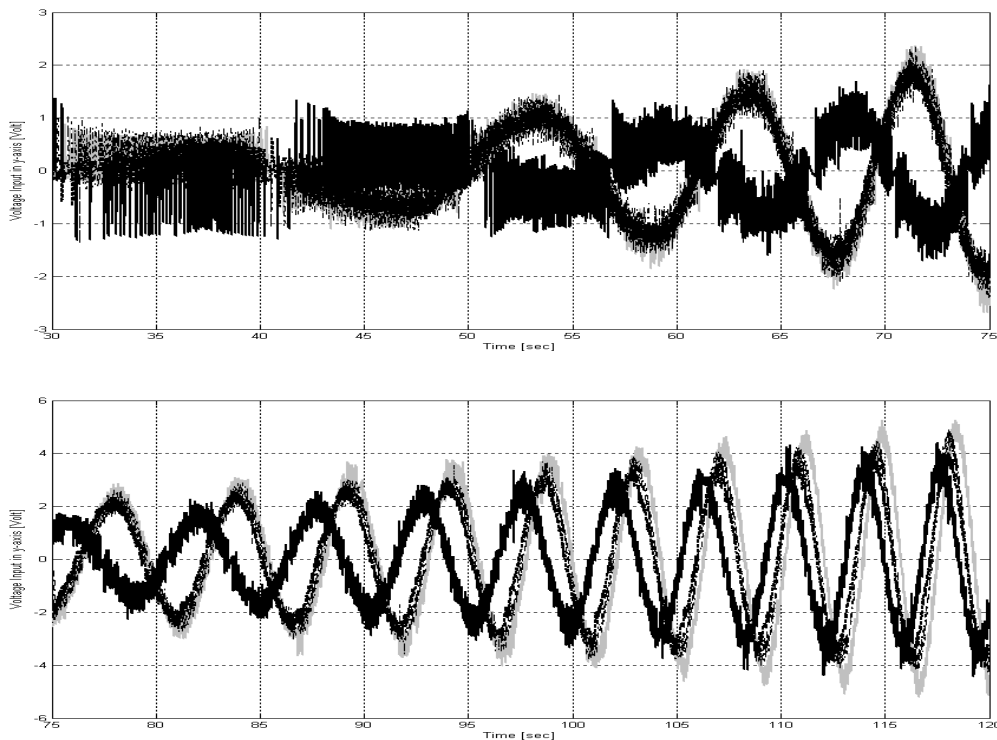


Figure 5.23 Comparison of the experimental responses of the control signal along y -axis for inconstant angular velocity case of tracking problem
 (— : State Feedback, — : Robust Tracking, - - - : MRAC and : Non-linear-MRAC)

Chapter 6

Conclusion and Further Development

6.1 Conclusion

The inverted pendulum system is one of the popular control problems and many researchers are interested to demonstrate and motivate various control techniques in order to stabilize the inverted pendulum in the unstable equilibrium position or the upright position. It can be classified into various classes such as the planar-, the rotational- or Futura-, 3D inverted pendulum and so on.

For this research 3D inverted pendulum placed on the cart, which was constructed by [Bro06] at IMR, Leibniz Universität Hannover, is considered to design with various control techniques. An accomplishment of this research is the calibration of the camera in order to transform 2D image coordinates into 3D world coordinates for the position of the ball at the end of the pendulum with a pin-hole camera model.

In the formulation of the dynamic equations of the inverted pendulum placed on the cart, it can be divided into 2 parts such as (1) the dynamics of the inverted pendulum (2) the dynamics of the motor and cart. To derive the equations of motion of the inverted pendulum, the parameters such as the inclination angle of the camera and table are considered in the system of the inverted pendulum using Lagrangian method in Chapter 3.1. The dynamics of the motor and cart for this research were referred from a previous work, which are identified by [Bro06].

For development of the controllers two basic type control problems are formulated such as regulation and tracking. The main aim for the regulation problem is to stabilize the pendulum in upright position and maintain the cart at the middle of the xy -table. The control structures for this problem are implemented such as PID, state feedback, model reference adaptive control (MRAC) using full state feedback and non-linear control as shown in Chapter 4.2.1. In case of the tracking problem the control structures are developed such as state feedback,

robust tracking control, MRAC using full state feedback and non-linear control plus MRAC for output tracking as shown in Chapter 4.2.2 so as to stabilize the pendulum while the cart is tracking a circle path.

From designing the controllers for the regulation problem in Chapter 4.2.1, the simulations and experiments are applied to compare the performance of each designed controller. The results show that all proposed controller can stabilize the pendulum and maintain the cart at the middle of the xy -table as shown in Chapters 4.2.1.5 and 5.2.1.

In the simulations and experiments for the tracking problem the circular path (4.94) and (4.95) with a constant radius of $R=5\text{ cm}$ is defined as the reference input for the cart position. The simulations and experiments are divided into 2 cases: (1) constant angular velocity of the circular reference input of $\omega=2\text{ rad/sec}$ (2) inconstant angular velocity of the circular reference input of $\omega=0.1t+0.5\text{ rad/sec}$ so that all controllers will be compared their performance. Their simulation and experimental results are shown in Chapter 4.2.2.5 and 5.2.2 respectively. For the constant angular velocity case, it can be seen that the robust tracking control can track the circular reference input better than the other. In case of the inconstant angular velocity, its results show that the non-linear controller plus MRAC for output tracking can adjust the control gains in order to track well the circular reference input.

6.2 Further Development

The findings in this research offer the opportunities for further developments and further researches as following.

- Hardware and Software

Since the motors used in this research are the stepping motors. Therefore, when these motors turn at low velocity, the cart will not move smooth. Consequently it effects on the inclination angle of the pendulum. If it is possible, the stepping motors should be changed to servo motors.

Since the software package is developed for xPC-Target Realtime OS of Mathworks, which must use 2 computers, in order to control the inverted pendulum. Therefore a delay time approximately 1 ms for sending the position of the pendulum in 2D-image coordinates from Host-PC to Target-PC will occur. If the software package is developed for a commercial Realtime OS such as Linux. It isn't necessary to use 2 computers and the delay time for communication between Host-PC and Target-PC will not occur.

- Dynamics of the system

In order that more accuracy of the dynamics of the system, two friction terms should be considered in the model, one is the viscous friction when the cart performs its linear motion on the ball screw, the other is the viscous friction when the pendulum rotates around its pivot.

A double 3D inverted pendulum placed on the cart is one of the challenging and interesting structure in order to design control techniques for the stabilization.

- Control Technique

Since CMOS camera is used to measure the position of the pendulum, it has the delay time approximately 8 ms for capturing the ball and calculating the inclination angles of the pendulum. It means that every 8 ms the position of the pendulum will change while the position of the cart changes every 1 ms. Therefore the inclination angles of the pendulum are not the actual inclination angles of the pendulum. In order to solve this problem, the predictive control is an effective method.

Bibliography

- [Aca82] Acarnley, P. P., *Stepping Motors: a guide to modern theory and practice*, Peter Peregrinus, UK, 1st ed., 1982.
- [Ban05] Banerjee, S., *Dynamics for Engineers*, Wiley, England, 1st ed., 2005.
- [Bar89] Bar-Kana, I. & Kaufman, H., “Simple adaptive control – a survey”, *Proc. IC-CON’89*, Jerusalem, Israel., Apr., 1989.
- [Bed92] Bedrossian, N. S., “Approximate feedback linearization: the cart-pole example”, *Proc. IEEE Int. Conf. on Robots and Automation*, Nice, France, May, 1992.
- [Bou00] Bouguecha, A., “Programmierung eines Bilderfassungsmoduls für einen Versuchstand der bildrückgeführten Regelung”, *Kleine Studienarbeit, Institut für Mess- und Regelungstechnik, Universität Hannover*, Sep., 2000.
- [Bro06] Brosig, S., “Modellierung, Identifikation und experimentelle Validierung zur bildrückgeführten Stabilisierung dynamischer Systeme”, *Dissertation, Institut für Mess- und Regelungstechnik, Universität Hannover*, Jun., 2006.
- [Bou01] Bouzid, N., “Simulation, Erarbeitung und Umsetzung von Konzepten für einen Versuchstand der bildrückgeführten Regelung”, *Große Studienarbeit, Institut für Mess- und Regelungstechnik, Universität Hannover*, Apr., 2001.
- [But92] Butler, H., *Model Reference Adaptive Control: From Theory to Practice*, Prentice-Hall, UK, 1st ed., 1992.
- [Cha95] Chan, M. & Davison, E. J., “The adaptive servomechanism problem for MIMO systems”, *Proc. IEEE Int. Conf. on Decision & Control*, LA, USA, Dec., 1995.

-
- [Che98] Chen, C. S. & Chen, W. L., "Robust adaptive sliding-mode control using fuzzy modeling for inverted-pendulum system", *IEEE Trans. Industrial Electronics*, vol. 45, no. 2, Apr., 1998.
- [Che02] Chen, B. M., Lee, T. H. & Venkataramanan, V., *Hard Disk Drive Servo Systems*, Springer-Verlag London, UK, 1st ed., 2002.
- [Chi90] Chinichian, M. and Kashani, R., "State space controller design for a spatial inverted cart/pendulum system", *Proc. the 32nd Midwest Symposium on Circuits and Systems*, Champaign, IL, Aug., 1990.
- [Chu99] Chung, C. Y., Lee, S. M., Lee, J. W. & Lee, B.H., "Balancing of an inverted pendulum with a kinematically redundant robot", *Proc. IEEE/RSJ Int. Conf. on Intelligent Robots and Systems*, Kyongiu, South Korea, Oct., 1999.
- [Cor96] Corke, P. I. , *Visual Control of Robots: High-Performance Visual Servoing*, Research Studies Press, UK, 1st ed., 1996.
- [Dav76] Davison, E. J., "The robust control of a servomechanism problem for linear time-invariant multivariable systems", *IEEE Trans. Automatic Control*, vol. AC-21, no. 1, Feb., 1976.
- [Dav87] Davison, E. J. & Scherzinger, B. M., "Perfect control of the robust servomechanism problem", *IEEE Trans. Automatic Control*, vol. AC-32, no. 8, Aug., 1987.
- [Die00] Diedrich, L., "PC-Simulation eines inversen 3D-Pendels mit Hilfe von MATLAB-Simulink als Machbarkeitsstudie (zur Parameterbestimmung) in einem realen System", *Große Studienarbeit, Institut für Mess- und Regelungstechnik, Universität Hannover*, Dec., 2000.
- [Dor01] Dorf, R. C., & Bishop, R. H., *Modern Control Systems*, Prentice-Hall, USA, 9th ed., 2001.
- [Elt98] Eltohamy, K. G. & Kuo, C. Y., "Nonlinear optimal control of a triple link inverted pendulum with single control input", *Int. J. Control*, vol. 69, no. 2, 239-256, 1998.
- [Fan01] Fang, L., Chen, W. J. & Cheang, S. U., "Friction compensation for a double inverted pendulum", *Proc. IEEE Int. Conf. on Control Applications*, Mexico City, Mexico, Sep., 2001.
- [Fra02] Franklin, G. F., Powell, J. D. & Emami-Naeini, A., *Feedback Control of Dynamic Systems*, Prentice Hall, USA, 4th ed., 2002.
- [Fra99] Franzrahe, O., "Erstellung eines Programmmoduls für die Online-Bildrückgeführte Regelung in C++ zur Einbindung in MATLAB", *Diplomarbeit, Institut für Mess- und Regelungstechnik, Universität Hannover*, Dec., 1999.
-

-
- [Fuj00] Fujinaka, T, Kishida, Y., Yoshioka, M. & Omatu, S., “Stabilization of double inverted pendulum with self-tuning Neuro-PID”, *Proc. IEEE-INNS-ENNS Int. Conf. on Neural Networks*, Como, Italy, Jul., 2000.
- [Gre77] Greenwood, D. T., *Classical Dynamics*, Prentice-Hall, USA, 1st ed., 1977.
- [Gro96] Grossimon, P. G., Barbieri, E. & Drakunov, S., “Sliding mode control of an inverted pendulum”, *Proc. Southeastern Sym. on System Theory*, Louisiana, USA, Mar./Apr., 1996.
- [Guz93] Guzella, L. & Isidori, A. “On approximate linearization of nonlinear control systems”, *Int. J. Robust and Nonlinear Control*, vol. 3, 1993.
- [Han04] Hangos, K. M., Bokor, J. & Szederkenyi, G., *Analysis and Control of Nonlinear Process Systems*, Springer-Verlag London, UK, 1st ed., 2004.
- [Hen04] Henmi, T., Deng, M. & Inoue, A., “Swing-up control of a serial double inverted pendulum”, *Proc. American Control Conf.*, Massachusetts, USA, Jun./Jul., 2004.
- [Hoh02] Hohl, A., “Simulation und Regelung eines Einfachpendels mittels Matlab/Simulink”, *Studienarbeit, Institut für Mess- und Regelungstechnik, Universität Hannover*, Mar., 2002.
- [Hor92] Horaud, R., Mohr, R. & Lorecki, B., “Linear-camera calibration”, *Proc. IEEE Int. Conf. on Robotics and Automation*, Nice, France, May, 1992.
- [Hua00] Huang, S. J., & Huang, C. L., “Control of an inverted pendulum using grey prediction model”, *IEEE Trans. Industry Applications*, vol. 36, no. 2, Mar./Apr., 2000.
- [Hwa93] Hwang, S. & Carmichael, R., “Adaptive tracking control for a DC motor”, *Proc. IEEE Reg. Conf. on Aerospace Control Systems*, California, USA, May, 1993.
- [Ish91] Ishida, T., Shiokawa, N., Nagado, T. & Ganeko, S., “Learning control of an inverted pendulum using a neural network”, *Proc. IEEE Int. Conf. on Industrial Electronics, Control and Instrumentation*, Nov., 1991.
- [Isi95] Isidori, A., *Nonlinear Control Systems*, Springer-Verlag London, UK, 3rd ed., 1995.
- [Kau98] Kaufman, H., Barkana, I. & Sobel, K., *Direct Adaptive Control Algorithms: Theory and Applications*, Springer-Verlag New York, USA, 2nd ed., 1998.
- [Ken94] Kenjo, T. & Sugawara, A., *Stepping Motors and their Microprocessor Controls*, Oxford, USA, 2nd ed., 1994.
- [Kre84] Krener, A. J., “Approximate linearization by state feedback and coordinate change”, *Systems & Control Letters*, vol. 5, no. 3, 1984.
-

-
- [Lan69] Landau, I. D., "A hyperstability criterion for model reference adaptive control systems", *IEEE Trans. on Automatic Control*, vol. 14, no. 5, Oct., 1969.
- [Lan79] Landau, Y. D., *Adaptive Control: The Model Reference Approach*, Marcel Dekker, 1st ed., 1979.
- [Lew95] Lewis, F. L. & Syrmos, V. L., *Optimal Control*, Wiley, Canada, 2nd ed., 1995.
- [Lun03] Lundberg, K. H. & Roberge, J. K., "Classical dual-inverted pendulum control", *Proc. IEEE Conf. On Decision and Control*, Hawaii, USA, Dec., 2003.
- [Mag98] Magana, M. E., & Holzapfel, F., "Fuzzy-logic control of an inverted pendulum with vision feedback", *IEEE Trans. Edu.*, vol. 41, no. 2, May, 1998.
- [Mar03] Marquez, H. J., *Nonlinear Control System: Analysis and Design*, Wiley, USA, 1st ed., 2003.
- [Mar89] Mareels, I. M. Y. & Ydstie, B. E., "Global stability for an MIT rule based adaptive control", *Proc. IEEE Int. Conf. On Decision and Control*, Florida, USA, Dec., 1989.
- [Mar99] Martinet, P. & Gallice, J., "Position based visual servoing using a nonlinear approach", *Proc. IEEE/RSJ Int. Conf. On Intelligent Robots and Systems*, Kyongju, South Korea, Oct., 1999.
- [Med97] Medrano-Cerda, G. A., "Robust stabilization of a triple inverted pendulum-cart", *Int. J. Control*, vol. 68, no. 5, 1997.
- [Mat01] MathWorks, *xPC Target Getting Started Guide*, online version, 2001.
- [Mat02] MathWorks, *xPC Target User's Guide*, online version, 2002.
- [Mor76] Mori, S., Nishihara, H. & Furuta, K., "Control of unstable mechanical system – control of pendulum", *Int. J. Control*, vol. 23, no. 5, 1976.
- [Nai02] Nair, S. & Leonard, N. E., "A normal form for energy shaping : application to the Furuta pendulum", *Proc. IEEE Conf. On Decision and Control*, Nevada, USA, Dec., 2002.
- [Nar89] Narendra, K. S. & Annaswamy, A. M., *Stable Adaptive Systems*, Prentice-Hall, USA, 1st ed., 1989.
- [Nor00] Norman S. Nise, *Control Systems Engineering*, John Wiley & Sons, USA, 3rd ed., 2000.
- [Oma00] Omatu, S., Fujinaka, T. & Yoshioka, M., "Neuro-PID control for inverted single and double pendulums", *Proc. IEEE Int. Conf. On Systems, Man and Cybernetics*, Nashville, TN, USA, Oct., 2000.
-

-
- [Par66] Parks, P. C., "Liapunov redesign of model reference adaptive control systems", *IEEE Trans. on Automatic Control*, vol. 11, no. 3, Jul., 1966.
- [Par95] Park, S.W. and Lee, C.S.G., "Very fast visual tracking algorithm using scanline", *Proc. IEEE Int. Conf. On Robotics and Automation*, Nagoya, Japan, May, 1995.
- [Ren96] Renou, S. & Saydy, L., "Real time control of an inverted pendulum based on approximate linearization", *Proc. IEEE/ Canadian Conf. on Electrical and Computer Engineering*, Calgary, Alta, May, 1996.
- [Sas99] Sastry, S., *Nonlinear Systems : Analysis, Stability and Control*, Springer-Verlag New York, USA, 1st ed., 1999.
- [Sea95] Seangwerapansiri, V., *Control of Dynamics Systems*, Chulalongkorn U., Thailand, 1st ed., 1995.
- [Slo91] Slotine, J. E. & Li, W., *Applied Nonlinear Control*, Prentice-Hall, USA, 1st ed., 1991.
- [Sob82] Sobel, K. Kaufman, H. & Mabijs, L., "Implicit adaptive control systems for a class of multi-input multi-output systems", *IEEE Trans. on Aerospace and Electronic Systems*, AES-18, no. 5, Sep., 1982.
- [Soo02] Soocharoen, P., *Control System Engineering*, KMITL, Thailand, 1st ed., 2002.
- [Spi67] Spiegel, M. R., *Theory and Problems of Theoretical Mechanics with an Introduction to Lagrange's Equations and Hamiltonian Theory*, Schaum's Outline Series, McGraw-Hill, USA, 1st ed., 1967.
- [Spr98] Sprenger, B., Kucera, L. & Mourad, S., "Balancing of an inverted pendulum with a SCARA robot", *IEEE/ASME Trans. on Mechatronics*, vol. 3, no. 2, Jun., 1998.
- [Sta02] Stanchev, S. P., Reithmeier, E. & Christov, N. D., "Pseudo indirect stabilizing adaptive controller design for a linearized model of an inverted pendulum around vertical position", *Proc. Automatics and Informatics Conf.*, 2002.
- [Sug98] Sugie, T. & Fujimoto, K., "Controller design for inverted pendulum based on approximate linearization", *Int. J. Robust Nonlinear Control*, vol. 8, issue 7, 1998.
- [Wan04] Wang, Z., Chen, Y & Fang, N., "Minimum-time swing-up of a rotary inverted pendulum by iterative impulsive control", *Proc. American Control Conf.*, Boston, USA, 2004.
- [Wen00] Wenzel, L., Vazquez, N., Nair, D. & Jamal, R., "Computer vision based inverted pendulum", *Proc. Instrumentation and Measurement Technology Conf.*, Maryland, USA, May, 2000.
-

-
- [Wil91] Williams, V. & Matsuoka, K., “Learning to balance the inverted pendulum using neural network”, *Proc. IEEE/IECON Int. Conf. on Neural Networks*, Kobe, Oct., 1991.
- [Win68] Winsor, C. A. & Roy, R. J., “Design of model reference adaptive control systems by Liapunov’s second method”, *IEEE Trans. on Automatic Control*, vol. 13, no. 2, Apr., 1968.
- [Xu01] Xu, Y., Iwase, M. & Furuta, K., “Time optimal swing-up control of single pendulum”, *ASME Trans. J. Dynamic Systems, Measurement, and Control*, vol. 123, Sep., 2001.
- [Yam02] Yamada, K. & Yuzawa, A., “Approximate feedback linearization for nonlinear systems and its application to the ACROBOT”, *Proc. American Control Conf.*, Anchorage, AK, May, 2002.
- [Yam99] Yamakita, M., Hoshino, T. & Furuta, K., “Control practice using pendulum”, *Proc. American Control Conf.*, California, USA, Jun., 1999.
- [Yi98] Yi, W., “A fast finding and fitting algorithm to detect circles”, *Proc. IGARSS’ 98*, Seattle, WA, USA., Jul., 1998.

Lebenslauf

- Persönliche Daten: Manusak Janthong
Schulenburg LandStr.32a
30165, Hannover, Deutschland
Tel: +49-(0)160-5107364
Rajamangala University of Technology Thunyaburi,
Faculty of Engineering,
39 Muh 1, Rangsit-Nakhonnayok Rd., Klong 6, Thanyaburi,
Pathum Thani, 12110, Thailand, Tel: +66-(0)2-5493430
Email: patnu@yahoo.com
geb. am 02. März 1973 in Thailand
verheiratet mit Patcharin Janthong
- Hochschulausbildung: Juni 1993 – November 1995
Studium der Maschinenbau: Mahanakorn University of
Technology in Thailand
Abschluss: B.Eng in Mechanical Engineering
- Juni 1996 – März 2000
Studium der Maschinenbau: Chulalongkorn University
in Thailand
Abschluss: M.Eng in Mechanical Engineering
- Berufstätigkeit: Oktober 2000 – November 2000
Mitarbeiter: Phatumwan Institute of Technology in Thailand
- seit November 2000
Mitarbeiter: Rajamangala University of Technology Thunyaburi
in Thailand